Thermalization in hydrodynamical systems

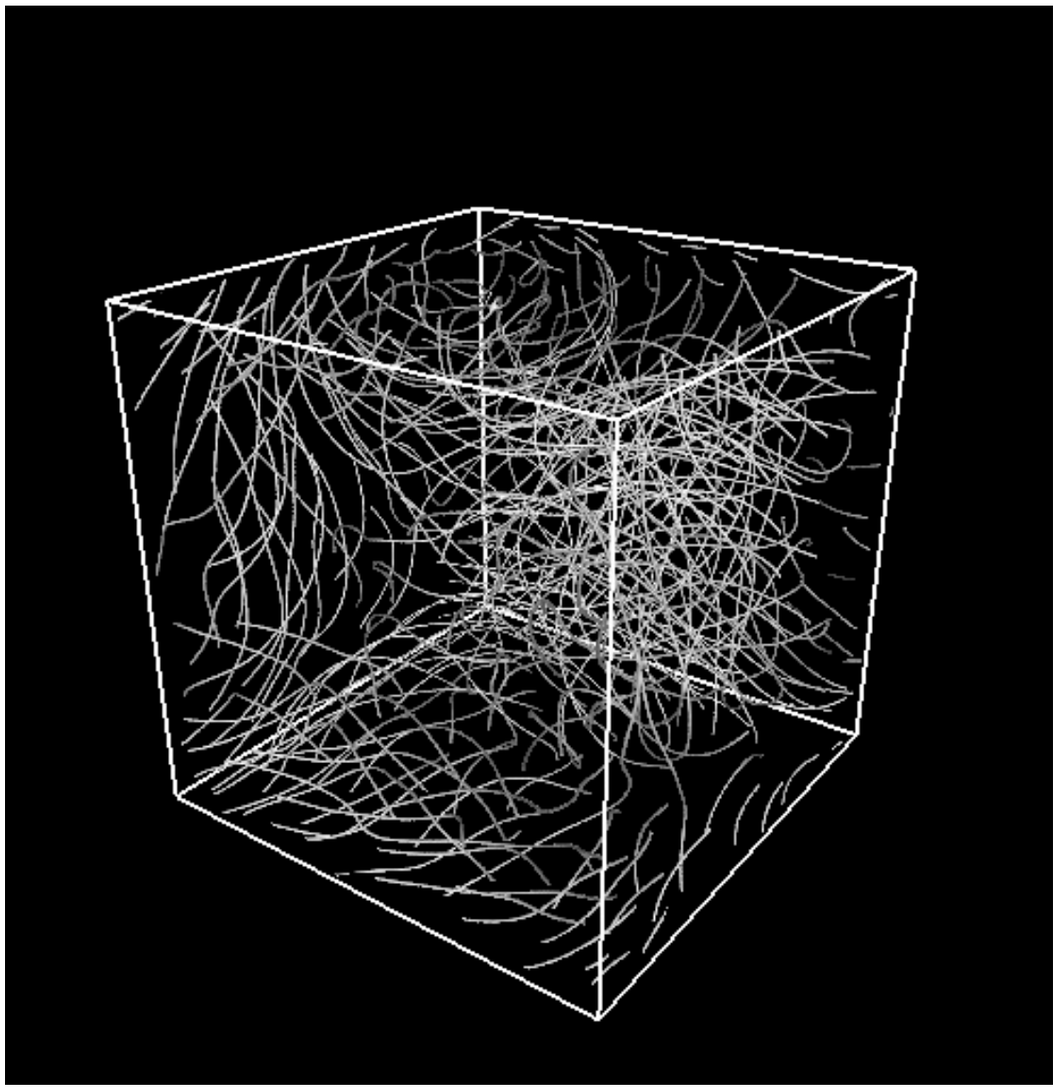

Marc Brachet
LPENS

TURBULENCE: PROBLEMS AT THE INTERFACE OF MATHEMATICS AND PHYSICS (ONLINE)
07 December 2020 to 18 December 2020

Talk Outline

- Definitions. Hydrodynamical systems: Burgers; Euler (compressible and inc.); Gross-Pitaevskii Equation (GPE=Nonlinear Schrödinger) Madelung's transformation. Example: Quantum shocks in (linear) Schrödinger Equation.

- Definitions. Thermalization: Examples: shocks and tygers in Burgers Equation. Thermalization of incompressible Euler with helical Arnold–Beltrami–Childress (ABC) initial data.

- Equilibrium, phase transition and thermalization in the GPE equation

- How close is helical turbulence in GPE ABC to Navier-Stokes ABC? Can we estimate the truncated GPE effective viscosity?

- Truncated 2D Euler dynamics and transitional dynamics in confined turbulence

- Truncated 3D Euler and energy spectrum in forced Navier-Stokes turbulence

- Conclusions

Definition. Hydodynamical Systems

- Perfect fluids
- Superfluids
- Simple examples using Burgers equation

What is a perfect fluid?

- Real classical fluids are viscous and conduct heat
- Perfect fluids are idealized models in which these mechanisms are neglected
- Perfect fluids have zero shear stresses, viscosities, and heat conduction
- Good approximation in some physical cases

Euler Equations

- A perfect fluid can be completely characterized by its velocity and two independent thermodynamic variables.

- If only one thermodynamic variable exists (e.g. isentropic perfect fluid) the fluid is barotropic.

- The density of a barotropic fluid is a function of pressure only.

Barotropic Euler equations

$$\partial_t \mathbf{v} + \mathbf{v} \cdot \nabla \mathbf{v} = -\frac{1}{\rho} \nabla p$$

$$\partial_t \rho + \nabla(\rho \mathbf{v}) = 0$$

Barotropic: $p(\mathbf{x}, t) = f(\rho(\mathbf{x}, t))$

Acoustic propagation: $c = \sqrt{\frac{\partial p}{\partial \rho}}$

Note that the system is time-reversible:

$$t \to -t \; ; \mathbf{v} \to -\mathbf{v} \; ; \rho \to \rho \; ; p \to p$$

Two useful limits

1. incompressible:

$$\rho = cte$$

$$\nabla \mathbf{v} = 0$$

$$c \to \infty$$

There is no equation of state and p is determined by maintaining the incompressibility

2. irrotational:

$$\nabla \times \mathbf{v} = 0$$

$$\mathbf{v} = \nabla \phi$$

$$c = \sqrt{\frac{\partial p}{\partial \rho}}$$

Only compressible modes...

Variational approach

- For the general case see e.g. : R. L. Seliger and G. B. Whitham, Variational Principles in Continuum Mechanics, Proc. R. Soc. Lond. A. 1968 305 1-25.

- Here I'll show how to deal only with the compressible irrotational case..

Irrotational case

$$\mathcal{L} = \rho\phi_t + \frac{\rho(\nabla\phi)^2}{2} + g(\rho)$$

$$\frac{\delta\mathcal{L}}{\delta\phi} = 0 \rightarrow \rho_t + \nabla(\rho(\nabla\phi)) = 0$$

define: $\mathbf{v} = \nabla\phi$

$$\rho g'' = p'$$

$$\frac{\delta\mathcal{L}}{\delta\rho} = 0 \rightarrow \phi_t + \frac{(\nabla\phi)^2}{2} + g' = 0$$

taking the gradient of the last equation:

$$\mathbf{v}_t + \mathbf{v}\cdot\nabla\mathbf{v} = -\nabla g' \quad = -\frac{\nabla p}{\rho}$$

What is a superfluid?
Is it just an Eulerian perfect fluid?

No! Superfluids obey the Gross-Pitaevskii equation (GPE)

The quantum nature of the GPE does disturb some classical traditions of fluid mechanics. This often makes it unpopular…

The Gross-Pitaeveski Equation (GPE)

$$i\hbar\partial_t\Psi = -\frac{\hbar^2}{2m}\nabla^2\Psi + g|\Psi|^2\Psi$$

$$\Psi = \sqrt{\rho/m}\exp i\frac{m}{\hbar}\Phi$$

- Describes a superfluid Bose-Einstein condensate at zero temperature
- Applies to a complex field
- Madelung's transformation gives hydrodynamical form
- Contains quantum vortices with quantized velocity circulation h/m

Variatitional formulation of the GPE

$$\mathcal{L} = -i\hbar\bar{\Psi}\partial_t\Psi + \frac{\hbar^2|\nabla\Psi|^2}{2m} + \frac{g|\Psi|^4}{2}$$

$$\Psi = \sqrt{\rho/m}\exp i\frac{m}{\hbar}\Phi$$

$$\mathcal{L} = \rho\partial_t\Phi + \frac{\rho\nabla\Phi^2}{2} + \frac{g\rho^2}{2m^2} + \frac{\hbar^2(\nabla\sqrt{\rho})^2}{2m^2}$$

Contrast and compare with Euler Equation Lagrangian:

$$\mathcal{L} = \rho\phi_t + \frac{\rho(\nabla\phi)^2}{2} + g(\rho)$$

GPE and Madelung

$$i\hbar\partial_t\Psi = -\frac{\hbar^2}{2m}\nabla^2\Psi + g|\Psi|^2\Psi$$

$$\psi(\mathbf{x},t) = \sqrt{\frac{\rho(\mathbf{x},t)}{m}}\exp\left[i\frac{m}{\hbar}\phi(\mathbf{x},t)\right], \qquad \mathbf{v} = \boldsymbol{\nabla}\phi$$

Speed of sound $c = \sqrt{g|A_0|^2/m}$

Coherence length $\xi = \sqrt{\hbar^2/2m|A_0|^2 g}.$

$$\frac{\partial\rho}{\partial t} + \boldsymbol{\nabla}\cdot(\rho\,\boldsymbol{\nabla}\,\phi) = 0, \qquad \frac{\partial\phi}{\partial t} + \frac{1}{2}(\nabla\phi)^2 = c^2(1-\rho) + c^2\xi^2\frac{\Delta\sqrt{\rho}}{\sqrt{\rho}}.$$

Continuity and Bernoulli equations for a compressible fluid

Irrotational fluid, except near nodal lines of ψ = superfluid vortices, with quantum of circulation $\Gamma = 4\pi c\xi/\sqrt{2}$, which can naturally reconnect in this model.

Energies

The GPE conserves the total energy E, which can be decomposed as [24, 25]: $E = E_{\rm kin} + E_{\rm int} + E_{\rm q}$, with $E_{\rm kin} = \langle|\sqrt{\rho}\mathbf{v}|^2/2\rangle$, $E_{\rm int} = \langle c^2(\rho-1)^2/2\rangle$ and $E_{\rm q} = \langle c^2\xi^2|\nabla\sqrt{\rho}|^2\rangle$. The kinetic energy $E_{\rm kin}$ can be also decomposed into compressible $E^{\rm c}_{\rm kin}$ and incompressible $E^{\rm i}_{\rm kin}$ components, using $(\sqrt{\rho}\mathbf{v}) = (\sqrt{\rho}\mathbf{v})^{\rm c} + (\sqrt{\rho}\mathbf{v})^{\rm i}$ with $\nabla\cdot(\sqrt{\rho}\mathbf{v})^{\rm i} = 0$.

- See e.g. Nore, et al., Phys. Rev. Lett. 78, 3896, 1997
- Paresval's theorem yields definition of energy spectra

1D Burgers equation,GPE and Madelung's transformation

- Euler, irrotational case with zero pressure is called inviscid Burgers

- In this case, the GPE reduces to the (linear) Schrödinger equation

- Madelung transforms yields inviscid Burgers with an extra quantum pressure term

- In what immediately follows, we will compare the (slightly) viscous 1D Burgers case with the quantum case

Viscous Burgers

$$\partial_t \phi + \frac{1}{2}(\partial_x \phi)^2 = \nu \partial_{xx} \phi$$

$$\phi(t=0) = -\cos x$$

$$v = \partial_x \phi$$

Pseudospectral calculation

$\nu = 0.006136$

$\frac{2}{3}$ dealiasing 1024 grid points

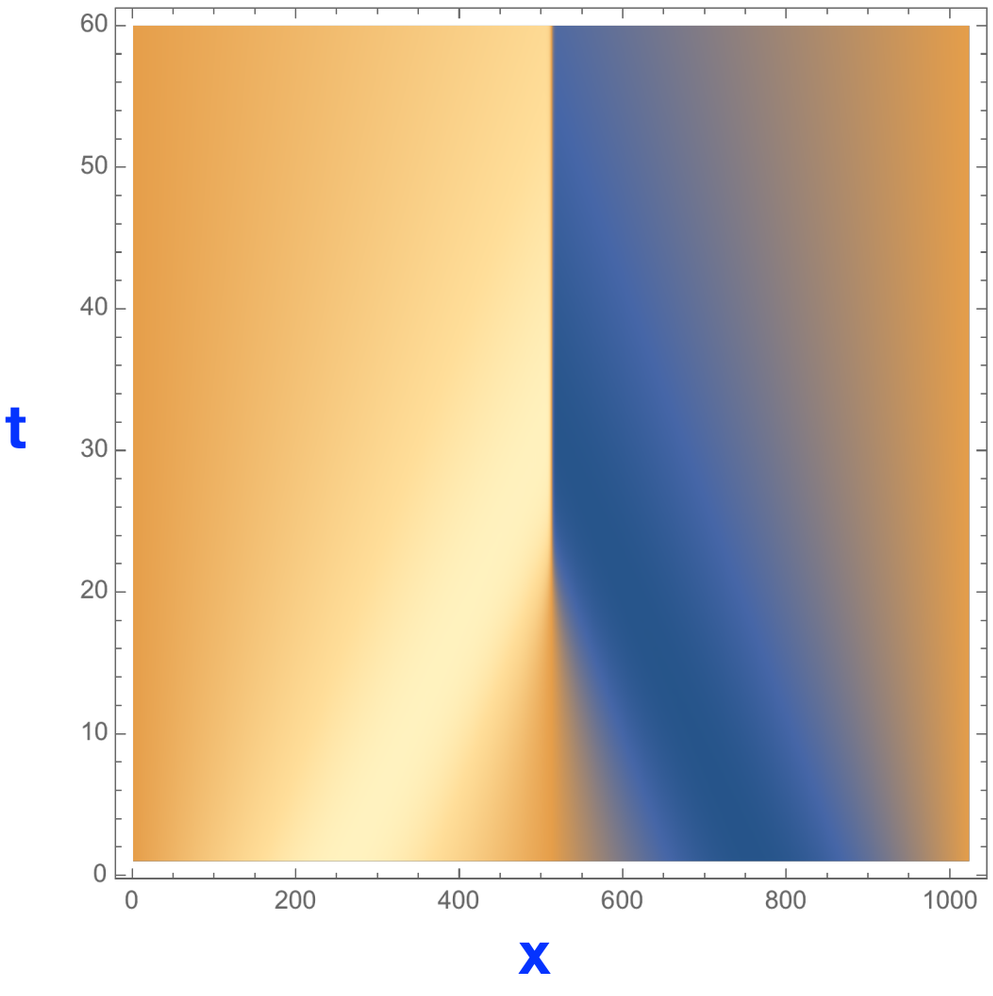

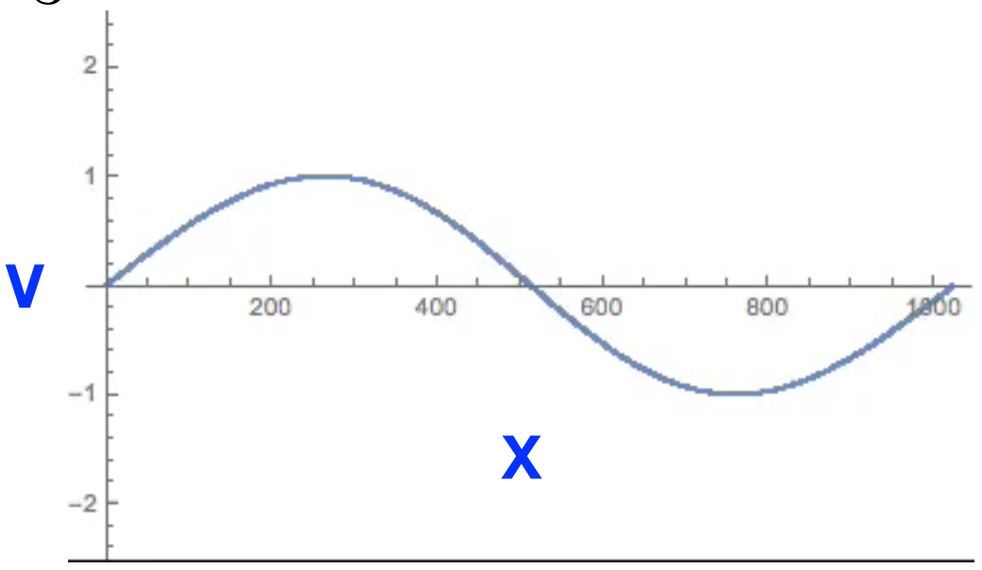

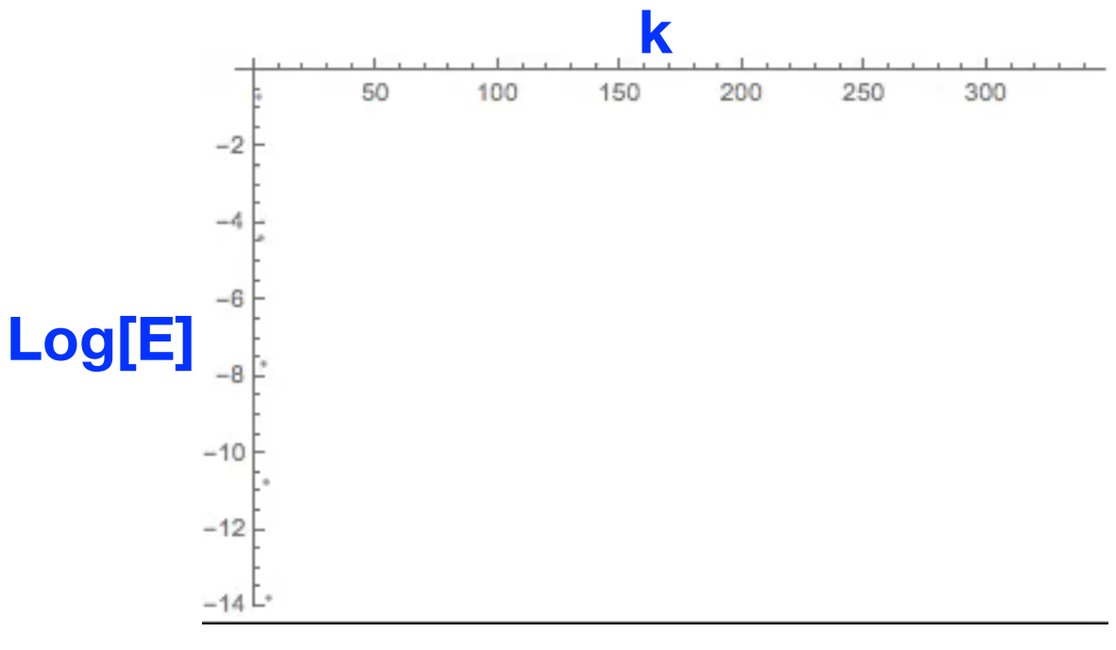

Quantum shocks in (linear) GPE

Schrödinger equation: $i\partial_t\psi = -\frac{\epsilon}{2}\partial_{xx}\psi$

Madelung's transformation: $\psi = \rho^{1/2}\exp i\frac{\phi}{\epsilon}$

Equations of motion:

$$\partial_t\phi + \tfrac{1}{2}(\partial_x\phi)^2 = \frac{\epsilon^2\partial_{xx}\sqrt{\rho}}{2\sqrt{\rho}}$$

$$\partial_t\rho + \partial_x(\rho\partial_x\phi) = 0$$

Initial data

$\phi(t=0) = -\cos x$

$\rho(t=0) = 1$

$v = \partial_x\phi$

$\epsilon = 0.0117188$

Single QFD shock

Density

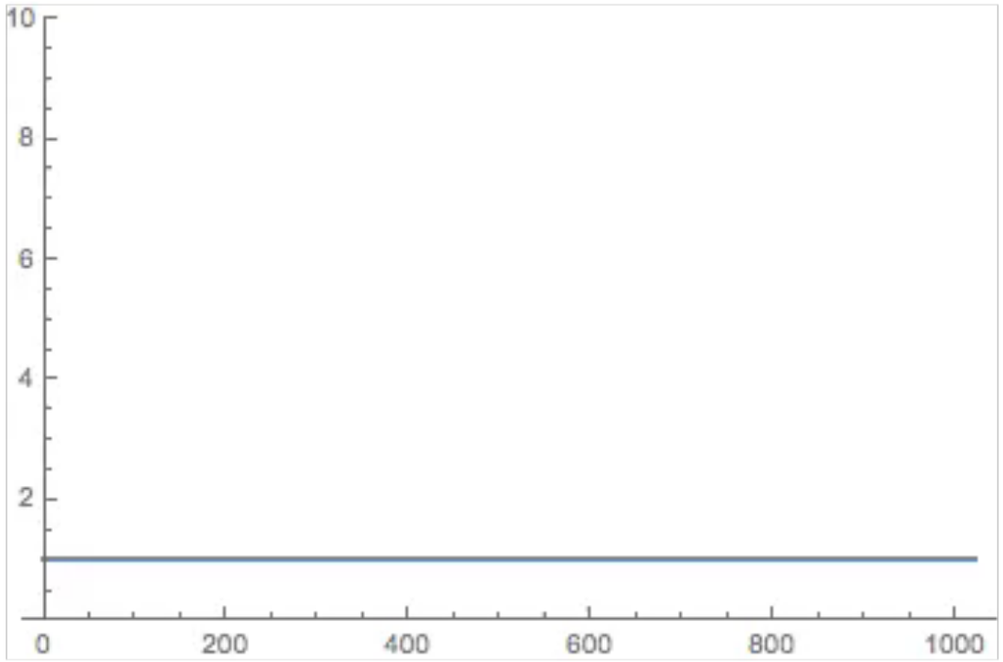

Velocity

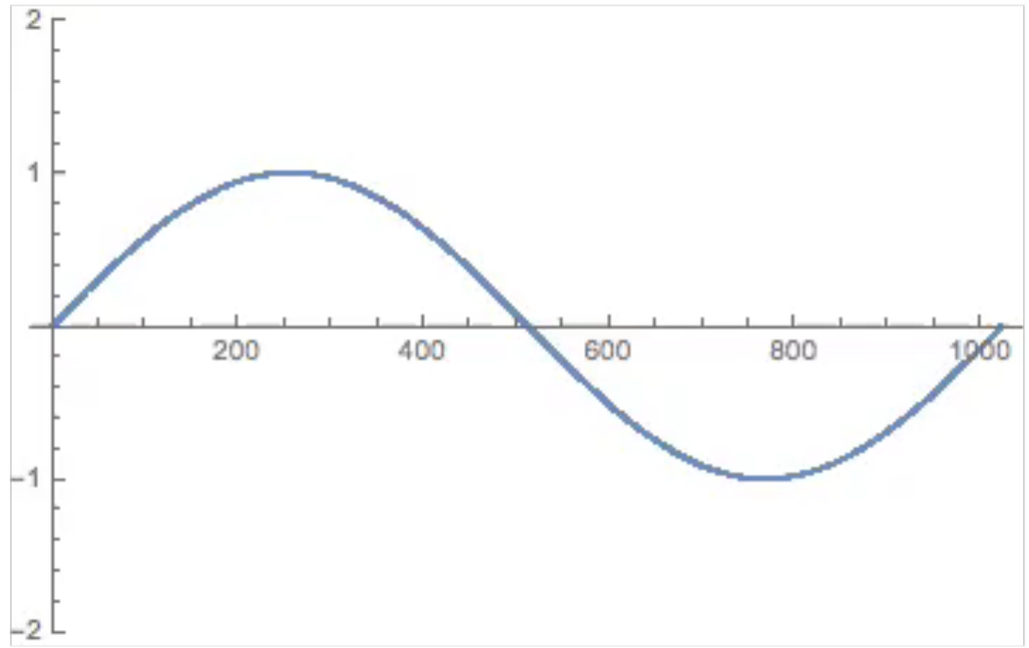

Density

Momentum=Density * Velocity

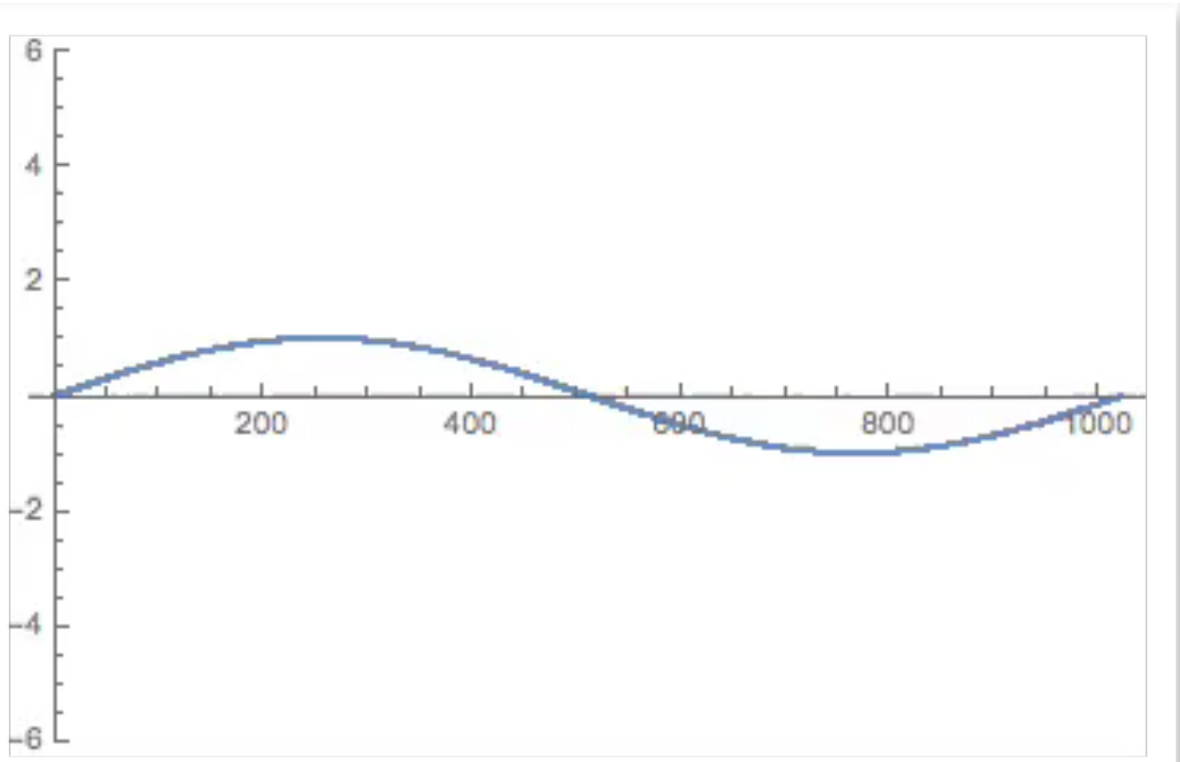

Single QFD shock

The Green function for Schrödinger's equation $i\partial_t\psi = -\frac{\epsilon}{2}\partial_{xx}\psi$ reads

$$G_0(x,t|x_0,t_0) = \sqrt{\frac{1}{2i\pi m(t-t_0)}}e^{\frac{i(x-x_0)^2}{2\epsilon(t-t_0)}}$$

The shock solution thus reads

$$\psi(\mathbf{x},t) = \int_{-\infty}^{\infty} dy \sqrt{\frac{1}{2i\pi\epsilon t}}e^{\frac{i}{\epsilon}\left(\frac{(y-x)^2}{2t}+\cos(y)\right)} \quad (1)$$

In the $\epsilon \to 0$ limit, this integral can be computed by using Pearcey's integral defined by

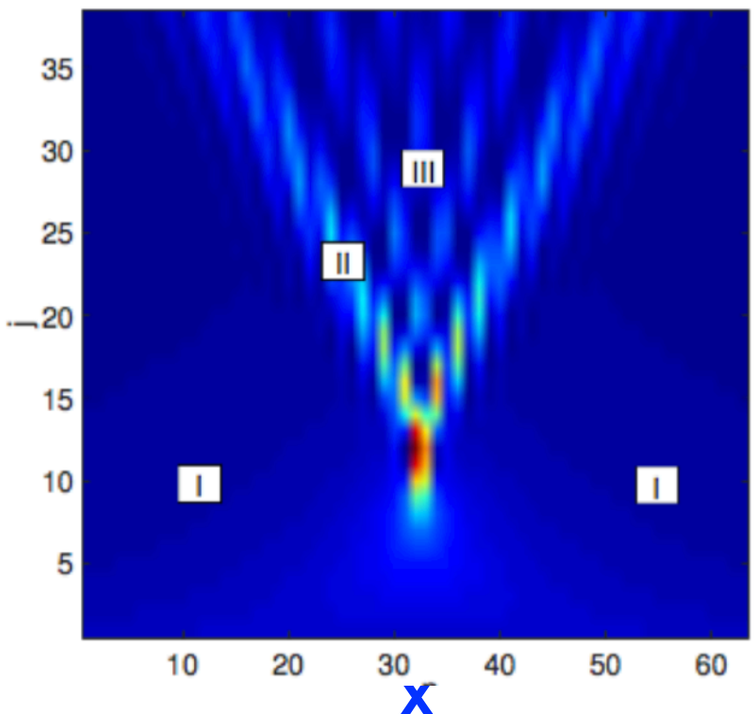

$$I_{\mathcal{P}}(T,X) = \int_{-\infty}^{\infty} dy\, e^{i\left(Xy+Ty^2+y^4\right)}$$

Asymptotic expressions can be readily obtained

see refs. in https://arxiv.org/abs/1709.10417

Definition. Thermalization

- By spectral truncation, the fluid mechanical PDE devolves into a large number of conservative time reversible ODE's
- Thermalization is defined as the standard thermal equilibrium of statistical mechanics for these ODE's
- Ergodicity is assumed
- Microcanonical and canonical distributions should give comparable results for large number of ODE's

Classical truncated systems

where first introduced in 1952 by TD Lee in hydrodynamics

T.D. Lee, Quart. Appl. Math., 10(1):69 (1952).

—NOTES—

ON SOME STATISTICAL PROPERTIES OF HYDRODYNAMICAL AND MAGNETO-HYDRODYNAMICAL FIELDS*

By T. D. LEE (*University of California, Berkeley*)

equilibrium distribution every mode of the Fourier components of magnetic field and velocity field must be in energy equipartition. Let $M(k)$ be the corresponding energy spectrum of magnetic field per unit volume, then we have

$$M(k) = F(k) \propto k^2. \tag{22}$$

2. Turbulence and magneto-turbulence. In the case of a real fluid, due to the energy

General definition of truncated systems

- The basic idea is to perform a truncation (in Fourier space) of the partial differential equation (PDE), as is always done whenever performing an actual numerical computation

- The truncated system is a large number of ordinary differential equations (ODE) with standard statistical mechanical properties

- It contains dissipative processes, thus furnishing a description finite temperature effects

Fourier-Galerkin truncation

Example: Let F be a non-linear function

$$\text{PDE:} \begin{cases} \dfrac{\partial \mathbf{u}}{\partial t}(\mathbf{x}, t) = \mathbf{F}[\mathbf{u}, \partial_i \mathbf{u}, \partial_{ij} \mathbf{u}, \ldots] \\ \text{Periodic B.C. on} \quad \Omega = [0, 2\pi]^D \end{cases}$$

with a conserved quantity E

$$\mathbf{u}(\mathbf{x}, t) = \sum_{\mathbf{k}} \hat{\mathbf{u}}(\mathbf{k}, t) e^{i\mathbf{k}\cdot\mathbf{x}}$$

Non linear terms imply convolutions in Fourier space

$$\frac{\partial \hat{\mathbf{u}}}{\partial t}(\mathbf{k}, t) = \hat{\mathbf{F}}[\hat{\mathbf{u}}, \mathbf{k}]$$

$$\mathbf{k} \in \mathbb{Z}^D$$

Galerkin-truncated equation

$$\frac{\partial \hat{\mathbf{u}}}{\partial t}(\mathbf{k}, t) = \hat{\mathbf{F}}[\hat{\mathbf{u}}, \mathbf{k}]$$

$$\hat{\mathbf{u}}(\mathbf{k}, t) = \mathbf{0} \quad \text{if} \qquad |\mathbf{k}| \geq k_{\max}$$

- Finite-dimensional system of ODE
- **PDE is approximated by the truncated system only as long as the spectral convergence is ensured**
  (dynamics is not influenced by the cut-off)
  - Inherits some of the conservation laws of the original PDE
  - The stationary solutions are given by the associated Liouville equation

$$\mathbb{P}[\hat{\mathbf{u}}(\mathbf{k})] = \mathcal{N} e^{-\eta E}$$

absolute equilibria

General properties of truncated system

- System relaxes toward the thermodynamical equilibrium
- Partial thermalization at small scales
- Thermalized modes generate an effective dissipation acting at large scales.

Truncated inviscid Burgers

$$\partial_t \phi + \frac{1}{2}(\partial_x \phi)^2 = 0$$

$$\phi(t=0) = -\cos x$$

$$v = \partial_x \phi$$

Pseudospectral calculation
$\frac{2}{3}$ dealiasing 1024 grid points

Tygers: See Frisch et al.

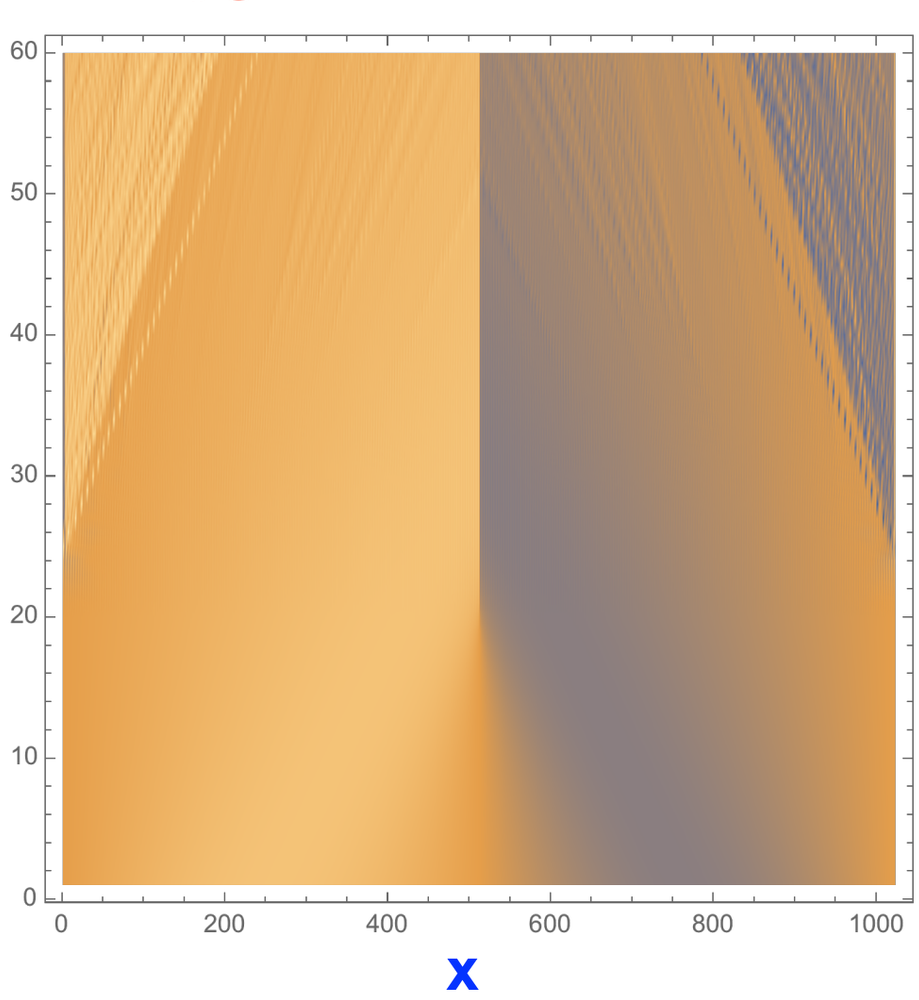

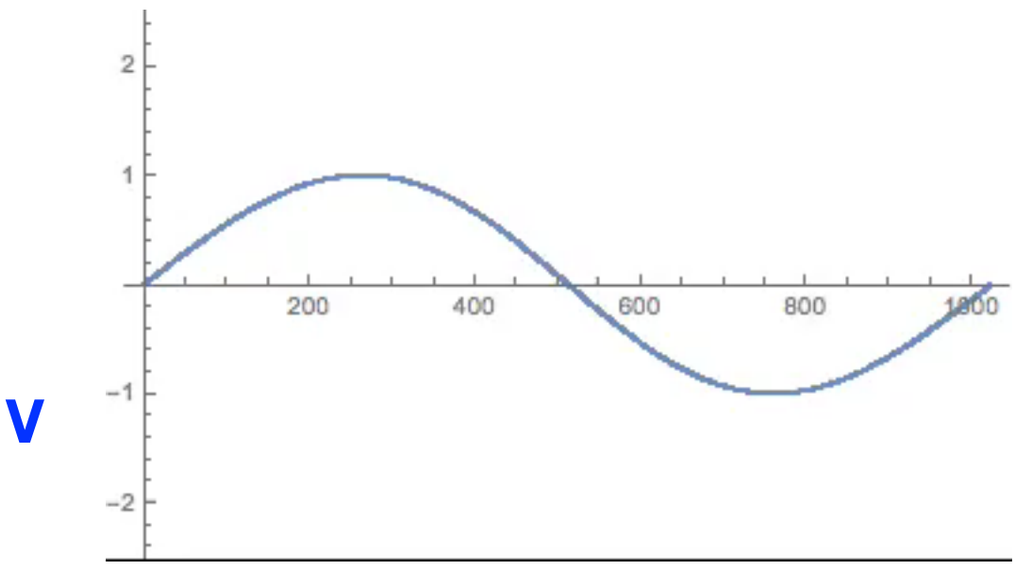

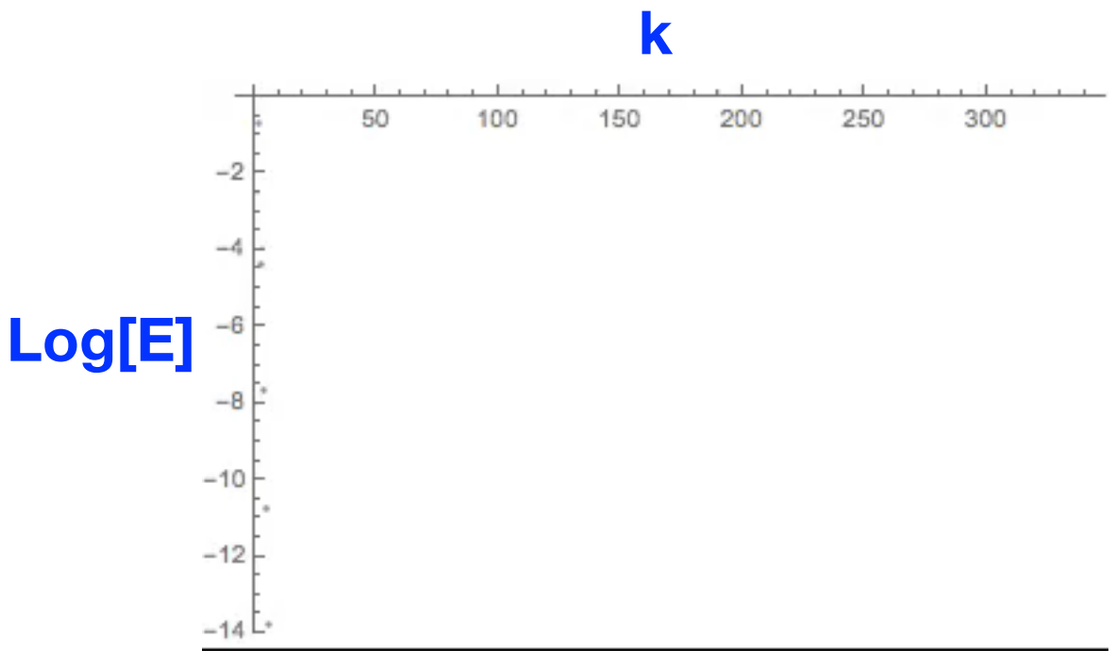

Truncated Euler equation

Euler PDE: $\partial_t \mathbf{u} + (\mathbf{u}\cdot\nabla)\mathbf{u} = -\nabla p$

$\nabla \cdot \mathbf{u} = 0$

$$\mathbf{u}(\mathbf{x},t) = \sum_{\mathbf{k}} \hat{\mathbf{u}}(\mathbf{k},t) e^{i\mathbf{k}\cdot\mathbf{x}}$$

$$\partial_t \hat{u}_\alpha(\mathbf{k},t) = -\frac{i}{2}\mathcal{P}_{\alpha\beta\gamma}(\mathbf{k}) \sum_{\mathbf{p}} \hat{u}_\beta(\mathbf{p},t)\hat{u}_\gamma(\mathbf{k}-\mathbf{p},t)$$

where $\mathcal{P}_{\alpha\beta\gamma} = k_\beta P_{\alpha\gamma} + k_\gamma P_{\alpha\beta}$ with $P_{\alpha\beta} = \delta_{\alpha\beta} - k_\alpha k_\beta / k$

Truncated Euler equation

Conserved quantities

Energy

$$E = \frac{1}{(2\pi)^3}\int \frac{|\mathbf{u}(\mathbf{x})|^2}{2}\, d^3x = \sum_k E(k)$$

Helicity

$$H = \frac{1}{(2\pi)^3}\int \mathbf{u}(\mathbf{x})\cdot\omega(\mathbf{x})\, d^3x = \sum_k H(k) \quad , \quad \omega = \nabla\times\mathbf{u}$$

H. Moffatt, J. Moreau in the 60's. Discovered 200 years after Euler work

$$E(k) = \sum_{k-\Delta k/2<|\mathbf{k}'|<k+\Delta k/2} \tfrac{1}{2}|\hat{\mathbf{u}}(\mathbf{k}',t)|^2$$

$$H(k) = \sum_{k-\Delta k/2<|\mathbf{k}'|<k+\Delta k/2} \hat{\mathbf{u}}(\mathbf{k}',t)\cdot\hat{\omega}(-\mathbf{k}',t)$$

Both Energy and Helicity are exactly conserved by the truncated dynamics

Kraichnan's Helical

Absolute Equilibrium

(J. FLuids Mech. 73)

$$\hat{\mathbf{u}}(\mathbf{k}) \sim e^{-\beta E - \alpha H}$$

Gaussian distribution

$$E(k) = \frac{k^2}{\beta} \frac{4\pi}{1 - \alpha^2 k^2/\beta^2} \sim k^2 \qquad H(k) = \frac{k^4 \alpha}{\beta^2} \frac{8\pi}{1 - \alpha^2 k^2/\beta^2} \sim k^4$$

For the case presented here: $\alpha^2 k_{\max}^2/\beta^2 \ll 1$

Numerical simulation ABC flow

Resolution of 512^3

$$\nabla \times \mathbf{u}^{(k)}_{\mathrm{ABC}} = \lambda_k \mathbf{u}^{(k)}_{\mathrm{ABC}}$$

G. Krstulovic, P. D. Mininni, M. E. Brachet and A. Pouquet, PRE 79(5) 056304, 2009

$$E(k) = \frac{k^2}{\beta} \frac{4\pi}{1 - \alpha^2 k^2/\beta^2} \sim k^2 \qquad H(k) = \frac{k^4 \alpha}{\beta^2} \frac{8\pi}{1 - \alpha^2 k^2/\beta^2} \sim k^4$$

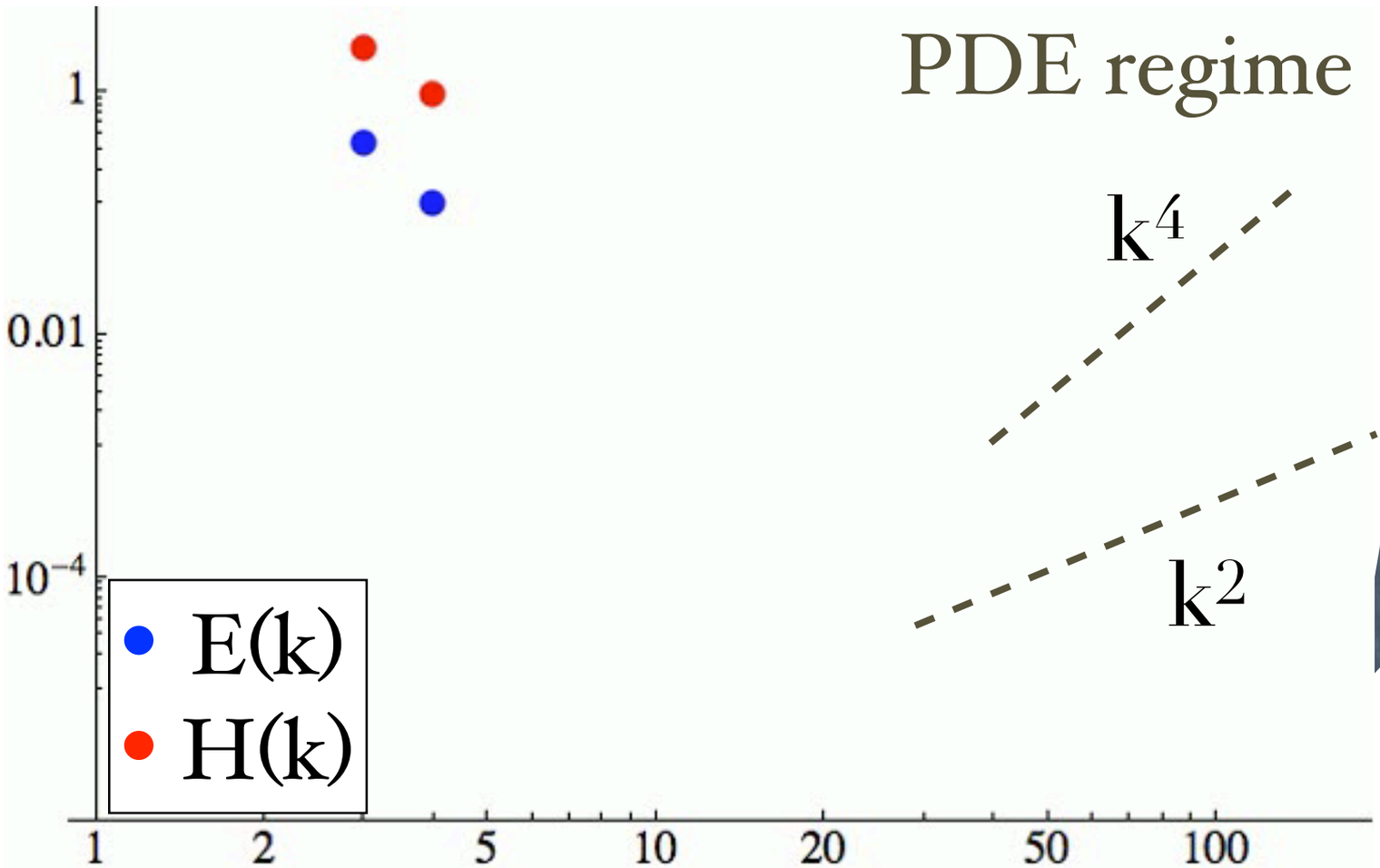

Truncated Euler: basic facts

- Relaxation toward Kraichnan helical absolute equilibrium
- Transient mixed energy and helicity cascades
- Thermalized small-scales act as microworld providing an effective dissipation in the system

Truncation of GPE

$$i\hbar\frac{\partial\psi}{\partial t} = \mathcal{P}_{\mathrm{G}}[-\frac{\hbar^2}{2m}\nabla^2\psi + g\mathcal{P}_{\mathrm{G}}[|\psi|^2]\psi]$$

$$H = \int d^3x \left(\frac{\hbar^2}{2m}|\nabla\psi|^2 + \frac{g}{2}[\mathcal{P}_{\mathrm{G}}|\psi|^2]^2\right).$$

$$\mathcal{P}_{\mathrm{G}}[\hat{\psi}_k] = \theta(k_{\mathrm{max}} - k)\hat{\psi}_k$$

Heaviside function

Description of BEC at finite temperature: classical field model

Conserved quantities

Energy, number of particles and momentum

$$
\begin{aligned}
H &= \int_V d^3x \left(\frac{\hbar^2}{2m} |\nabla \psi|^2 + \frac{g}{2} |\psi|^4 \right) \\
N &= \int_V |\psi|^2 \, d^3x \\
\mathbf{P} &= \int_V \frac{i\hbar}{2} \left(\psi \nabla \overline{\psi} - \overline{\psi} \nabla \psi \right) \, d^3x.
\end{aligned}
$$

Conservation laws are valid in the truncated system, if dealiasing is done carefully enough

Thermalized microcanonical states

Condensation transition in TGPE

It was previously known that the k=0 mode of ψ vanishes at finite energy

MJ. Davis, SA. Morgan and K. Burnett
PRL **87,** (2001)

In fact: standard 2nd order phase transition with complex order parameter

For a full discussion of the subject, see:

Krstulovic and Brachet, Phys. Rev. E 83, 066311 (2011)

What is an 'absolute equilibrium' for GPE?

$$P_{\rm stat} = \frac{1}{\mathcal{Z}} e^{-\beta F}$$

is non Gaussian
because H is quartic!

$$F = H - \mu N - \mathbf{W} \cdot \mathrm{P}$$

$$H = \int_V d^3x \left(\frac{\hbar^2}{2m} |\nabla \psi|^2 + \frac{g}{2} |\psi|^4 \right)$$

Stochastic pde used to generate absolute equilibrium

$$\begin{aligned} \hbar \frac{\partial A_{\mathbf{k}}}{\partial t} &= -\frac{1}{V} \frac{\partial F}{\partial A^*_{\mathbf{k}}} + \sqrt{\frac{2\hbar}{V\beta}}\, \hat{\zeta}(\mathbf{k}, t) \\ \langle \zeta(\mathbf{x}, t) \zeta^*(\mathbf{x}', t') \rangle &= \delta(t - t') \delta(\mathbf{x} - \mathbf{x}'), \end{aligned}$$

$$\hbar \frac{\partial \psi}{\partial t} = \mathcal{P}_{\rm G} [\frac{\hbar^2}{2m} \nabla^2 \psi + \mu \psi - g \mathcal{P}_{\rm G} [|\psi|^2] \psi - i\hbar \mathbf{W} \cdot \nabla \psi] + \sqrt{\frac{2\hbar}{V\beta}} \mathcal{P}_{\rm G} [\zeta(\mathbf{x}, t)]$$

Micro canonical versus grand canonical

H	T	TGPE time steps	SGLE time steps
0.09	0.09	40000	9600
0.5	0.5	20000	9600
1.96	1.8	20000	9600
4.68	4	20000	5000

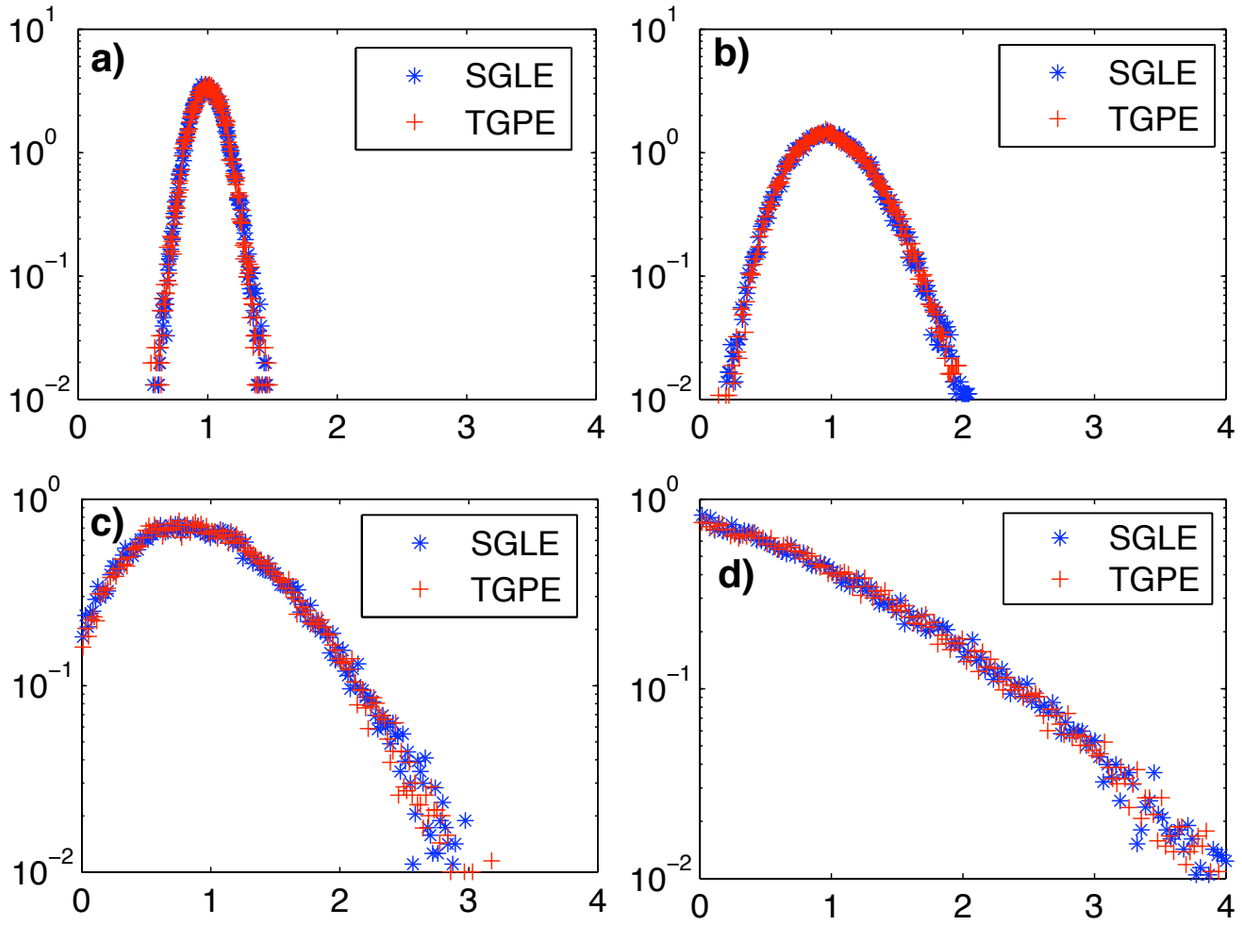

Density histograms

Condensation transition

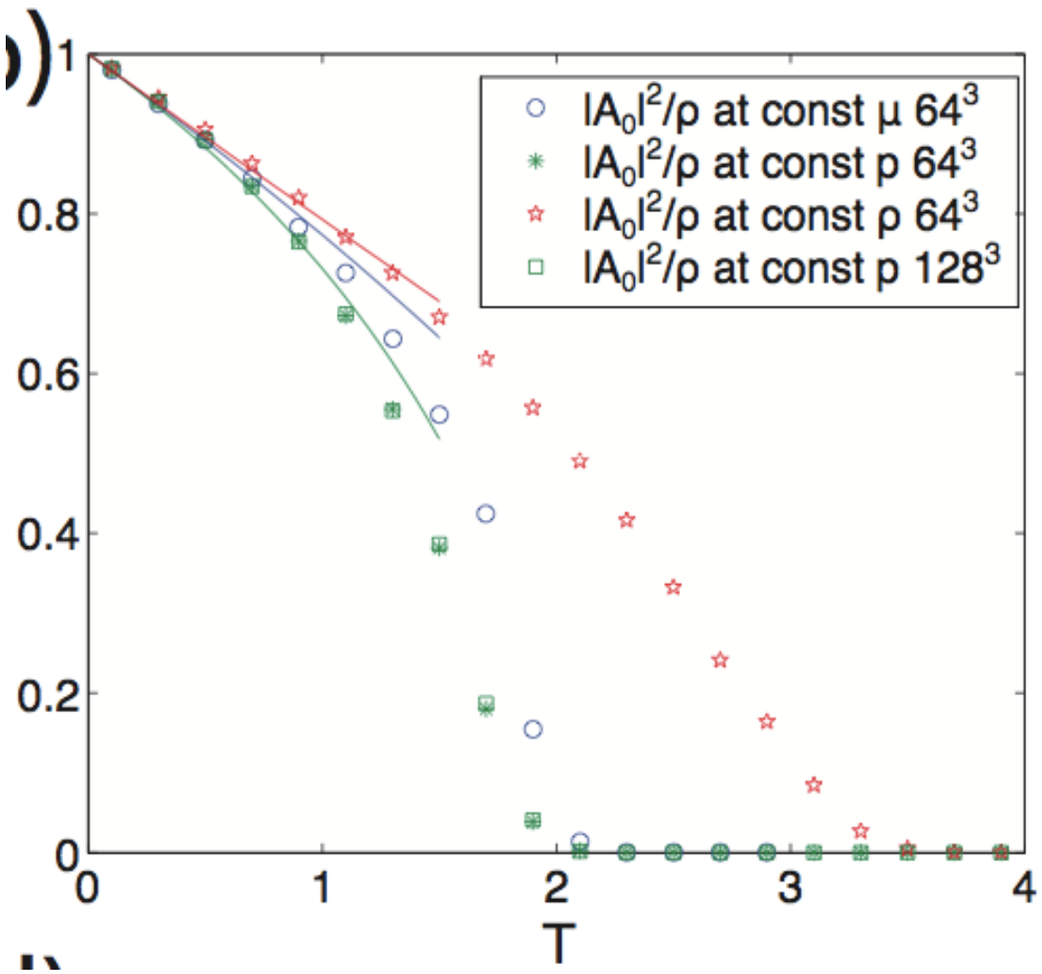

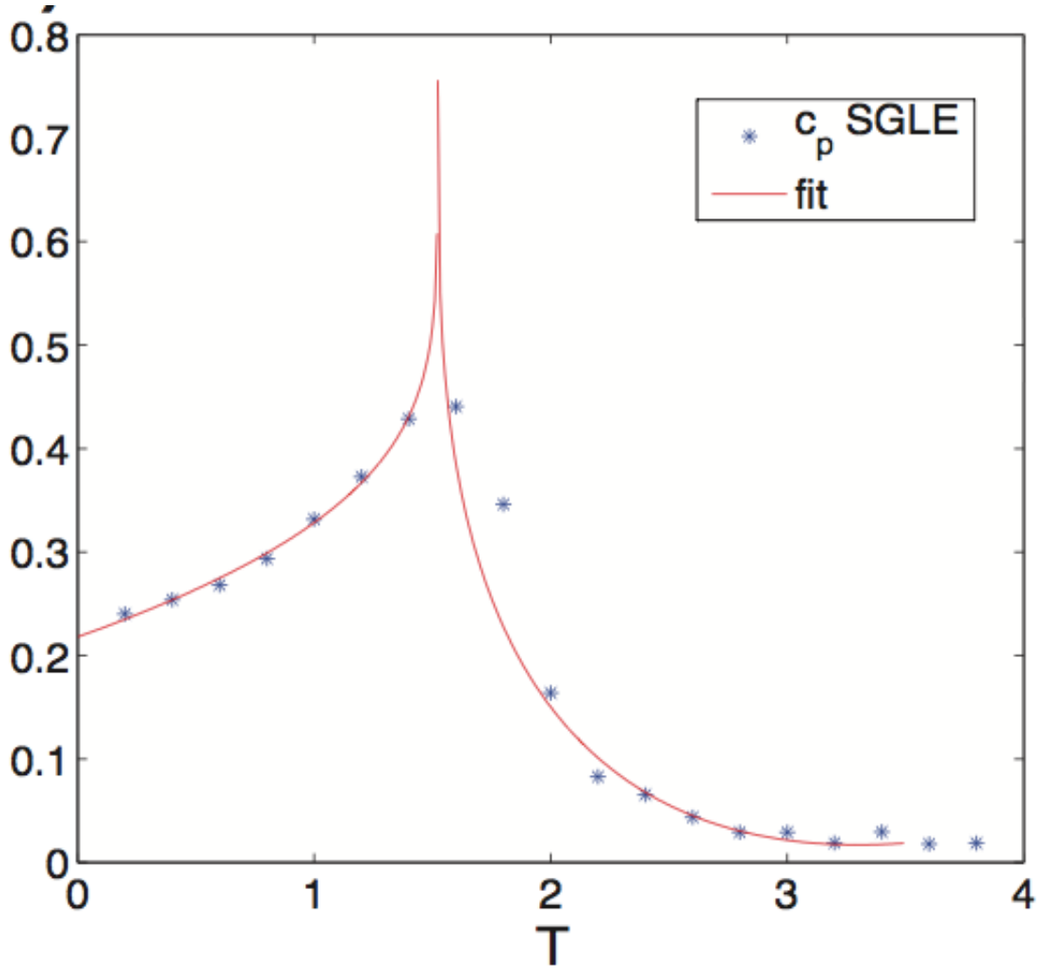

$\lambda - \phi^4 \quad (D = 3, n = 2)$

2D BKT transition

Vishwanath Shukla, Marc Brachet and Rahul Pandit

Turbulence in the two-dimensional Fourier-truncated Gross–Pitaevskii equation

New J. Phys. 15 113025 (2013)

Below transition

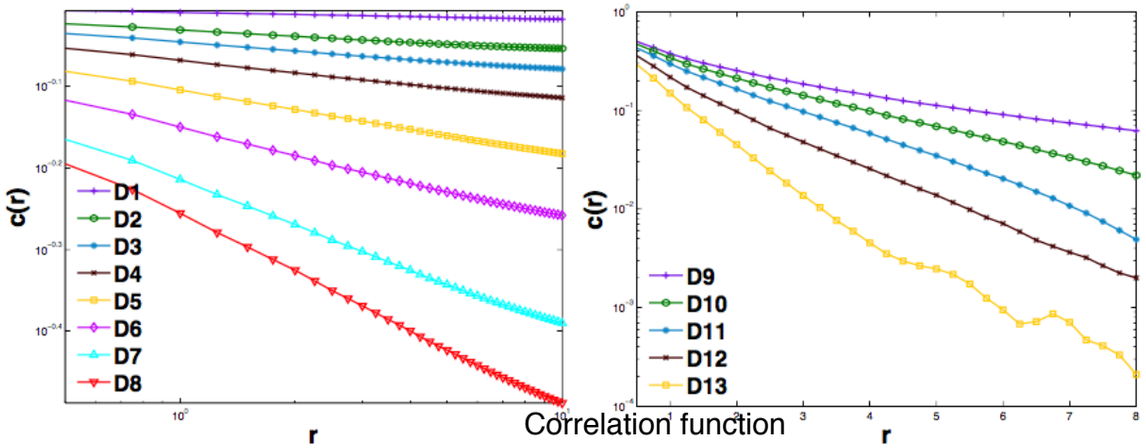

Above transition

Correlation function

[Left] Log-log plot of $c(r)$ vs. r ($E < E_{\mathrm{BKT}}$, $N_c = 128$); [Right] Semilog-y plot $c(r)$ vs. r ($E > E_{\mathrm{BKT}}$, $N_c = 128$).

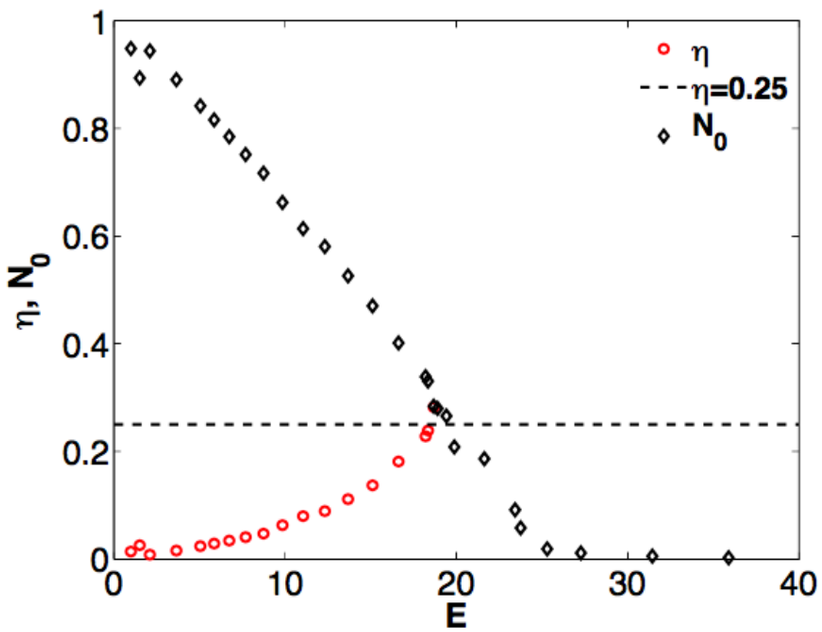

Condensate fraction
and
Power exponent

Dynamics of thermalization in the GPE

Kinetic energy spectrum

- $E_{kin\ tot}(k)$
- $E_{kin\ inc}(k)$
- $E_{kin\ comp}(k)$

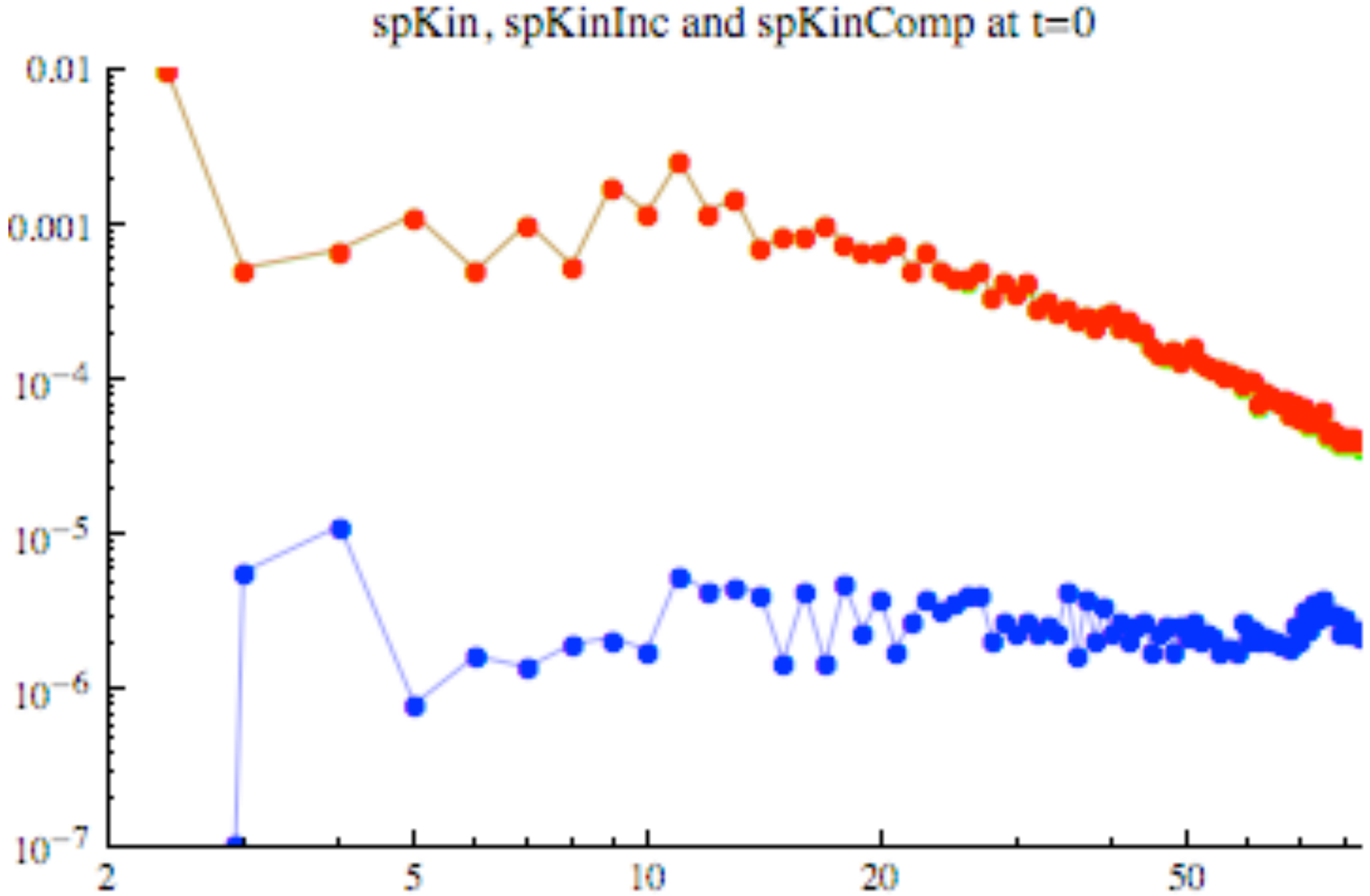

Taylor-Green vortex

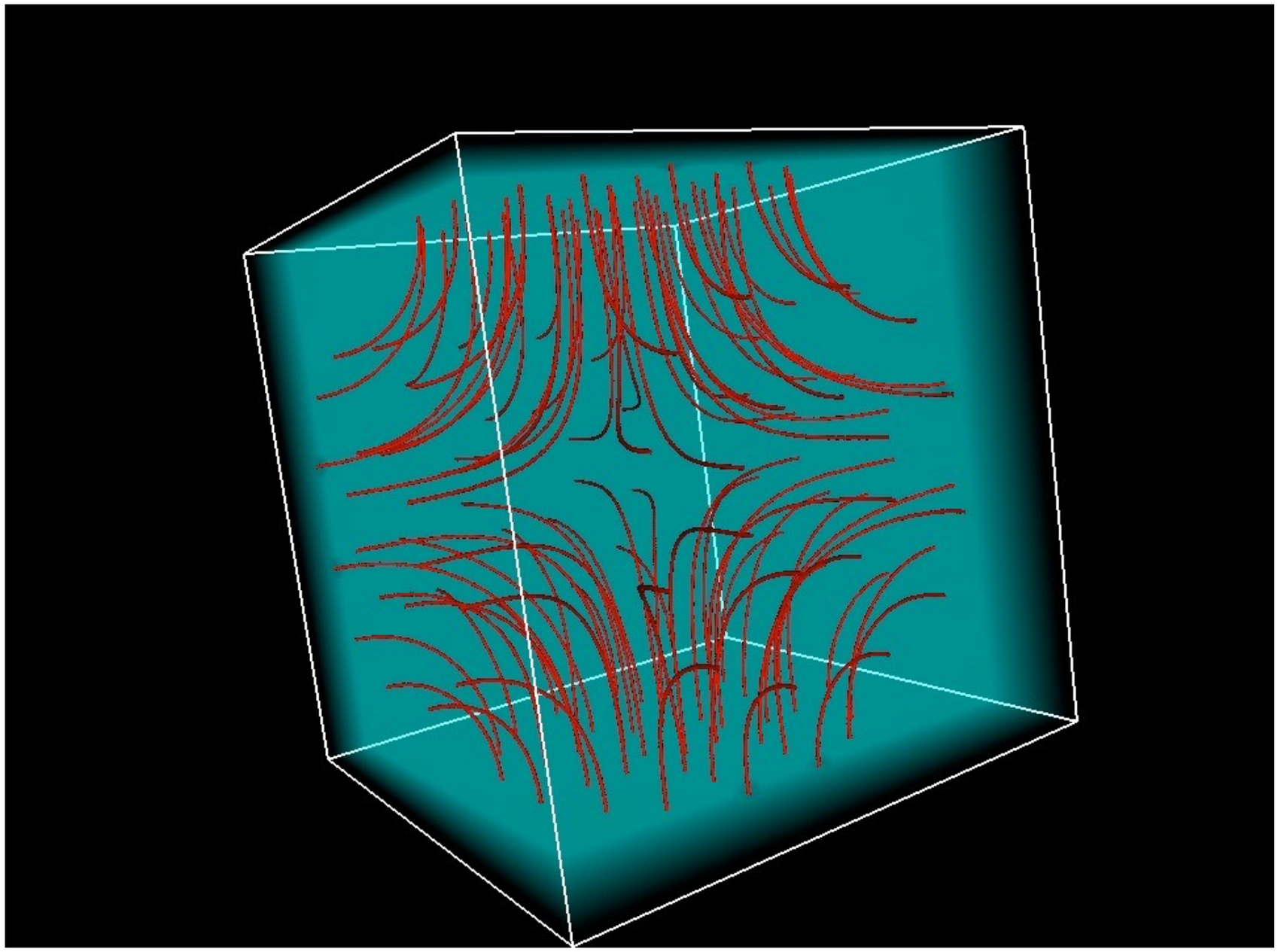

Taylor-Green vortex

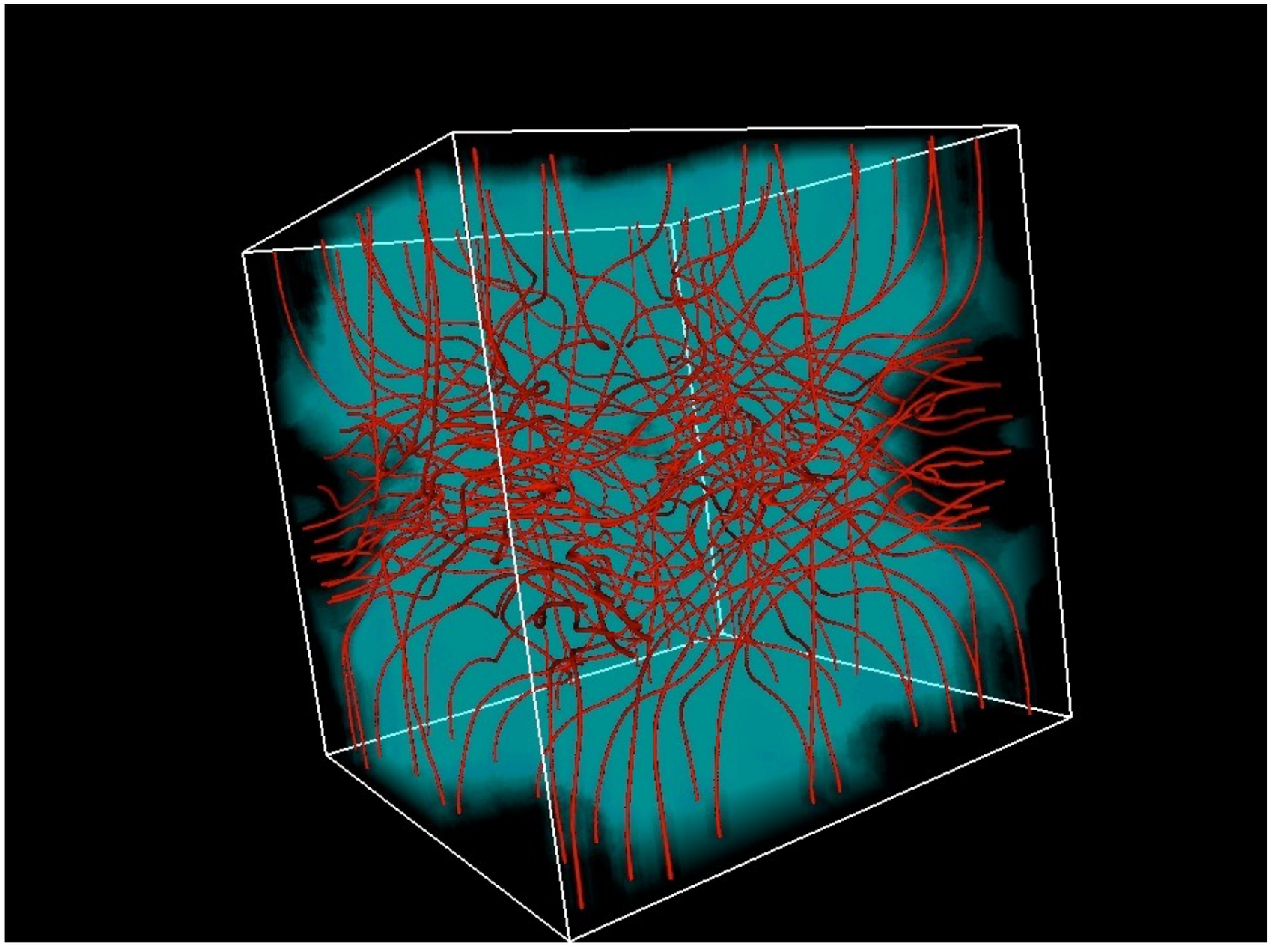

Taylor-Green vortex

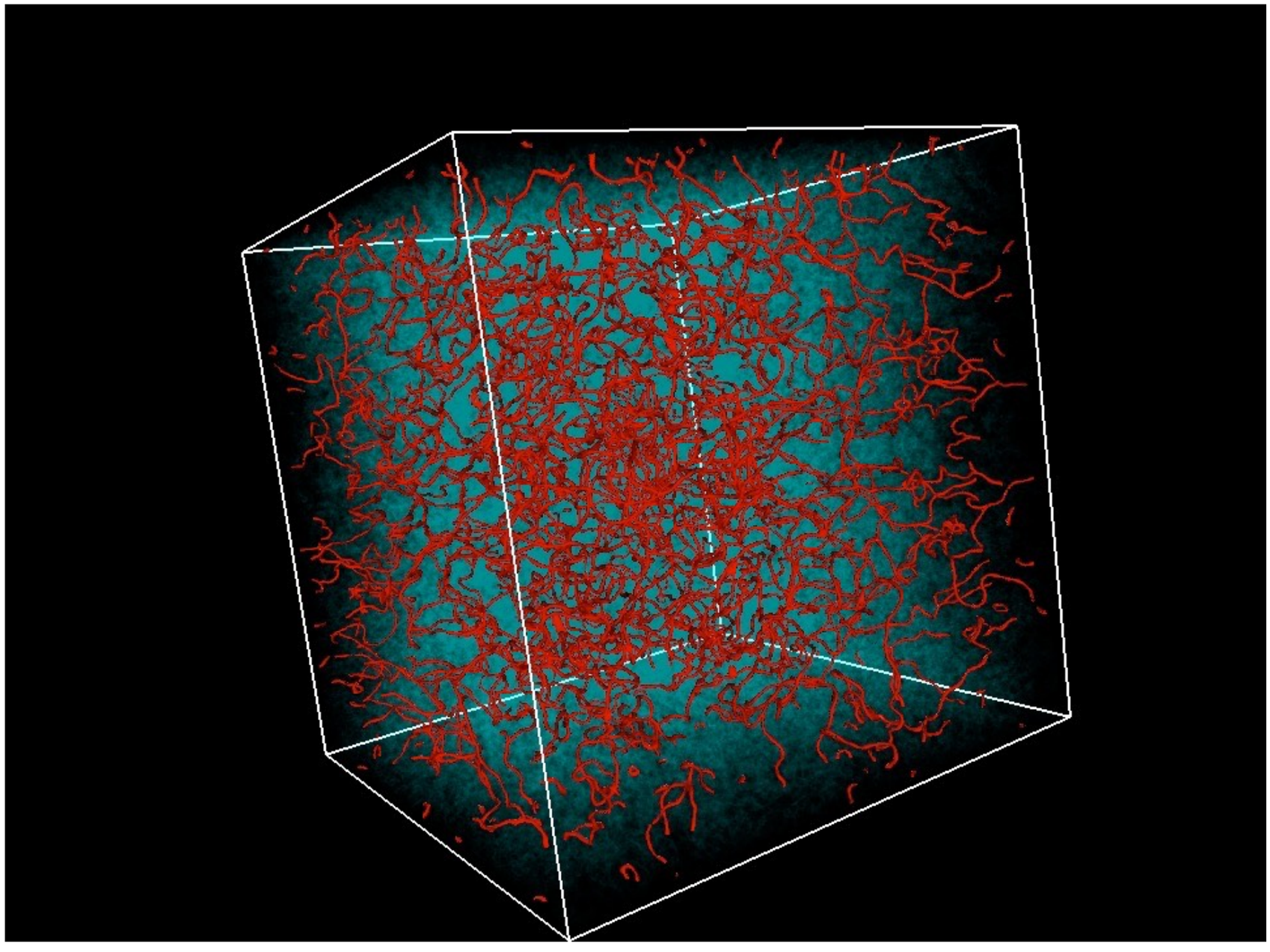

Taylor-Green vortex

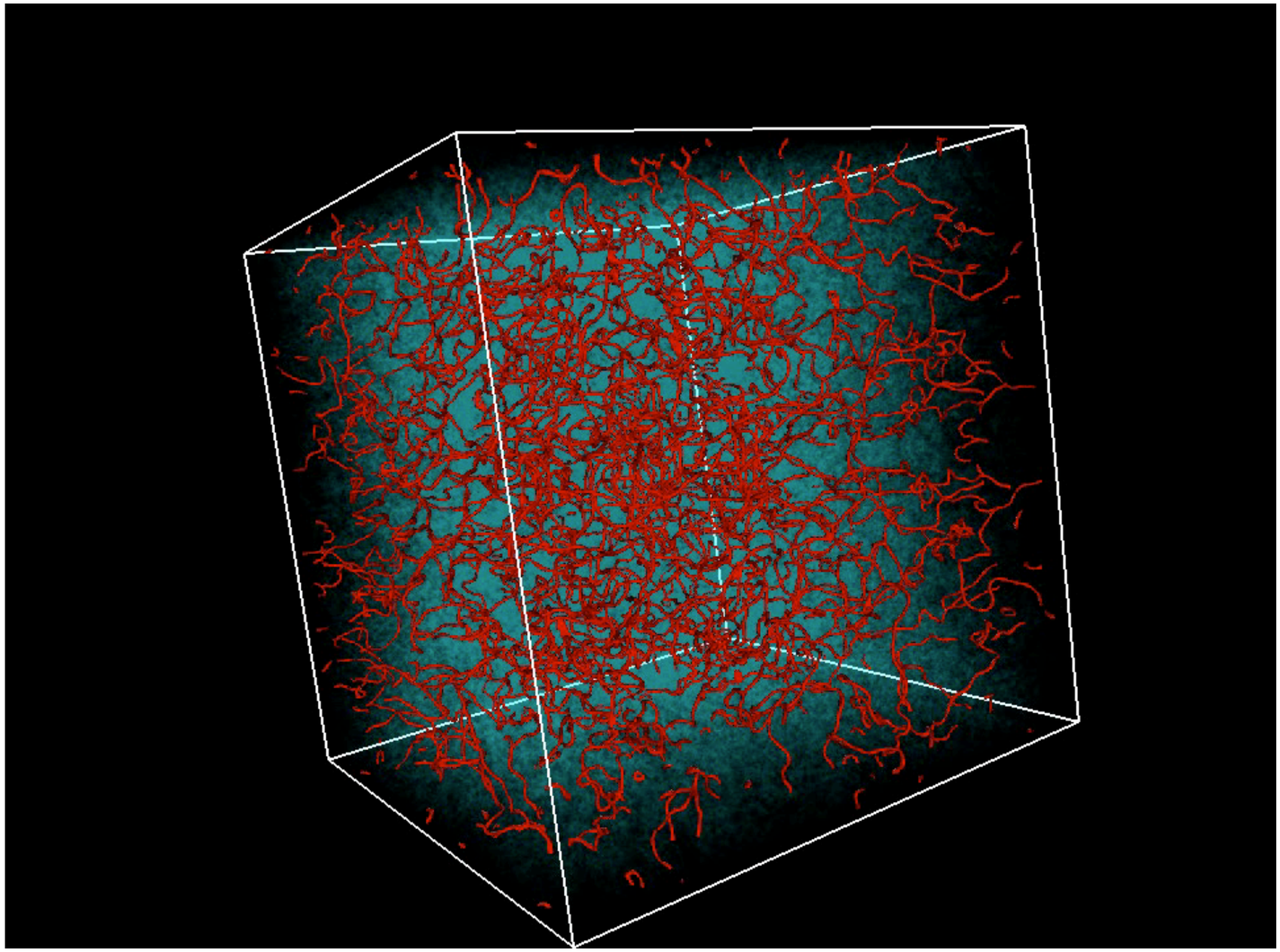

Dispersive "bottleneck" for thermalization of waves

Variable $\xi k_{\max}$ (ξ fixed, different resolutions)

Kinetic energy spectrum

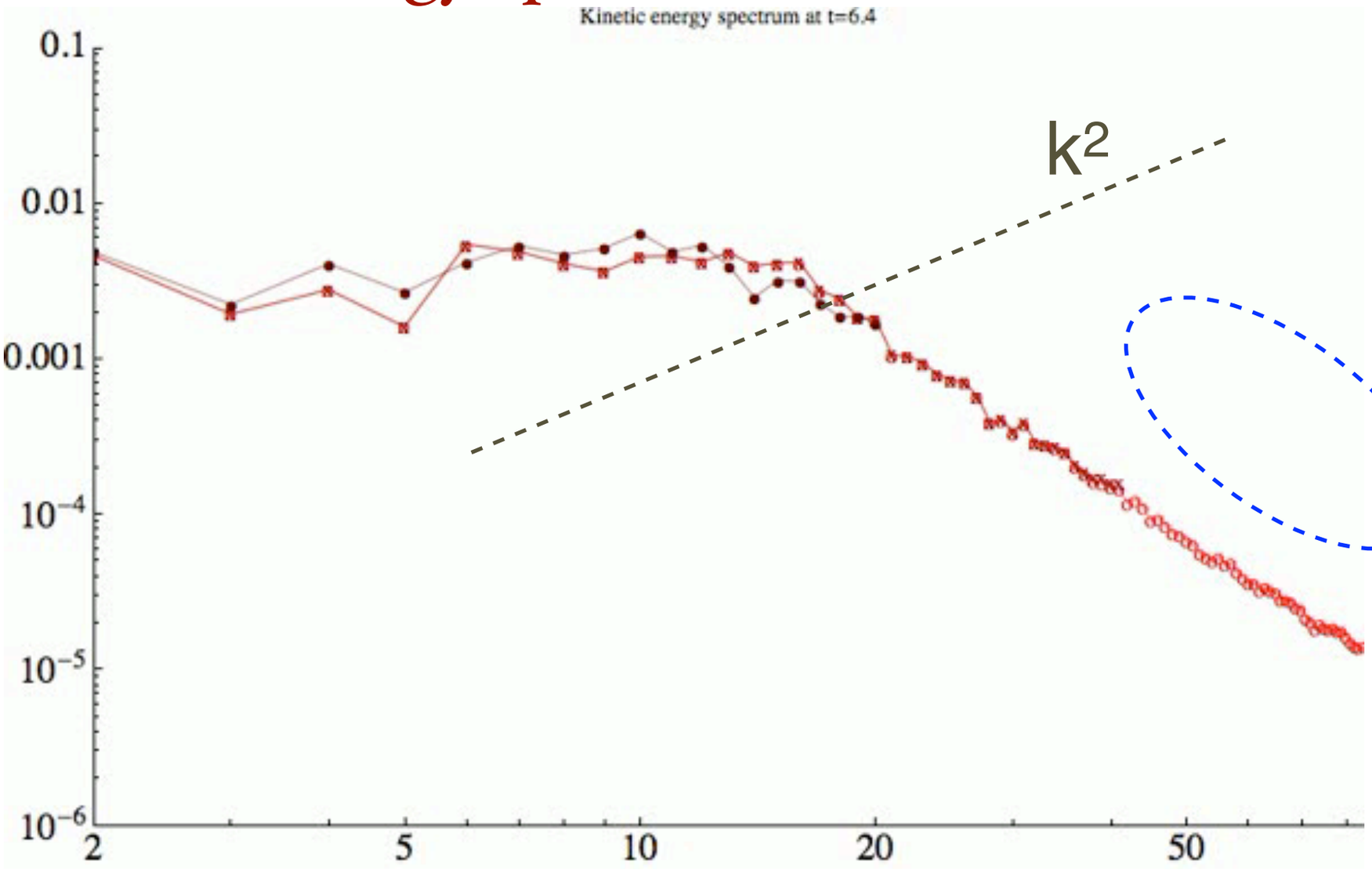

Partial thermalization starts

Spectral convergence

$k_{\max}$-independent bottleneck

see: Krstulovic and Brachet, Phys. Rev. Lett. 106, 115303 (2011)

Self truncation in 2D

Vishwanath Shukla, Marc Brachet and Rahul Pandit

Turbulence in the two-dimensional Fourier-truncated Gross–Pitaevskii equation

New J. Phys. 15 113025 (2013)

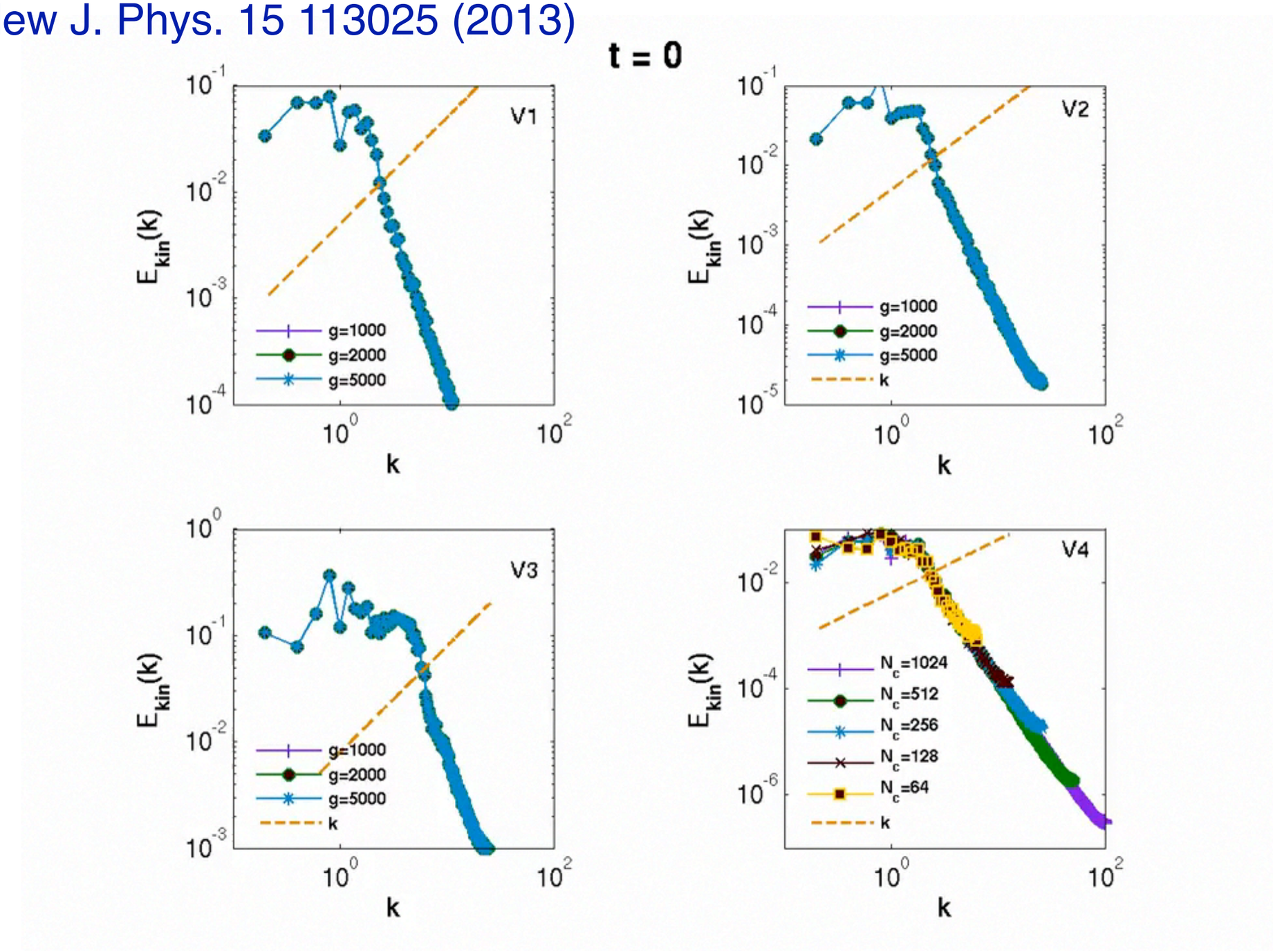

[Top Left] $k_0 = 5\Delta k$ and $\sigma = 2\Delta k$, [Top Right] $k_0 = 15\Delta k$ and $\sigma = 2\Delta k$, [Bottom Left] $k_0 = 35\Delta k$ and $\sigma = 5\Delta k$, and [Bottom Right] different Nc.

Dual cascade

- Dual cascade in helical quantum turbulence
- Initial Data: ABC flow
- GPE turbulent decay
- Evolutions of energies and helicity
- Evolution of spectra
- Kelvin waves and large scale structures

ABC initial data

As initial condition we use a superposition of $k = 1$ and $k = 2$ basic ABC flows: $\mathbf{v}_{\rm ABC} = \mathbf{v}^{(1)}_{\rm ABC} + \mathbf{v}^{(2)}_{\rm ABC}$, with

$$\mathbf{v}^{(k)}_{\rm ABC} = [B\cos(ky) + C\sin(kz)]\,\hat{x} + [C\cos(kz) + A\sin(kx)]\,\hat{y} + [A\cos(kx) + B\sin(ky)]\,\hat{z}, \quad (2)$$

and $(A, B, C) = (0.9, 1, 1.1)/\sqrt{3}$. The basic ABC flow is a 2π-periodic stationary solution of the Euler equation with maximal helicity. To build its quantum version we first take the flow with $B = C = 0$ and use Madelung transformation to obtain a wavefunction $\Psi^{x,y,z}_{A,k} = \exp\{i[A\sin(kx)\,m/\hbar]y + i[A\cos(kx)\,m/\hbar]z\}$, where $[a]$ stands for the nearest integer to a to enforce periodicity. The wavefunction of the quantum ABC flow is then obtained as $\Psi^{(k)}_{\rm ABC} = \Psi^{x,y,z}_{A,k} \times \Psi^{y,z,x}_{B,k} \times \Psi^{z,x,y}_{C,k}$. Finally, $\Psi_{\rm ABC} = \Psi^{(1)}_{\rm ABC} \times \Psi^{(2)}_{\rm ABC}$ corresponds to the initial flow $\mathbf{v}_{\rm ABC}$. In practice, to correctly set the initial density with defects along the vortex lines and to correct frustration errors arising from periodicity, following [24, 25] we first evolve $\Psi_{\rm ABC}$ using the advected real Guinzburg-Landau equation [31], whose stationary solutions are solutions of the GPE with minimal emission of acoustic energy.

2048^3 ABC initial data with 45000 quanta of helicity

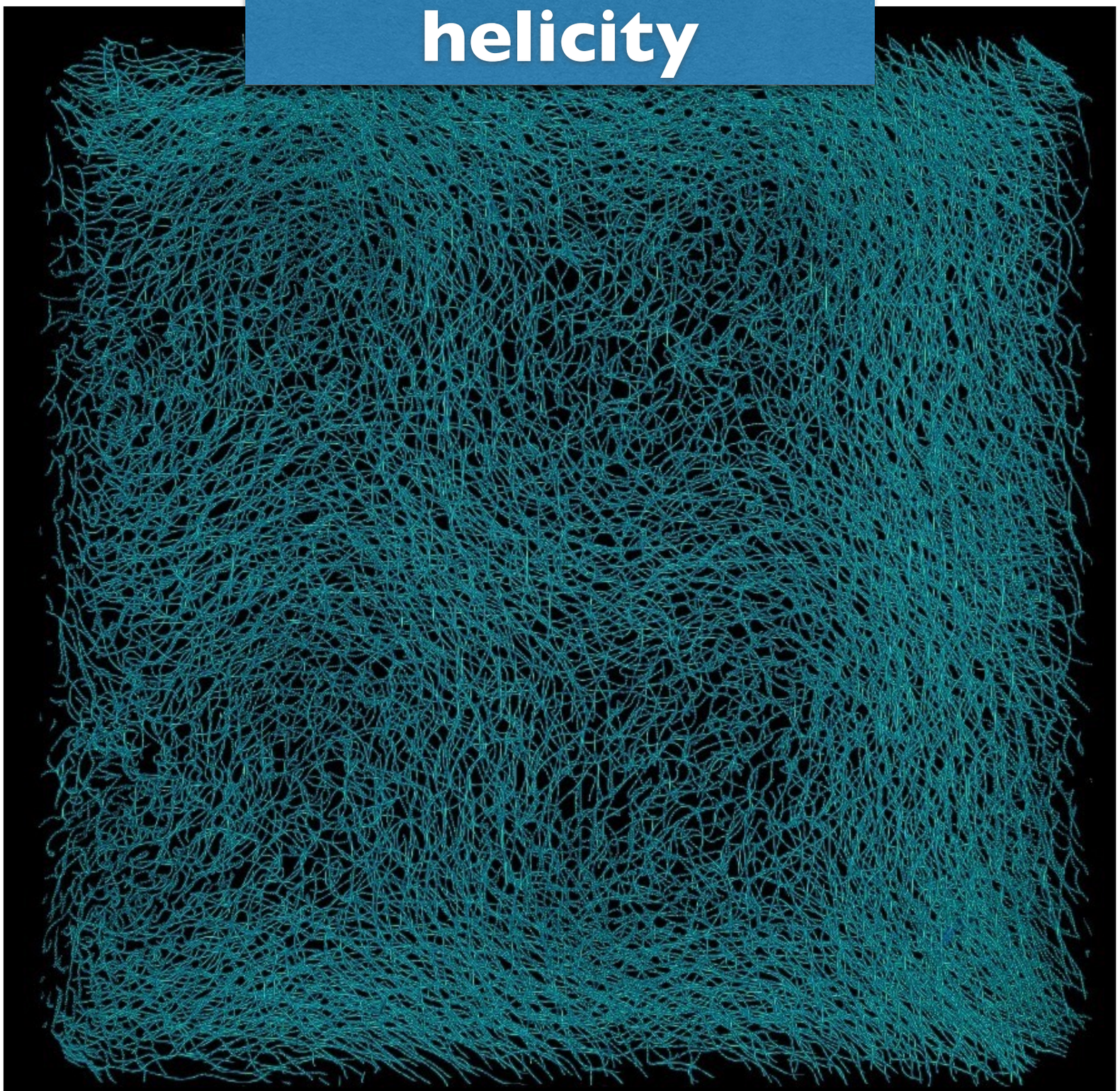

Time-evolution of energy and helicity

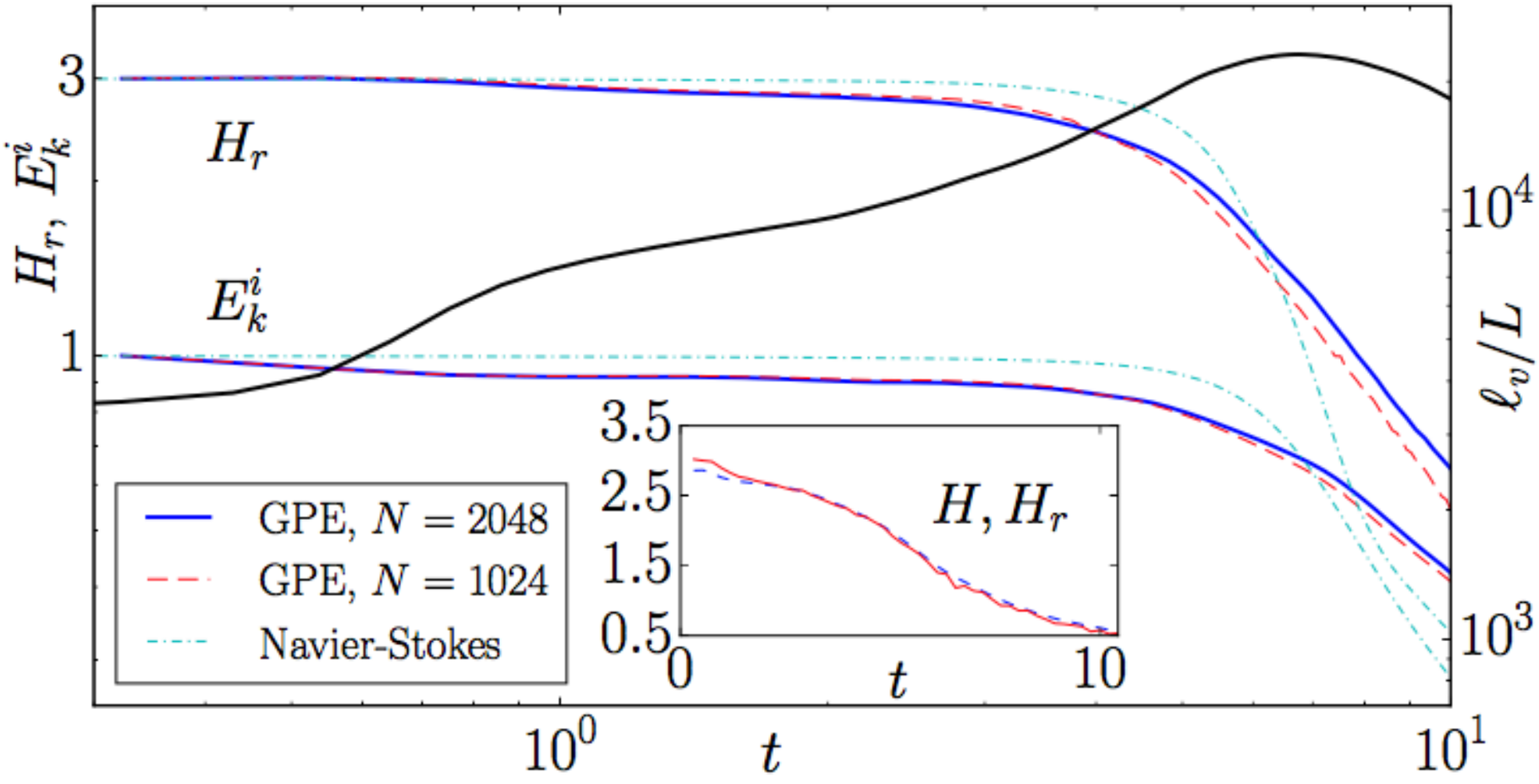

FIG. 1. Evolution of the incompressible energy E_k^i and of the regularized helicity H_r in the 1024^3 and 2048^3 GPE runs, and in Navier-Stokes. Note the early "inviscid" phase in which quantities are approximately constant. The solid black line shows the total vortex length in the 2048^3 GPE run. Inset: $H_r(t)$ (dashed blue line) and the nonregularized helicity $H(t)$ (solid red line) in the 2048^3 GPE run.

Dual energy-helicity cascade

$$E(k) \approx \epsilon^{2/3} k^{-5/3}, \qquad H(k) \approx \eta \epsilon^{-1/3} k^{-5/3}, \tag{3}$$

and with ϵ and η calculated directly using

$$\epsilon = -dE_k^i/dt, \quad \eta = -dH/dt, \tag{4}$$

A. Brissaud, U. Frisch, J. Leorat, M. Lesieur, and A. Mazure, Phys. Fluids **16**, 1366 (1973).

Dual cascade spectra

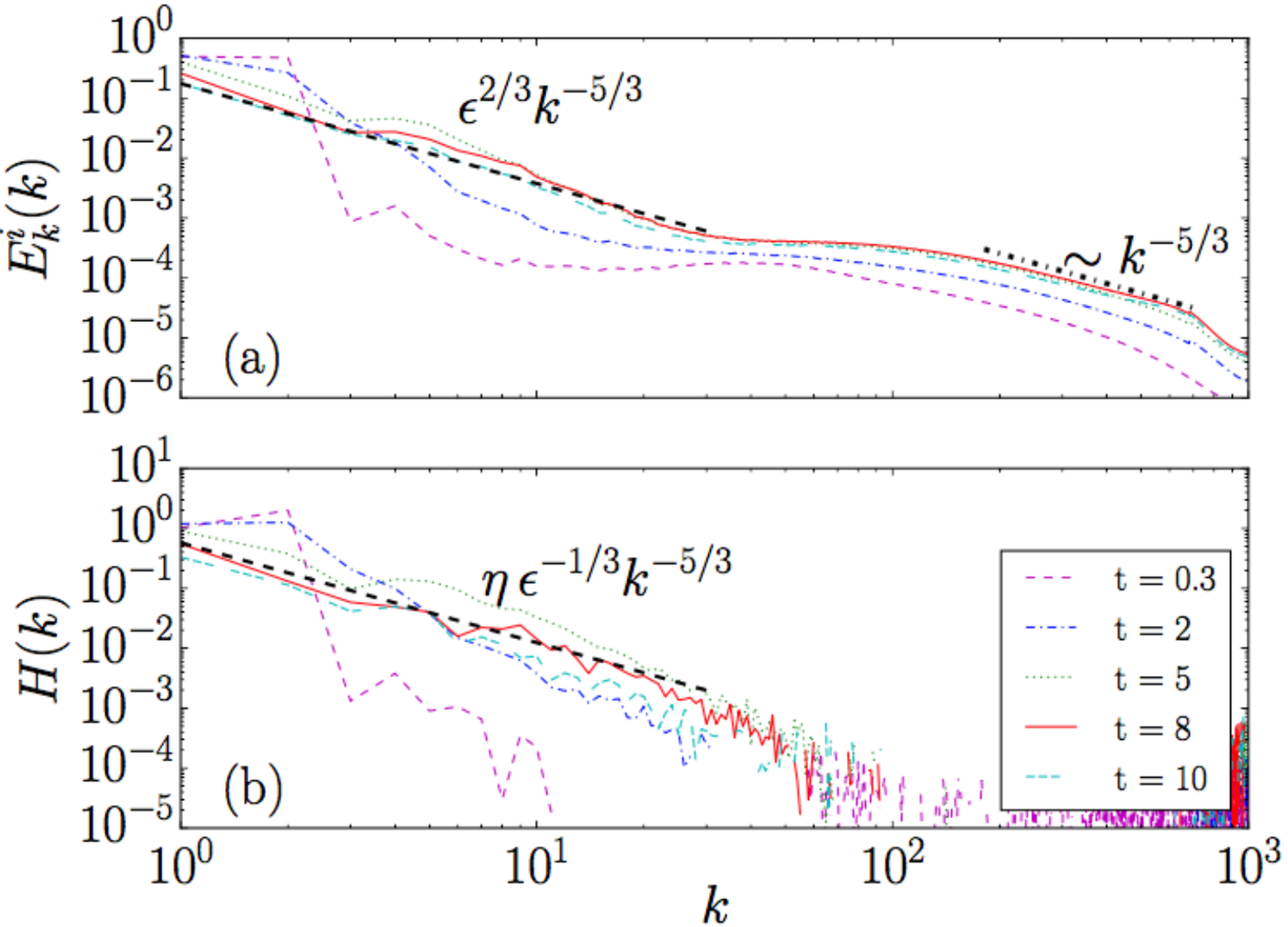

FIG. 2. Spectrum of the (a) incompressible kinetic energy, and (b) helicity in the 2048^3 GPE run. At large scales both follow a scaling compatible with a classical dual cascade (thick dashed lines). At scales smaller than the intervortex scale ($k_\ell \approx 80$) a second range compatible with a Kelvin wave cascade is observed in E_k^i (thick dash-dotted line). The helicity spectrum broadens in time indicating a direct transfer.

compensated helicity spectra

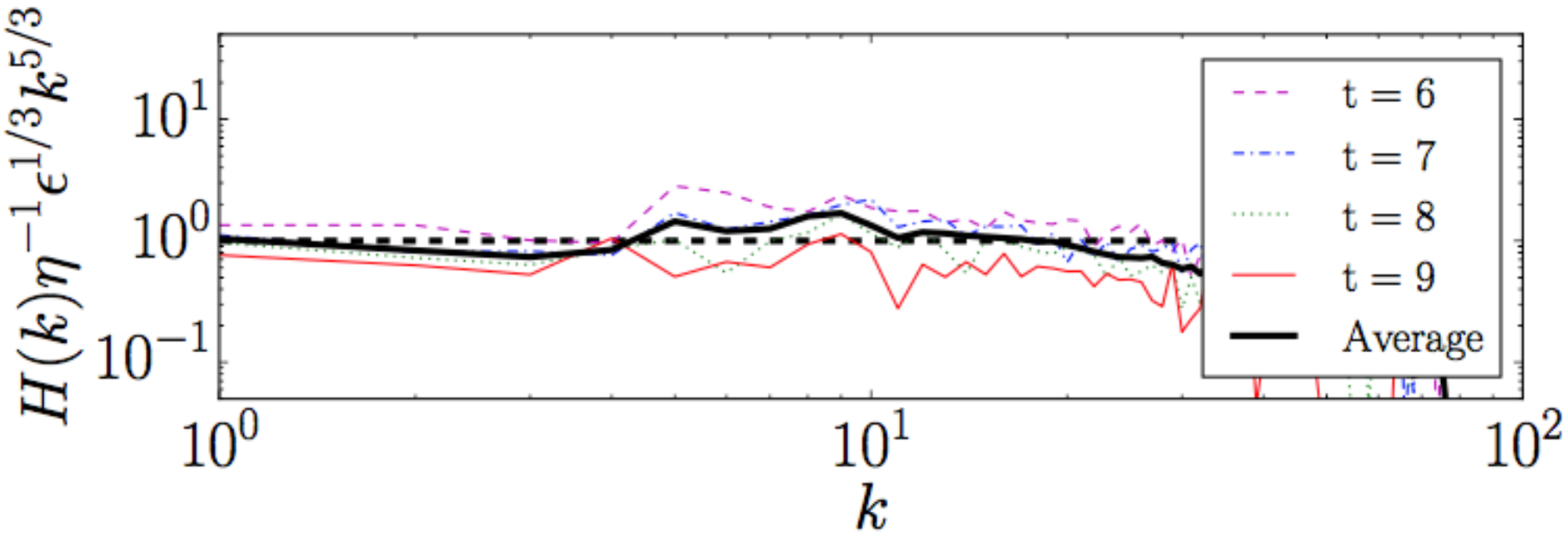

FIG. 3. Compensated helicity spectra in the 2048^3 GPE run. The spectrum is compatible with $\eta\epsilon^{-1/3}k^{-5/3}$ scaling. The time-averaged spectrum is also shown.

Kelvin waves

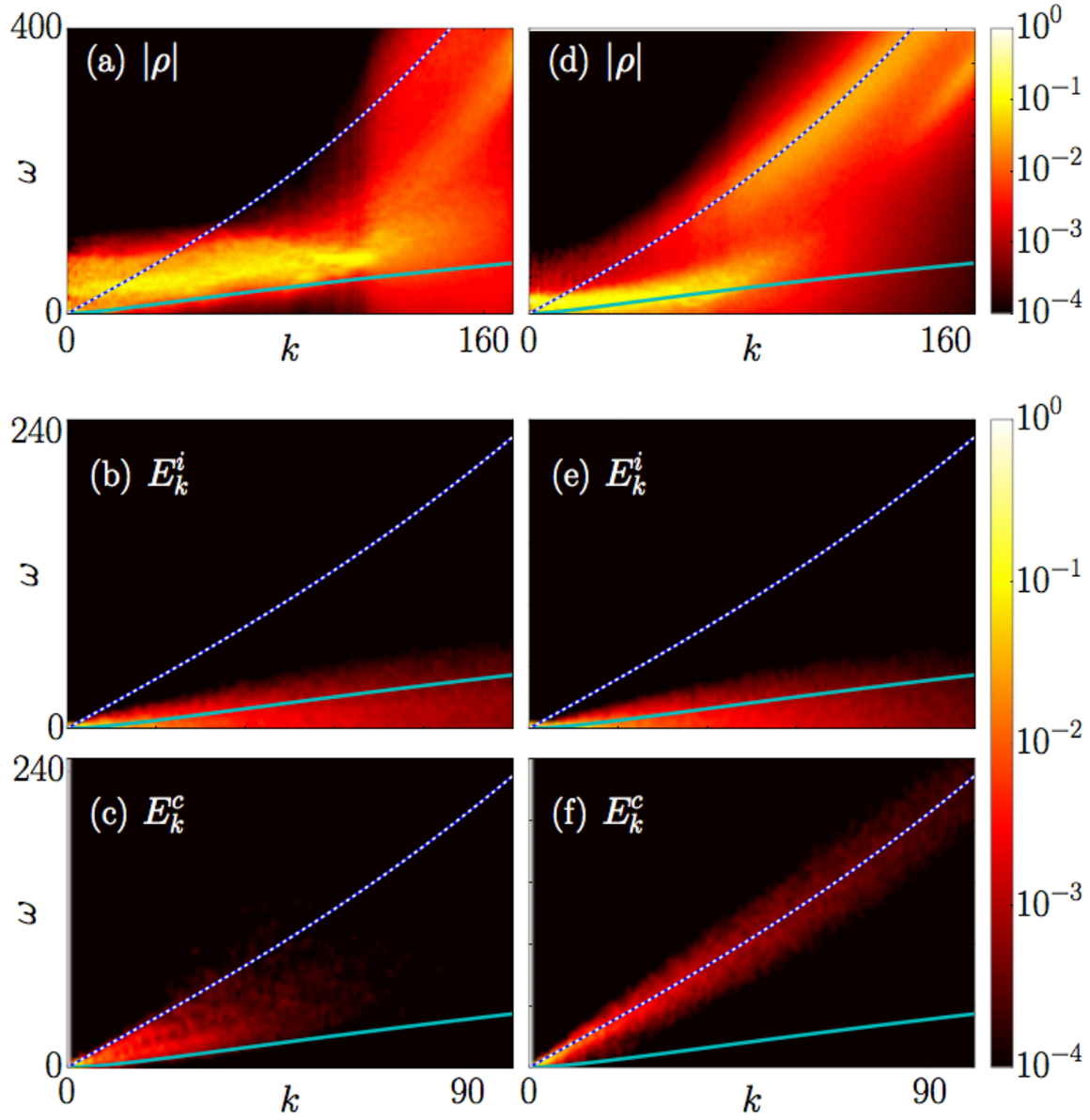

FIG. 4. Spatiotemporal power spectra for the 512^3 GPE run between $t = 0$ and 2 for (a) the mass density ρ, and zooms between $k = 0$ and 100 for (b) the incompressible and (c) compressible velocity. Same for late times ($t \in [8,10]$) are shown in (d), (e), and (f). The solid (green) curve is the dispersion relation of Kelvin waves, while the dotted (white) curve corresponds to sound waves.

Quantum tornados?

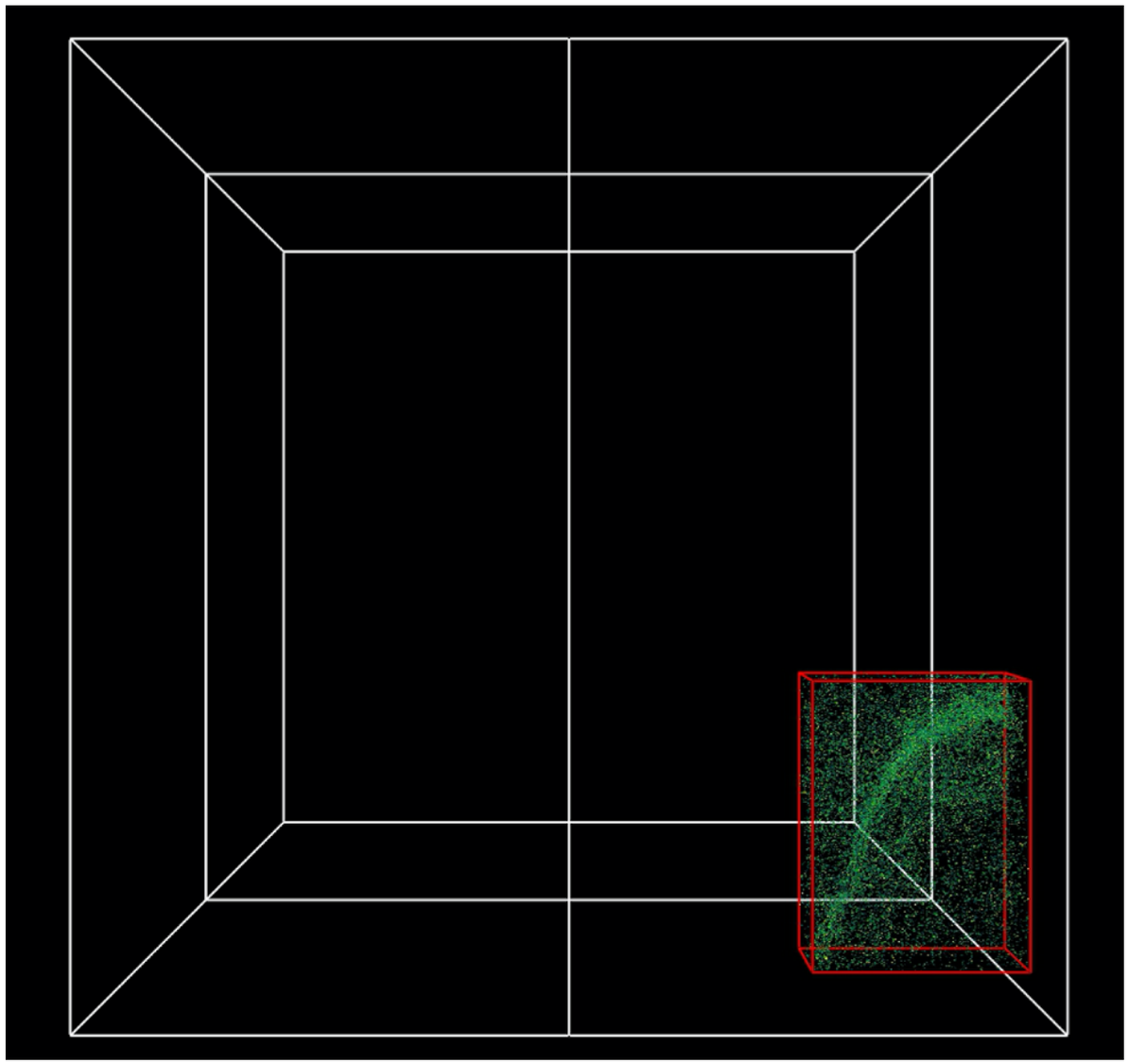

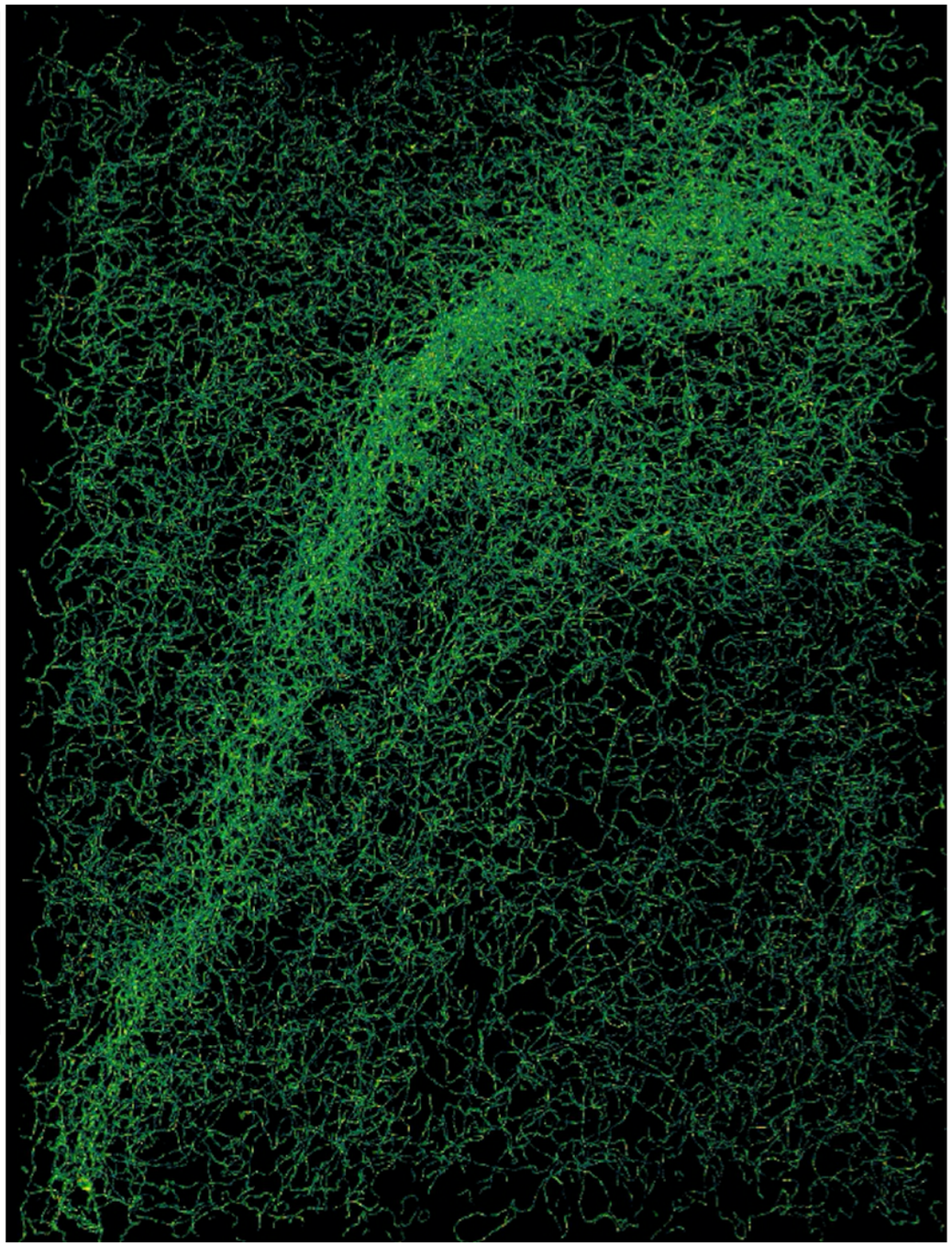

Link with classical vortex tubes

Helicity and the Călugăreanu invariant†

By H. K. Moffatt and Renzo L. Ricca‡
Department of Applied Mathematics and Theoretical Physics, Silver Street, Cambridge CB3 9EW, U.K.

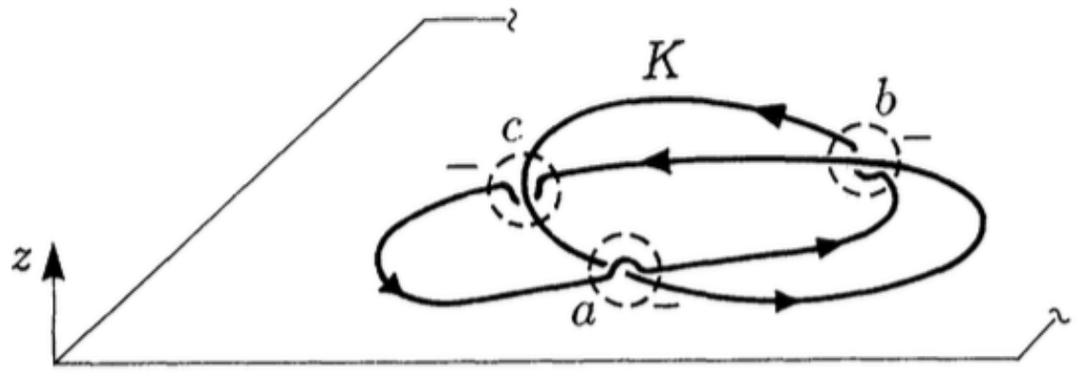

Figure 4

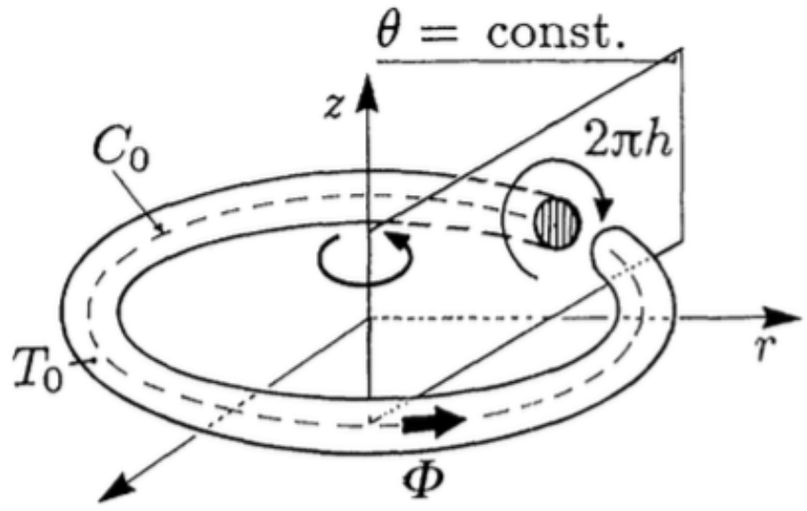

Figure 5

Link with classical vortex tubes

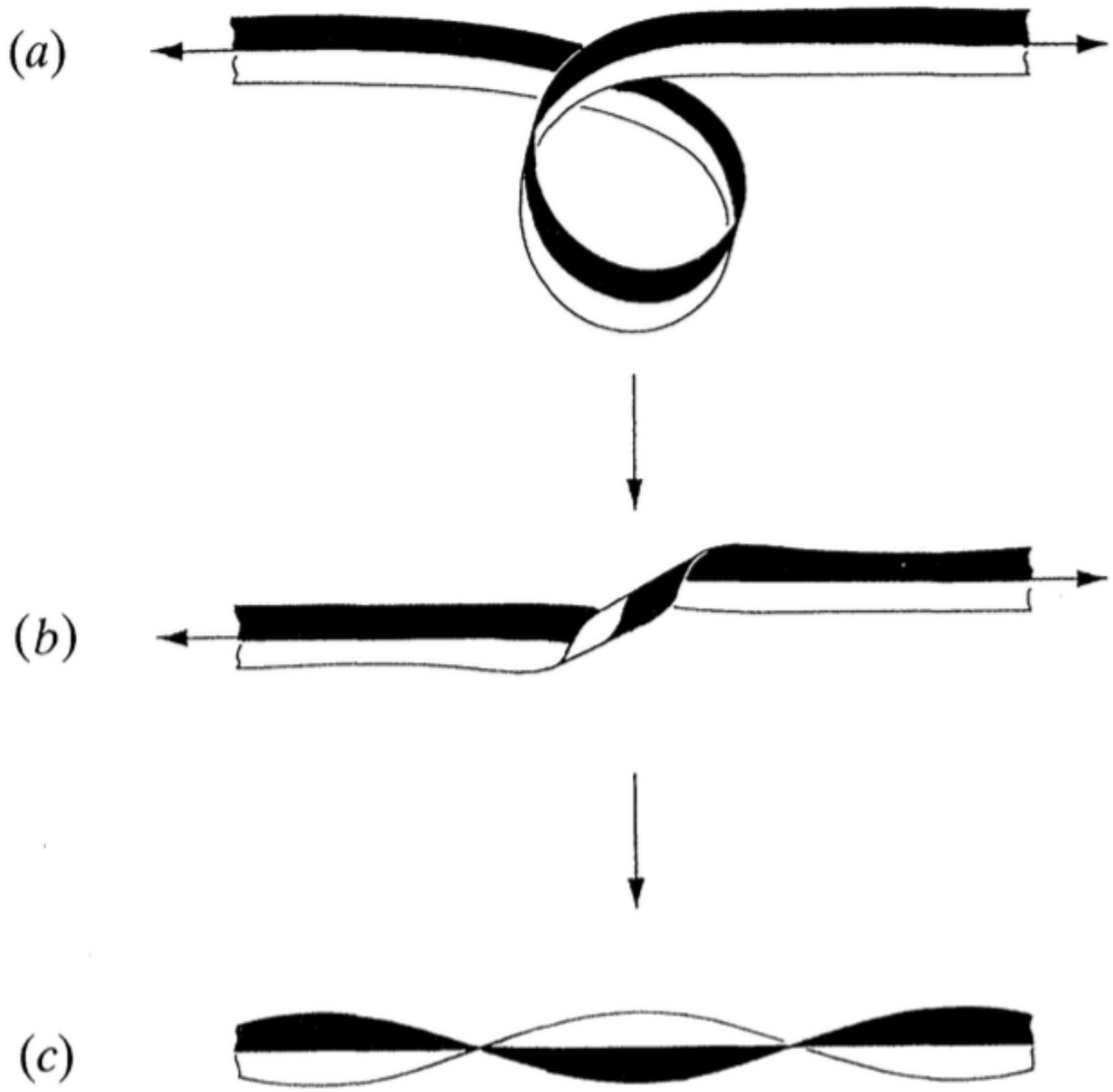

Figure 12. (*a*) Writhe, (*b*) torsion and (*c*) twist contributions of a ribbon to the Călugăreanu invariant. If a coiled ribbon is stretched so that its centre-line becomes straight, then the initial torsion of the centre-line is converted to the final twist of the ribbon about its centre-line.

Quantum tornados?

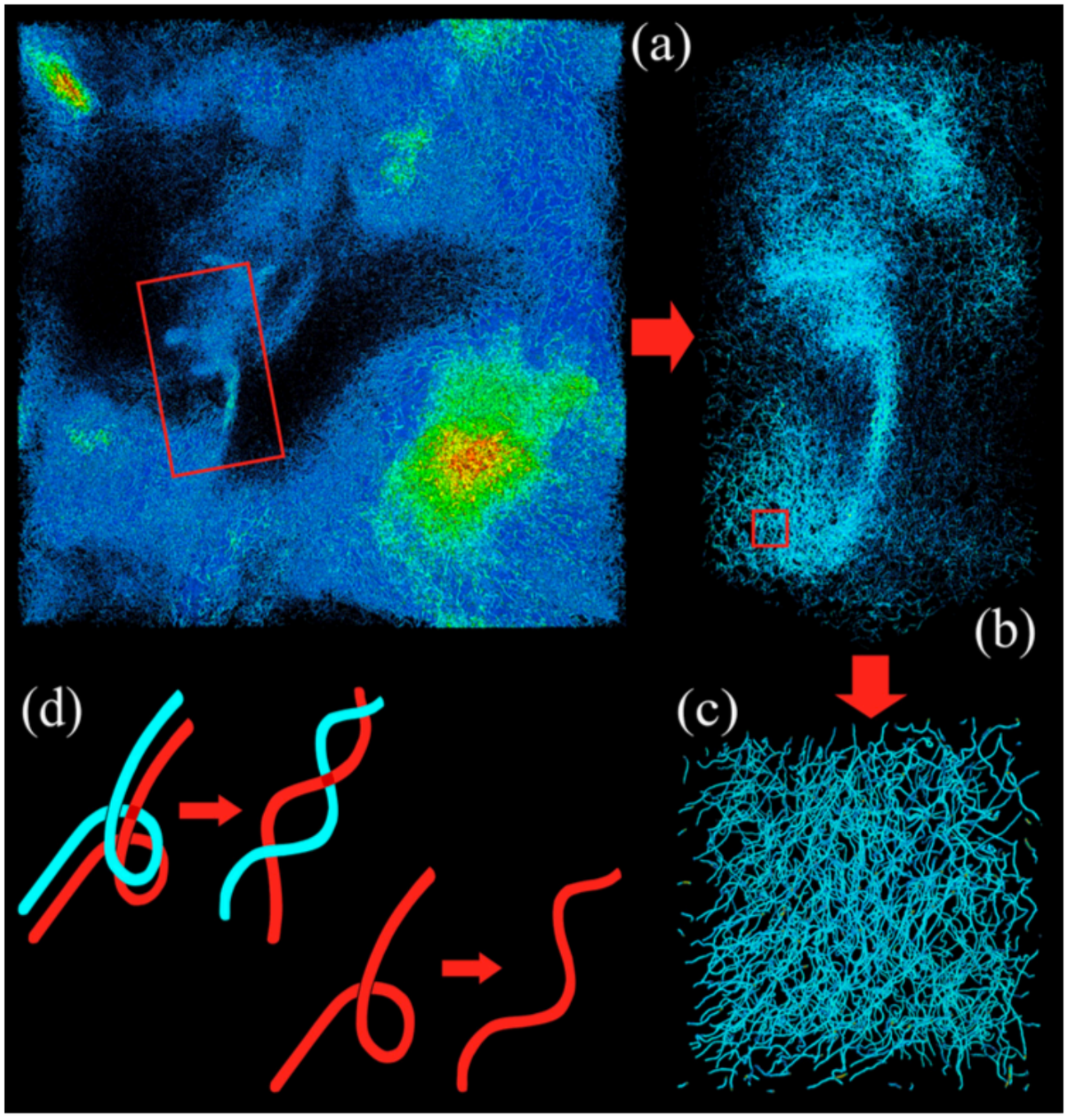

FIG. 5. Three-dimensional rendering of vortex lines at the onset of the decay in the 2048^4 GPE run of (a) a slice of the full box, and successive zooms in (b) and (c) into the regions indicated by the (red) rectangles. (d) Sketch of the transfer of helicity from writhe to twist in a bundle of vortices, and for an individual vortex.

Polarization of vortex bundles and density correlations

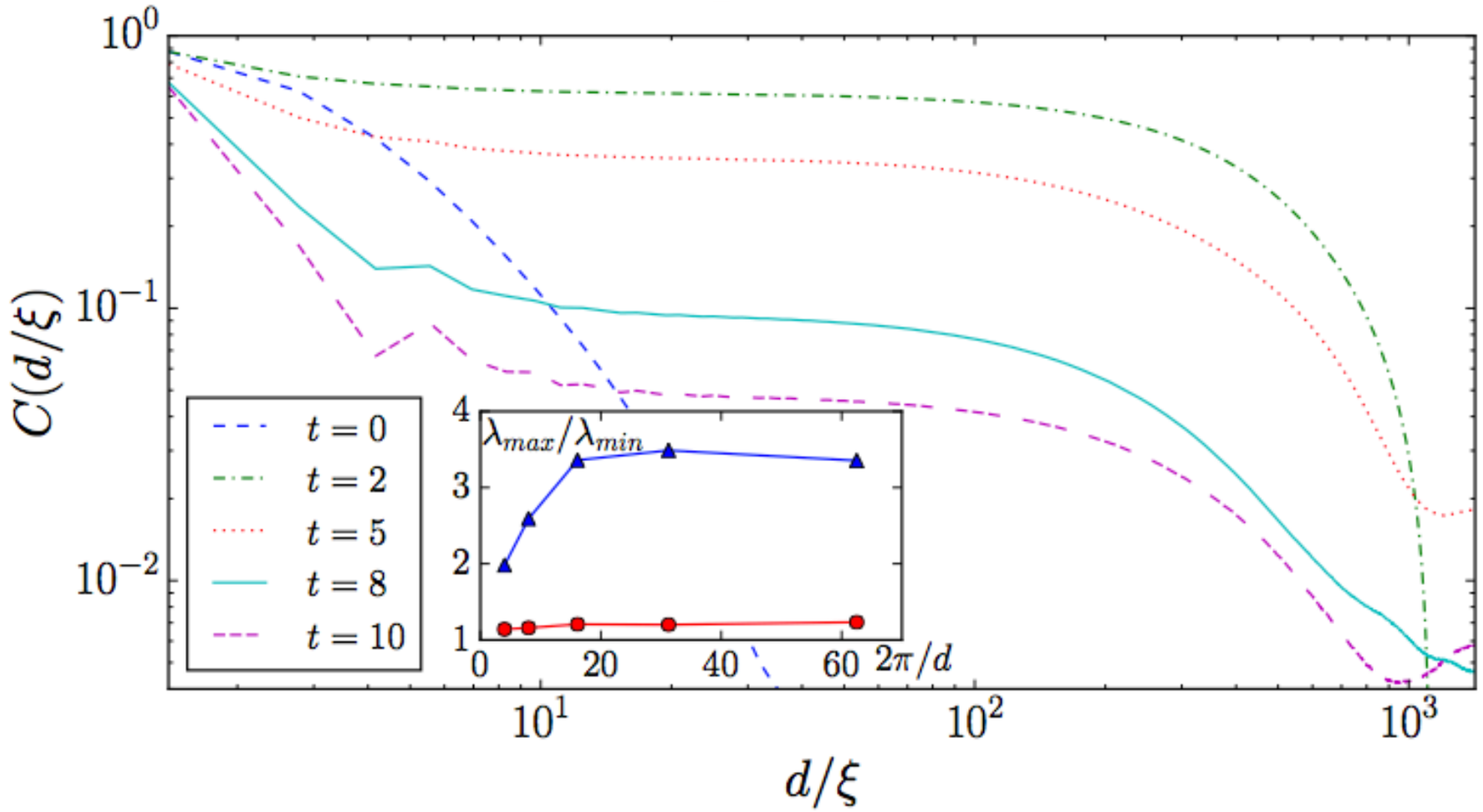

FIG. 6. Correlation function of ρ in the 2048^3 GPE run. At $t = 0$ it decays rapidly in units of the healing length ξ, but then quickly develops long-range correlations. Inset: Ratio of eigenvalues $\lambda_{\rm max}/\lambda_{\rm min}$ as a function of $2\pi/d$, with d the size of the box used for the average (blue triangles: regions with structures; red triangles: regions of quiescence).

Quantitative estimation of effective viscosity in quantum turbulence

With: Vishwanath Shukla, Pablo D. Mininni, Giorgio Krstulovic, Patricio Clark di Leoni

- PHYSICAL REVIEW A 99, 043605 (2019)

- High resolution numerical simulations of the Gross-Pitaevskii equation (GPE) in the Taylor-Green geometry.

- Presence of both a Kolmogorov scaling range for scales larger than the intervortex scale l, and a second inertial range for scales smaller than l.

- Finite temperature effects using thermal states, and evolving a combination of these thermal states with the Taylor-Green initial conditions using the GPE.

- Mean free path determined by spectral broadening of the Bogoliubov dispersion relation used to quantify the effective viscosity as a function of the temperature. To further calibrate this estimations of viscosity we perform low Reynolds number simulations of the Navier-Stokes equations.

Time evolution at T=0

Incompressible kinetic Energy

Vortex Length

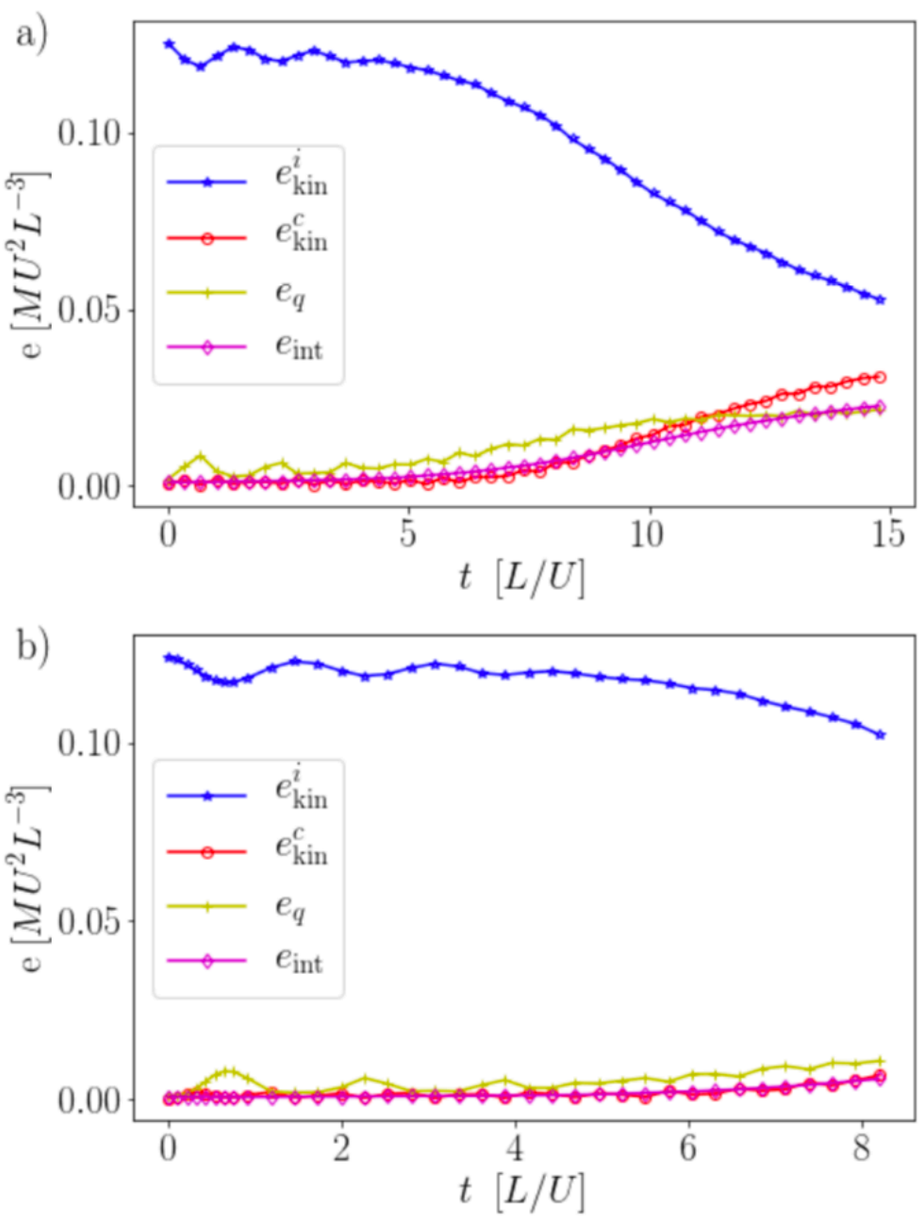

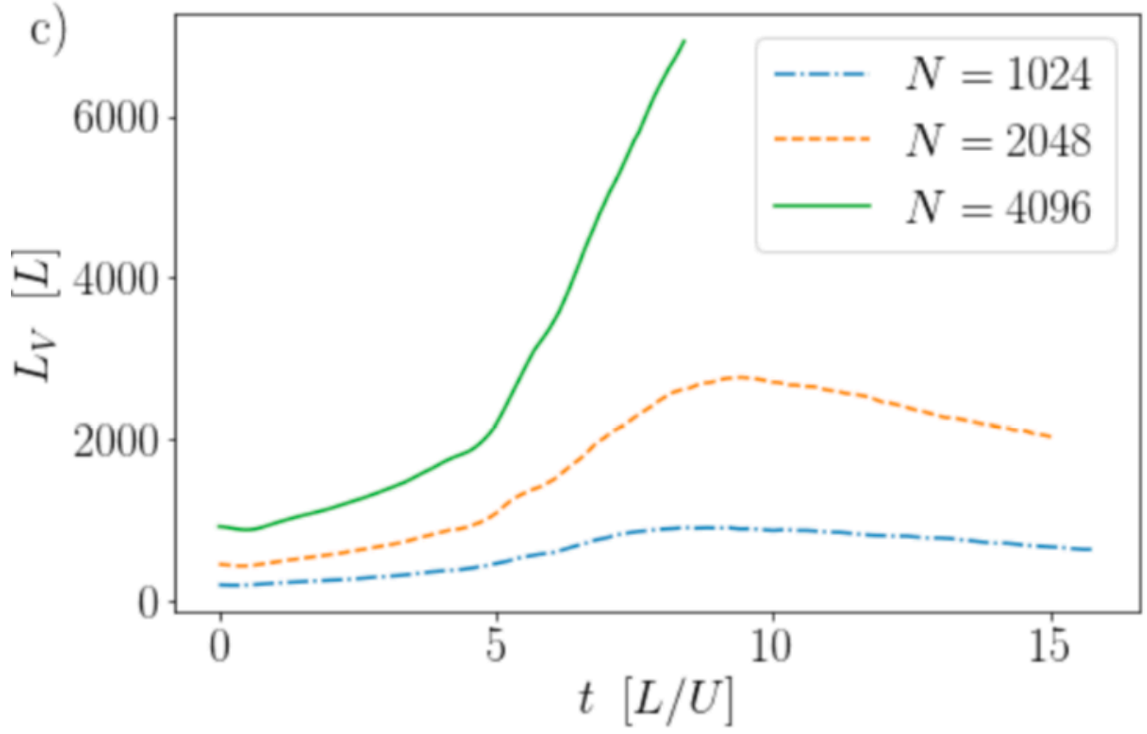

FIG. 1: *(Color online)* Time evolution of the different energy components at zero temperature in (a) a 3D simulation with $N = 2048$ grid points in each spatial direction, and (b) with $N = 4096$ grid points in each direction. Both DNSs have $\xi k_{\rm max} = 2.5$. (c) Time evolution of the total vortex line length L in simulations at different spatial resolutions.

Inc. kin. Energy Spectra

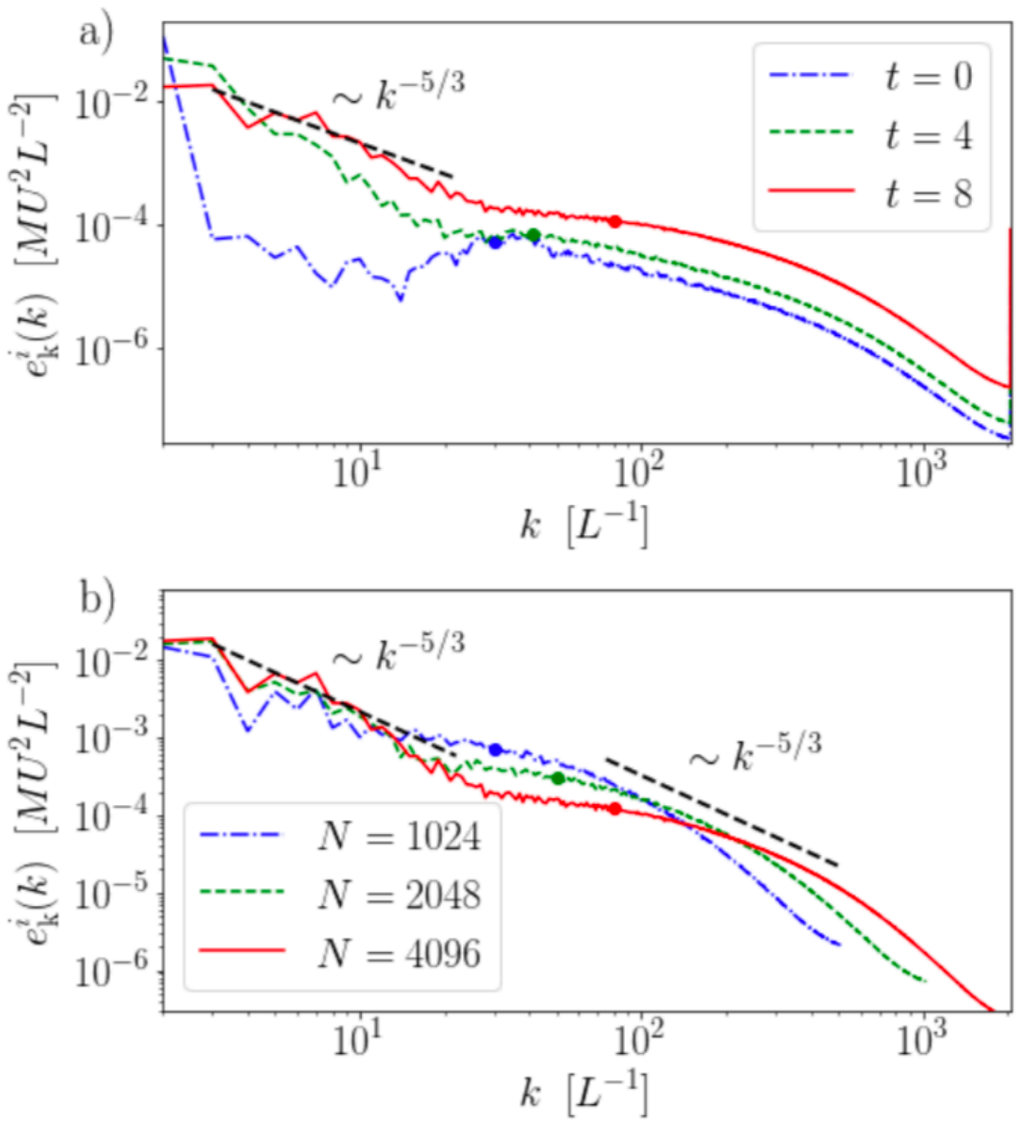

(a) Incompressible kinetic energy spectra at zero temperature, at different times for the N = 4096 simulation. b) Spectra at t = 8 for three DNSs at different spatial resolution. In both panels, the circular marks indicate the mean intervortex wavenumber.

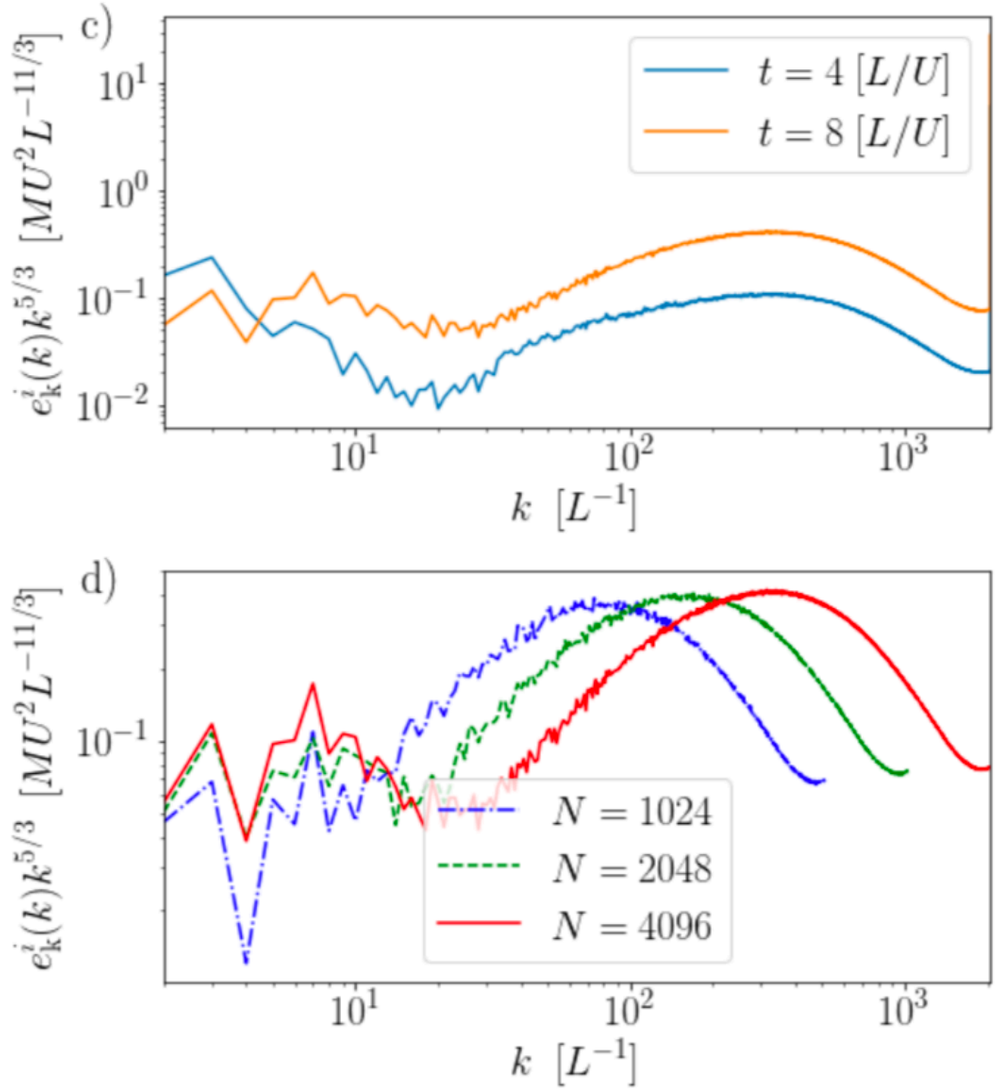

Note the emergence of a second intertial range, after a bottleneck, for scales smaler than the intervortex scale. (c) and (d) show the spectra from panel (a) and (b), but compensated by Kolmogorov scaling.

Compensated inc Ekin

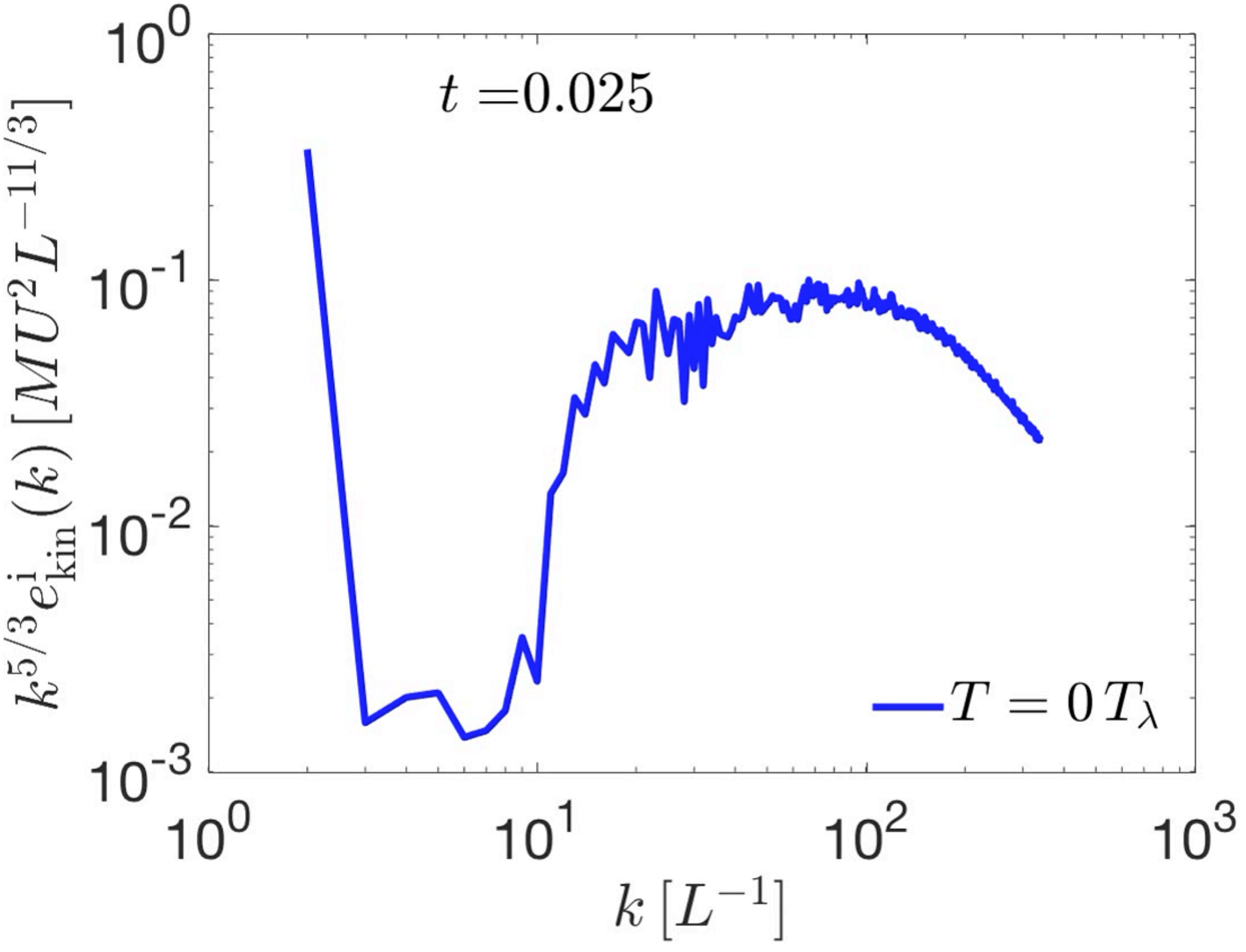

3D rendering T=0

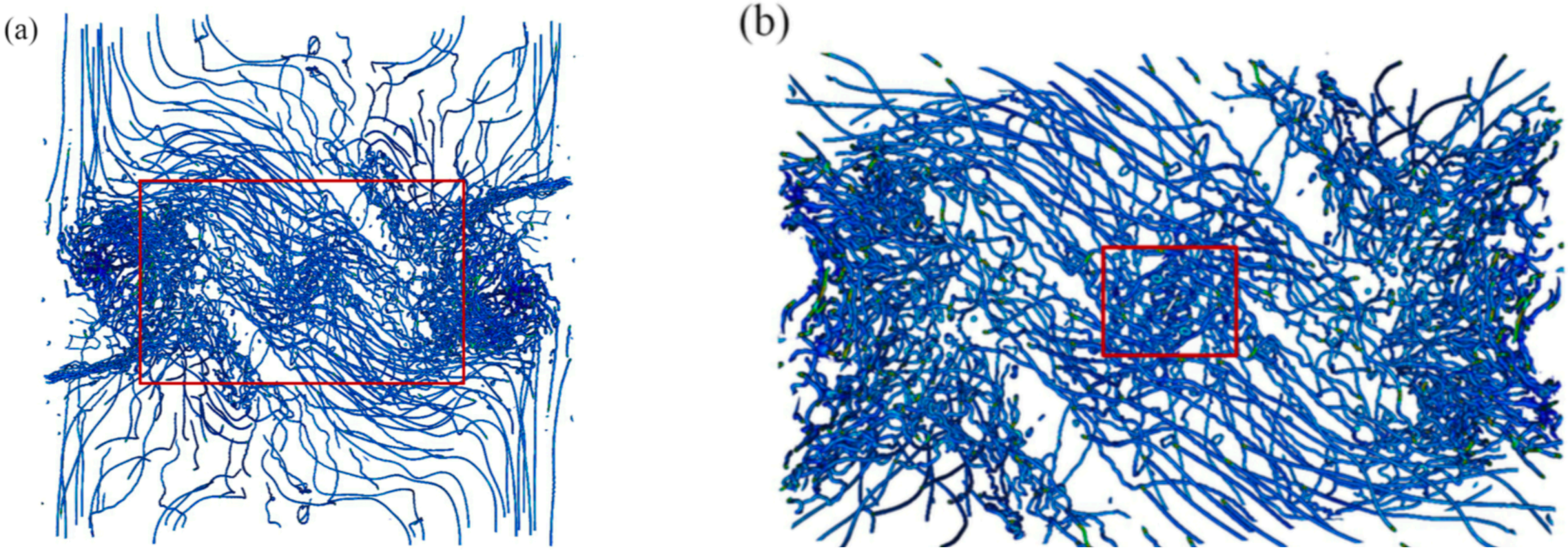

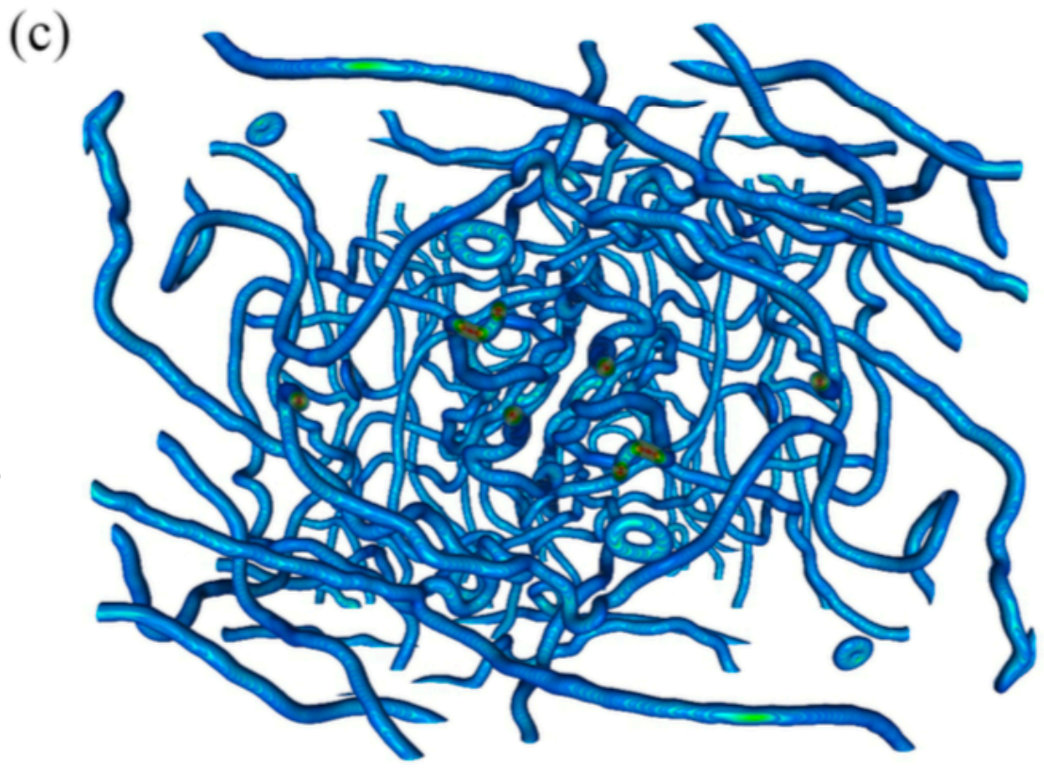

FIG. 3: *(Color online)* Three-dimensional renderings of vortex lines at the onset of the decay in the 4096^4 GPE run. (a) The full impermeable box. The (red) box indicates the region shown in panel (b), which shows a zoom into a region of the domain with large shear of the vortex lines. Again, the (red) box in this panel indicates the region zoomed into in panel (c). Note in the latter panel the tangle of vortices, the many links between vortices, and the helical deformations of individual vortices along the vortex line. Visualizations were prepared using the software VAPOR [53].

Energy dissipation at finite Temperature

$$\xi k_{max} = 2.5$$

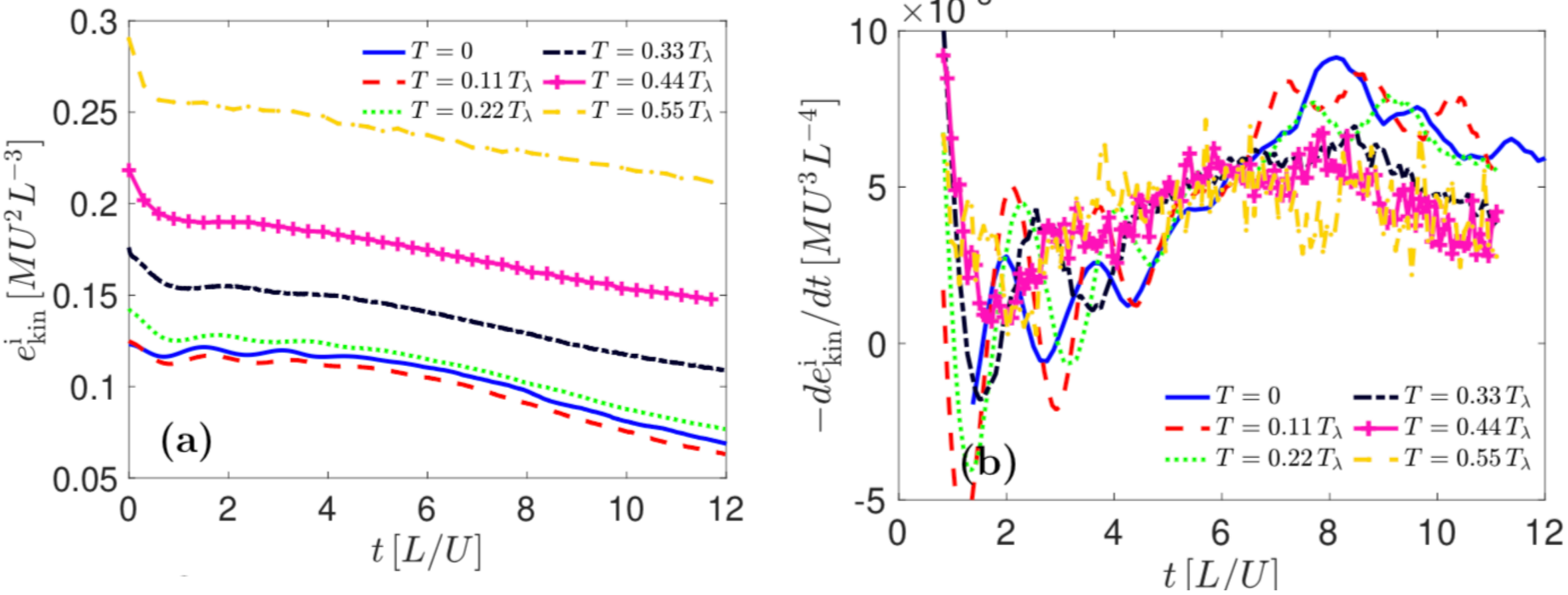

FIG. 7: *(Color online)* Time evolution of: (a) The incompressible kinetic energy $e^i_{\rm kin}$, and of (b) the incompressible kinetic energy dissipation rate $-de^i_{\rm kin}/dt$, at six different temperatures in TGPE runs with linear spatial resolution $N = 1024$ and $\xi k_{max} = 2.5$. The incompressible kinetic energy is given in units of MU^2L^{-3}, its time derivative in units of MU^3L^{-4},

Compensated inc Ekin

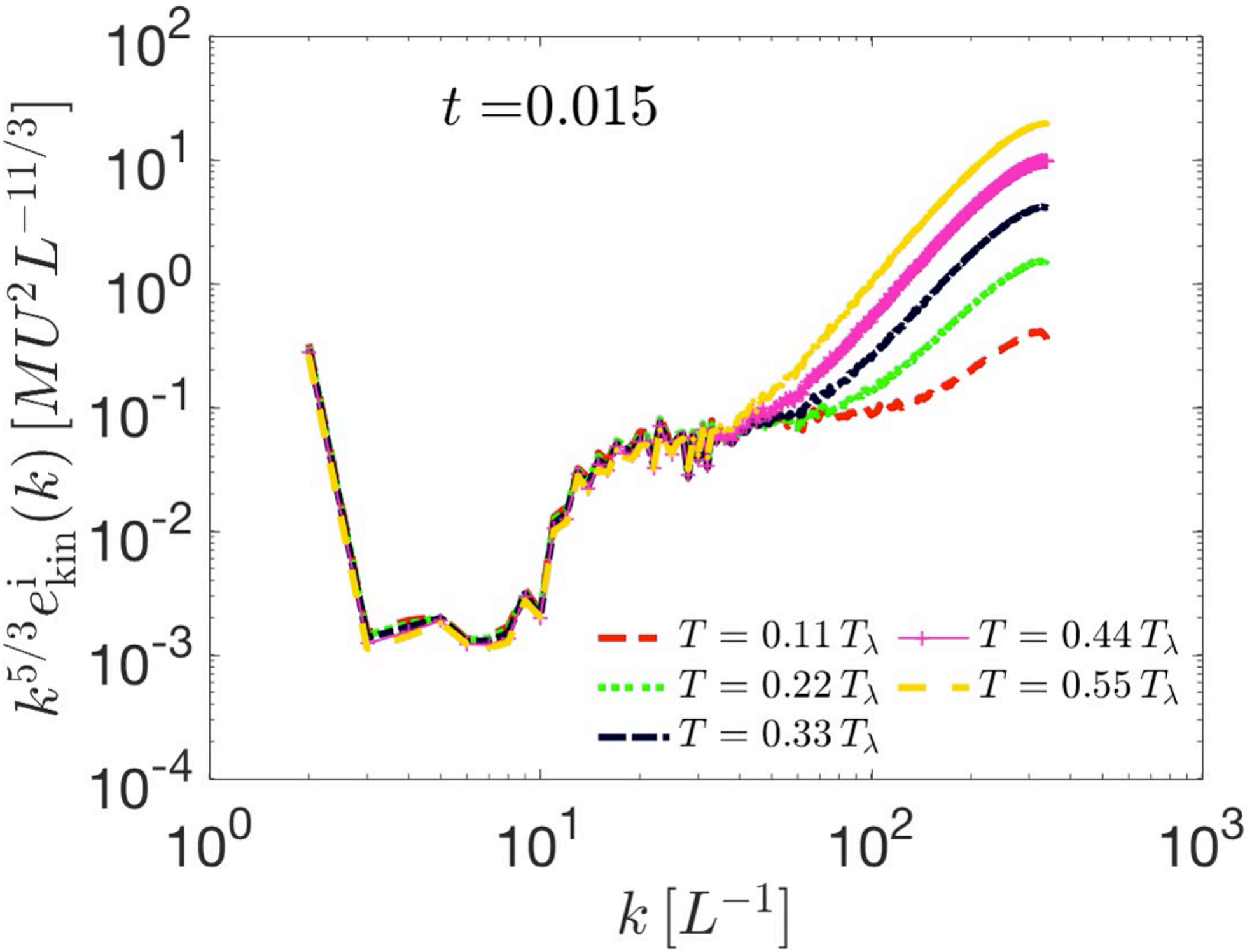

equilibrium spatiotemporal spectra

$\xi k_{\max} = 1.5$

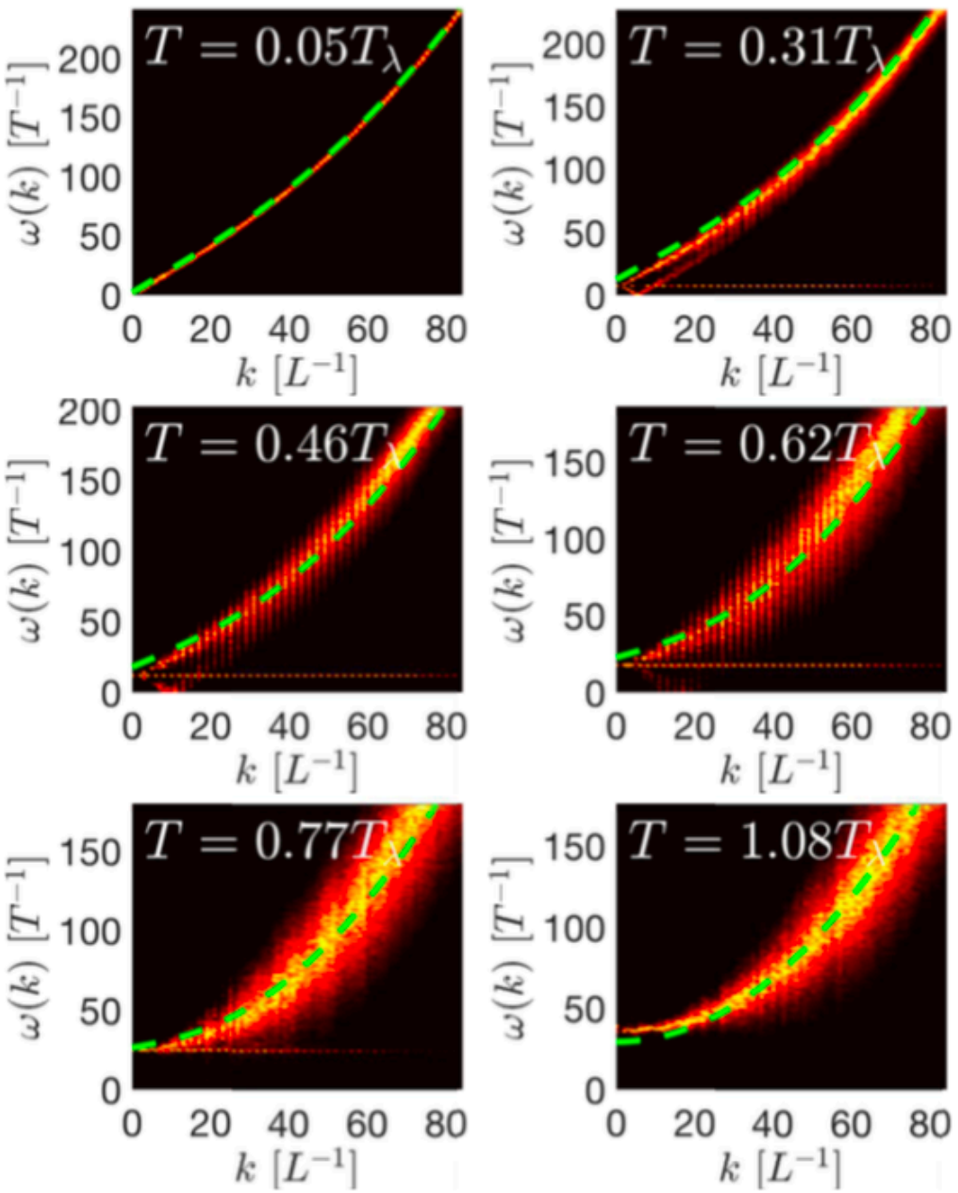

FIG. 10: *(Color online)* Spatio-temporal spectra with $\xi k_{\max} = 1.5$ and $N = 256^3$, for different temperatures as indicated in each panel. The (green) dashed line indicates the theoretical Bogoliubov dispersion relation. Bright (red to yellow) areas indicate modes with large excitation.

$\xi k_{max} = 2.5$

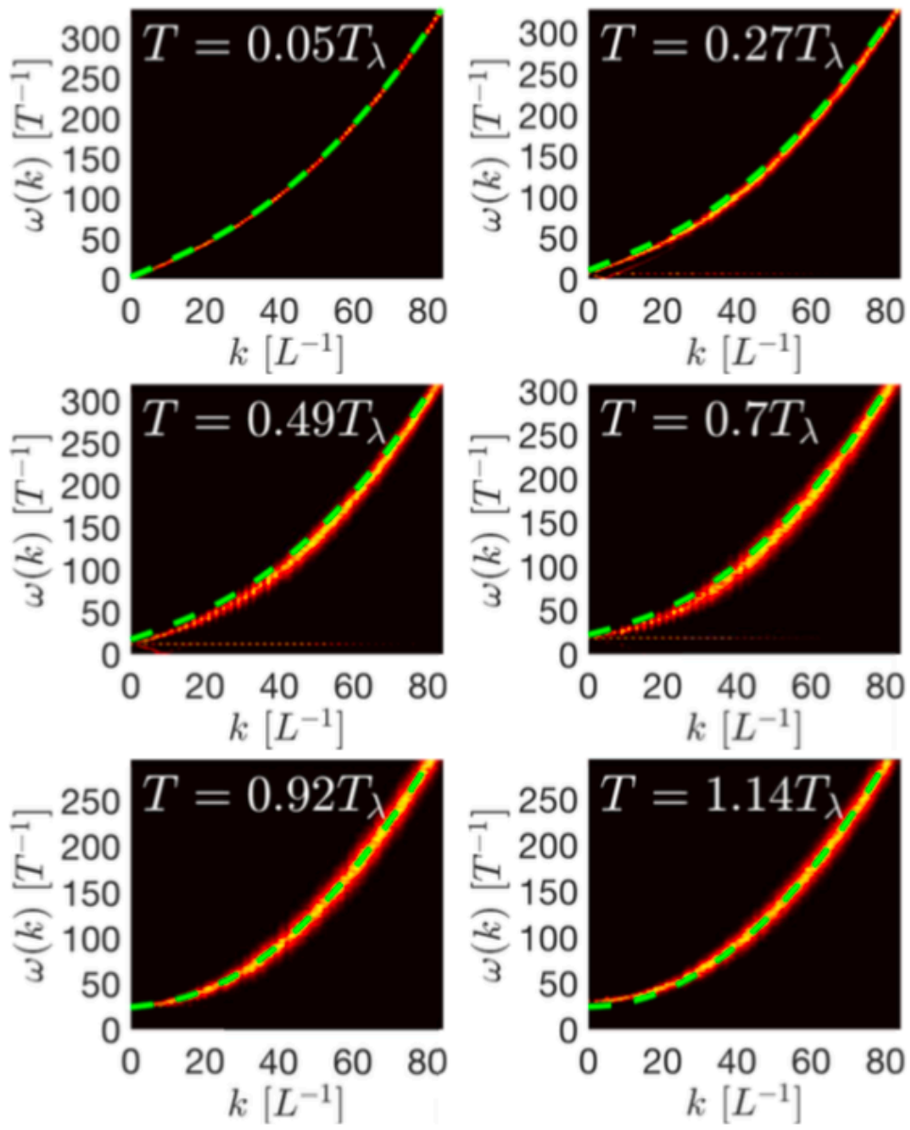

FIG. 11: *(Color online)* Spatio-temporal spectra with $\xi k_{\max} = 2.5$ and $N = 256^3$, for different temperatures as indicated in each figure. The (green) dashed line indicates the theoretical Bogoliubov dispersion relation. Bright (red to yellow) areas indicate modes with large excitation.

Thermal Broadening

$\xi k_{\max} = 1.5$

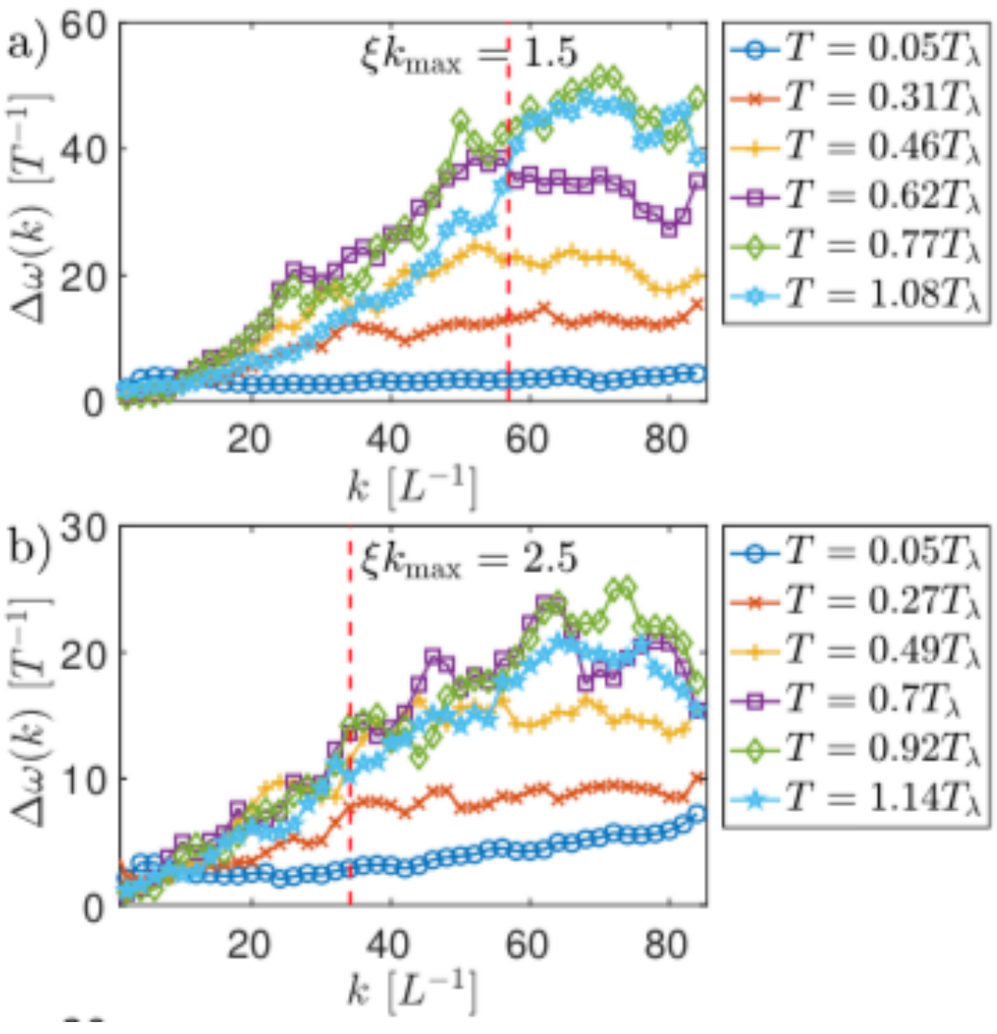

$\xi k_{max} = 2.5$

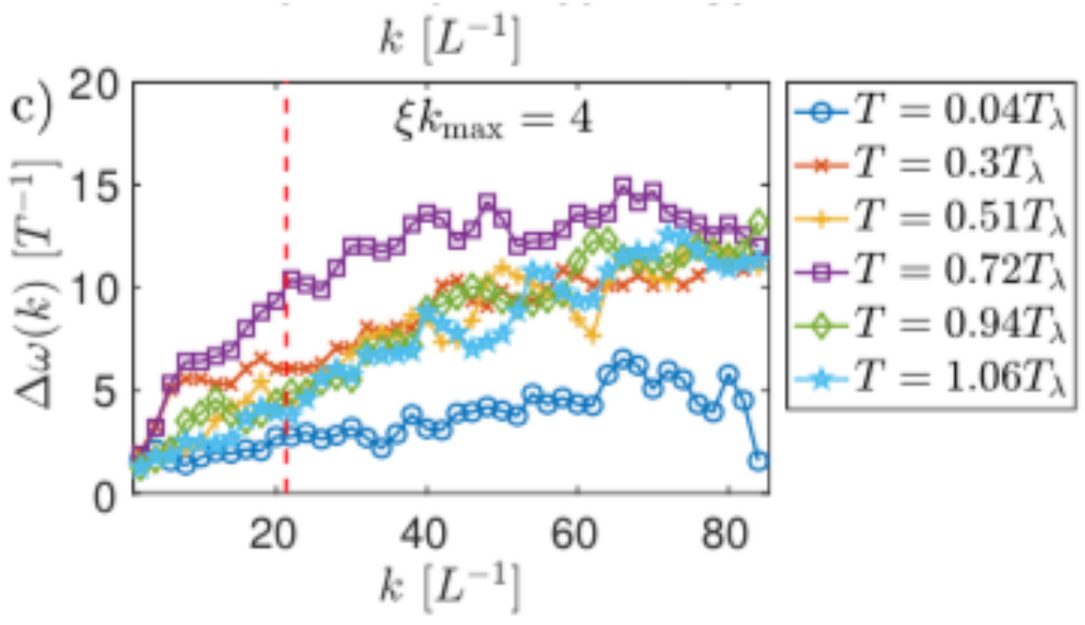

FIG. 12: *(Color online)* Spectral broadening $\Delta\omega(k)$ of the dispersion relation, for different temperatures and values of $\xi k_{\max}$. The vertical dashed lines indicate the value of $1/\xi$ in each case: (a) as a function of k for different temperatures and for $\xi k_{\max} = 1.5$, (b) same for $\xi k_{\max} = 2.5$, and (c) same for $\xi k_{\max} = 4$.The frequency $\Delta\omega(k)$ is given in units of T^{-1}, and k is in units of L^{-1}.

$\xi k_{\max} = 4$

Broadening, Mean Free Path & Effective viscosity

waves [56]. As a result, the mean free path can be constructed as

$$\lambda(k,T) \sim \frac{1}{\Delta\omega(k,T)} \frac{d\omega_B}{dk}. \tag{38}$$

From the mean free path, we can estimate the effective viscosity by writing

$$\nu_{\rm eff}(T) \sim \lambda(T) \left.\frac{d\omega_B}{dk}\right|_{k\approx k_{\rm max}} = \frac{\left(\left.\frac{d\omega_B}{dk}\right|_{k\approx k_{\rm max}}\right)^2}{\Delta\omega(k\approx k_{\rm max},T)}; \tag{39}$$

Mean Free Path

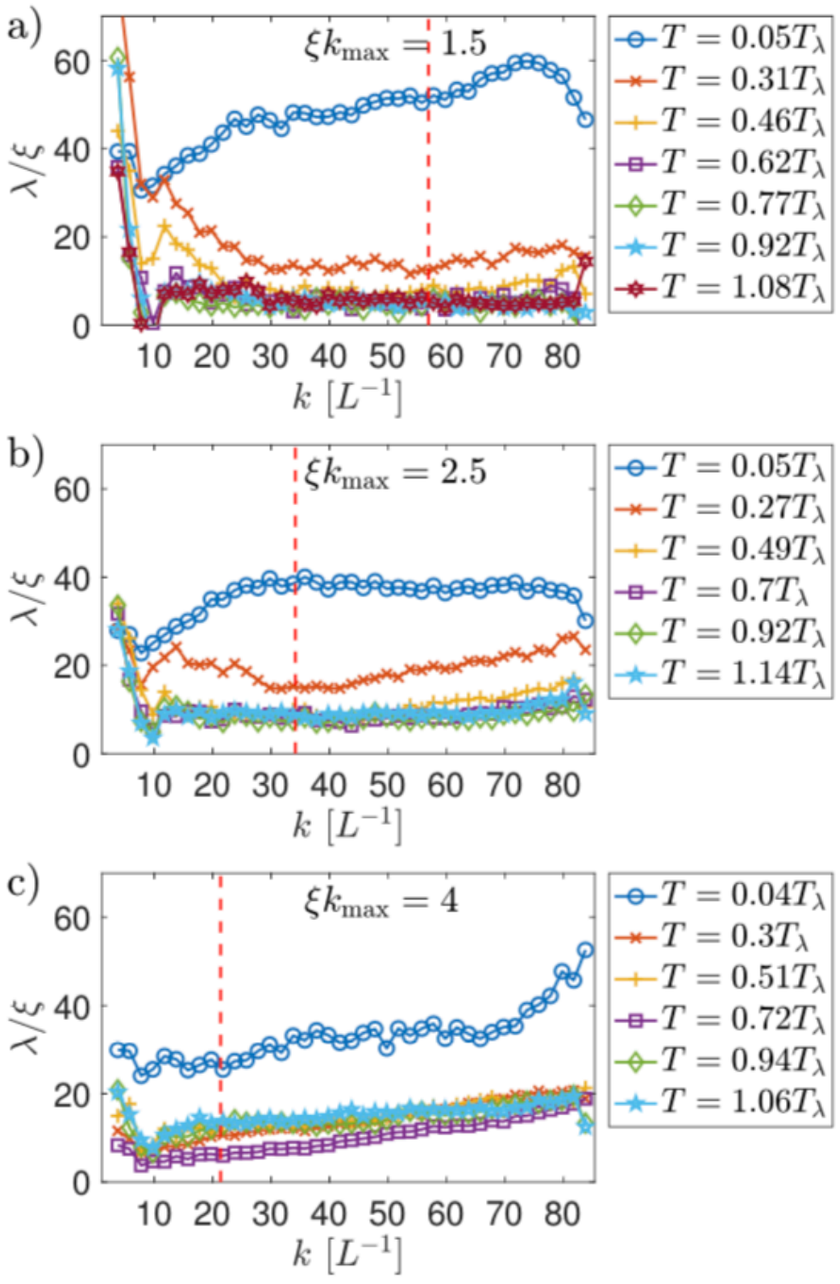

FIG. 13: *(Color online)* Mean free-path as a function of k for different temperatures in simulations with $\xi k_{\max} = 1.5$ (a), $\xi k_{\max} = 2.5$ (b) and $\xi k_{\max} = 4$ (c). The vertical dashed line indicates the value of $1/\xi$.

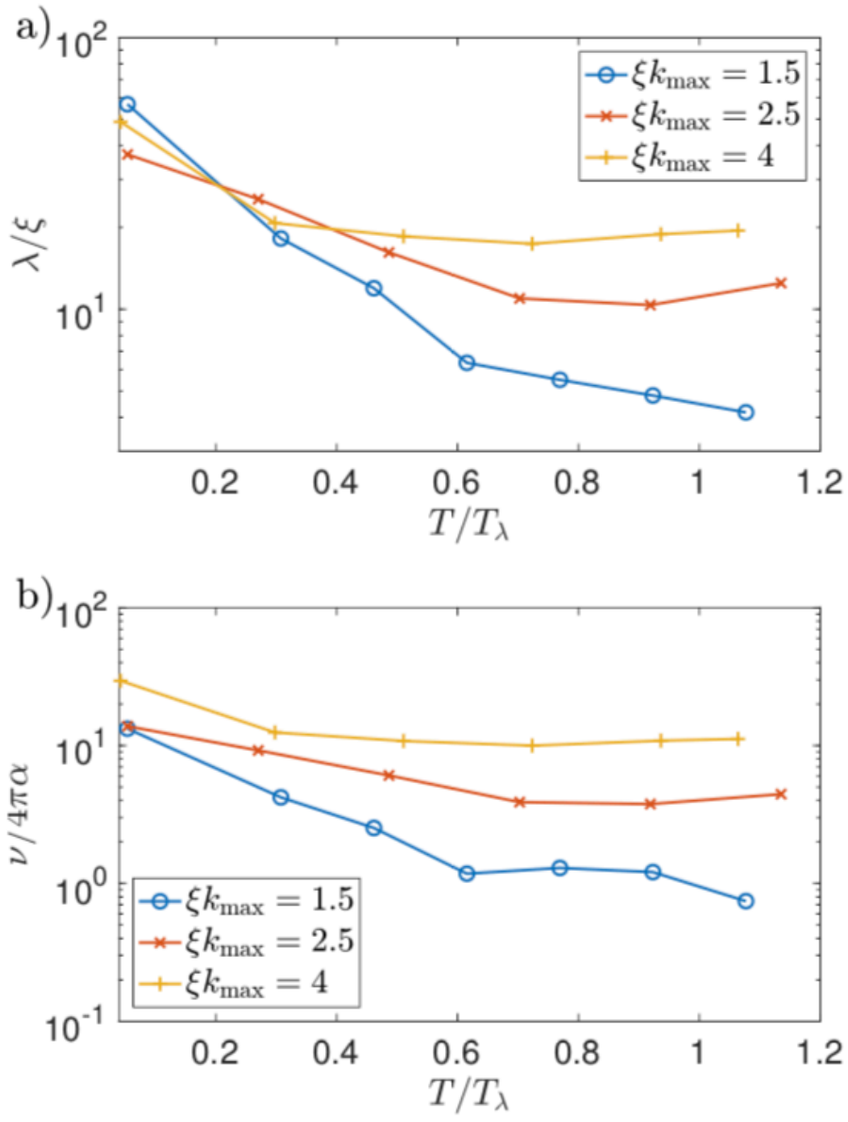

FIG. 14: *(Color online)* (a) Mean free-path as a function of temperature T for different values of $\xi k_{\max}$. (b) Effective viscosity (acting on the normal fluid), normalized by the quantum of circulation $4\pi\alpha = 4\pi c\xi/\sqrt{2}$, as a function of temperature T for different values of $\xi k_{\max}$.

Effective Reynolds number

note that we evaluate $\Delta\omega(T)$ and $d\omega_B/dk$ at $k = 80 \approx k_{\max}$. In Fig. 14(b) we show $\nu_{\rm eff}(T)$ normalized by the quantum of circulation $4\pi\alpha = 4\pi c\xi\sqrt{2}$. For temperatures above $0.5T_\lambda$, both λ and $\nu_{\rm eff}$ are relatively constant. For the runs with $\xi k_{\max} = 2.5$ we have

$$\lambda(T) \sim 10\xi, \tag{40}$$

$$\nu_{\rm eff}(T) \sim 50\alpha = 50c\xi/\sqrt{2}. \tag{41}$$

Equation (41) gives a physical estimation of the scaling of the effective viscosity in terms of the sound velocity c and of the healing length ξ. In the simulations, using $c = 2U$ and $\xi = 2.5/k_{\max} = 2.5 \times 3L/N$, the effective viscosity then becomes

$$\nu_{\rm eff}(T) \sim L\,U\frac{500}{N}, \tag{42}$$

where U and L are the unit velocity and length, and N is the linear spatial resolution. In dimensionless units, with $U = L = 1$, the Reynolds number can then be estimated as

$$\mathrm{Re}^{(\mathrm{TG})} = \frac{C}{\nu_{\rm eff}} = \frac{CN}{500}, \tag{43}$$

Effective Reynolds number

r.m.s. flow velocity

$$U_0 = \sqrt{2E} \tag{44}$$

and the flow correlation length

$$L_0 = 2\pi \frac{\int E(k)/k\, dk}{\int E(k)\, dk} \tag{45}$$

(i.e., the flow integral scale). Writing U_0 and L_0 in units of U and L, this Reynolds number is

$$\mathrm{Re} = C\frac{U_0 L_0}{\nu_{\mathrm{eff}}} = C\frac{U_0 L_0 N}{500}. \tag{46}$$

It is worth pointing out that $\nu_{\mathrm{eff}}(T)$ depends on the value of ξk_{max}, and that the strength of the nonlinear interactions goes down with increasing ξk_{max}. Thus, in the simulations with $\xi k_{\mathrm{max}} = 1.5$ we have stronger turbulence. Moreover, the mean free path (see Fig. 14) in these runs is $\lambda(T) \sim 5\xi$, which gives a smaller $\nu_{\mathrm{eff}}(T) \sim 15\alpha$. This results, for $\xi k_{\mathrm{max}} = 1.5$, in a larger Reynolds number

$$\mathrm{Re} = C\frac{U_0 L_0}{\nu_{\mathrm{eff}}} = C\frac{U_0 L_0 N}{90} \tag{47}$$

However, we cannot arbitrarily decrease ξk_{max} to obtain higher values of Re. At a fixed spatial resolution, ξk_{max} must be larger than unity if we want to properly resolve the vortices in simulations.

C is about 7

$$\xi k_{max} = 2.5$$

$$Re \sim U_0 L_0 \frac{N}{71}$$

$$\xi k_{\mathrm{max}} = 1.5$$

$$Re \sim U_0 L_0 \frac{N}{13}$$

Back to Truncated Euler and classical turbulence

- Truncated Euler describes the relaxation toward Kraichnan helical absolute equilibrium and transient mixed energy and helicity cascades
- Can Truncated Euler describe reversals in two-dimensional confined turbulent flows?
- Can truncated Euler describe the large scales of 3D turbulence forced at small scales?

Statistical theory of reversals in two-dimensional confined turbulent flows

Vishwanath Shukla, Stephan Fauve, and Marc Brachet,
Statistical theory of reversals in two-dimensional confined turbulent flows,
PHYSICAL REVIEW E 94, 061101(R) (2016)

The problem is to model a transition on a turbulent background (seen in experiments and DNS) where the global circulation of a 2D flow (forced at smaller scales) goes from unimodal to bimodal (reversals) and then to condensate (no reversal)

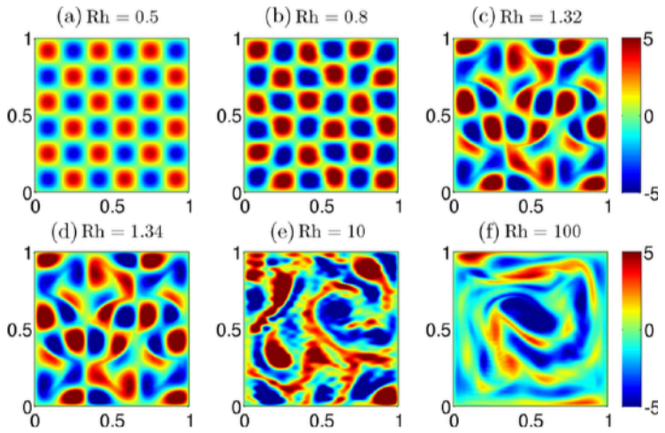

FIG. 2. (Color online) Vorticity patterns for Re = 5000: (a) Linear response to the forcing (Rh = 0.5), (b) stationary nonlinear regime (Rh = 0.8), (c) time-periodic regime (Rh = 1.32), (d) quasiperiodic regime (Rh = 1.34), (e) chaotic flow with zero-mean velocity (Rh = 10), and (f) condensate state (Rh = 100).

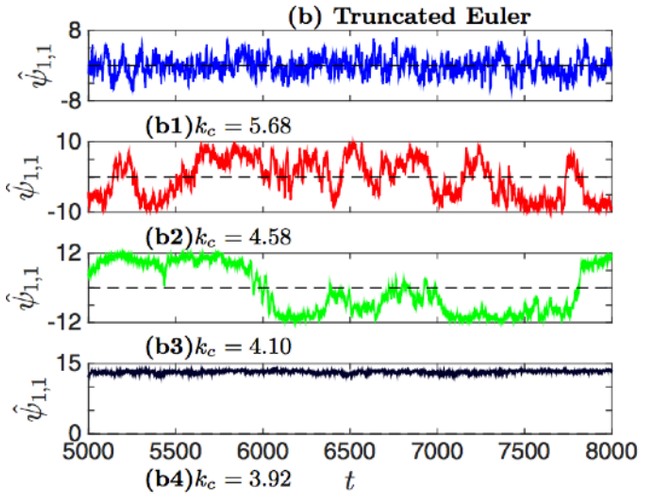

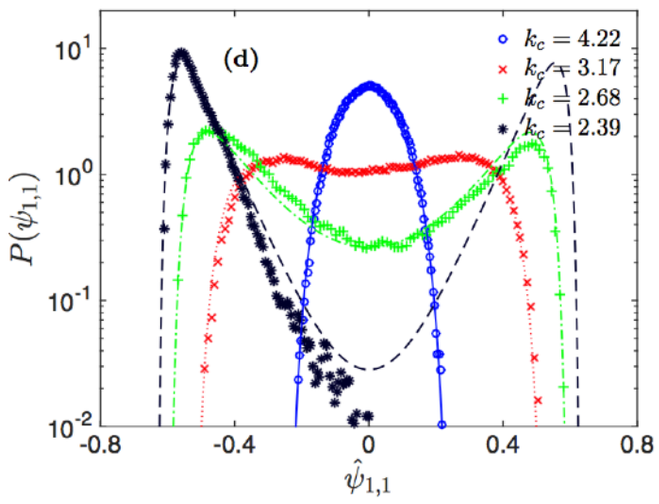

Large scale circulation

Experiment

G. Michel, J. Herault, F. Pétrélis and S. Fauve,
Bifurcations of a large-scale circulation in a quasi-bidimensional turbulent flow,
EPL, 115 (2016) 64004

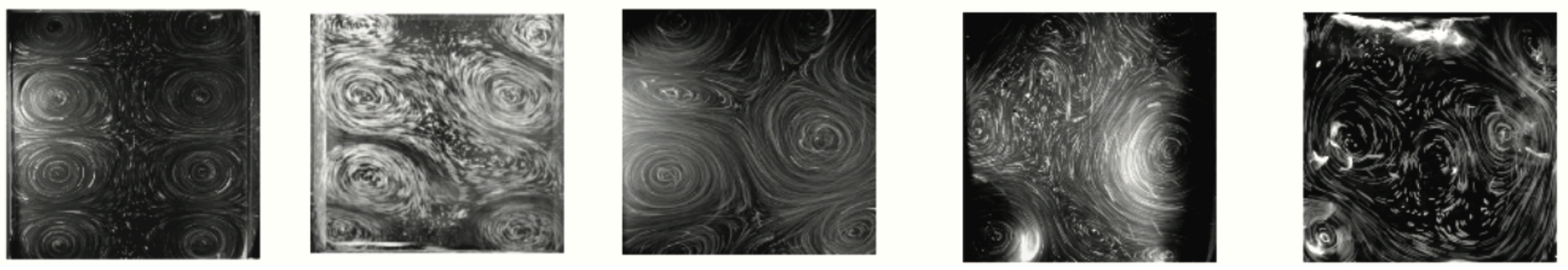

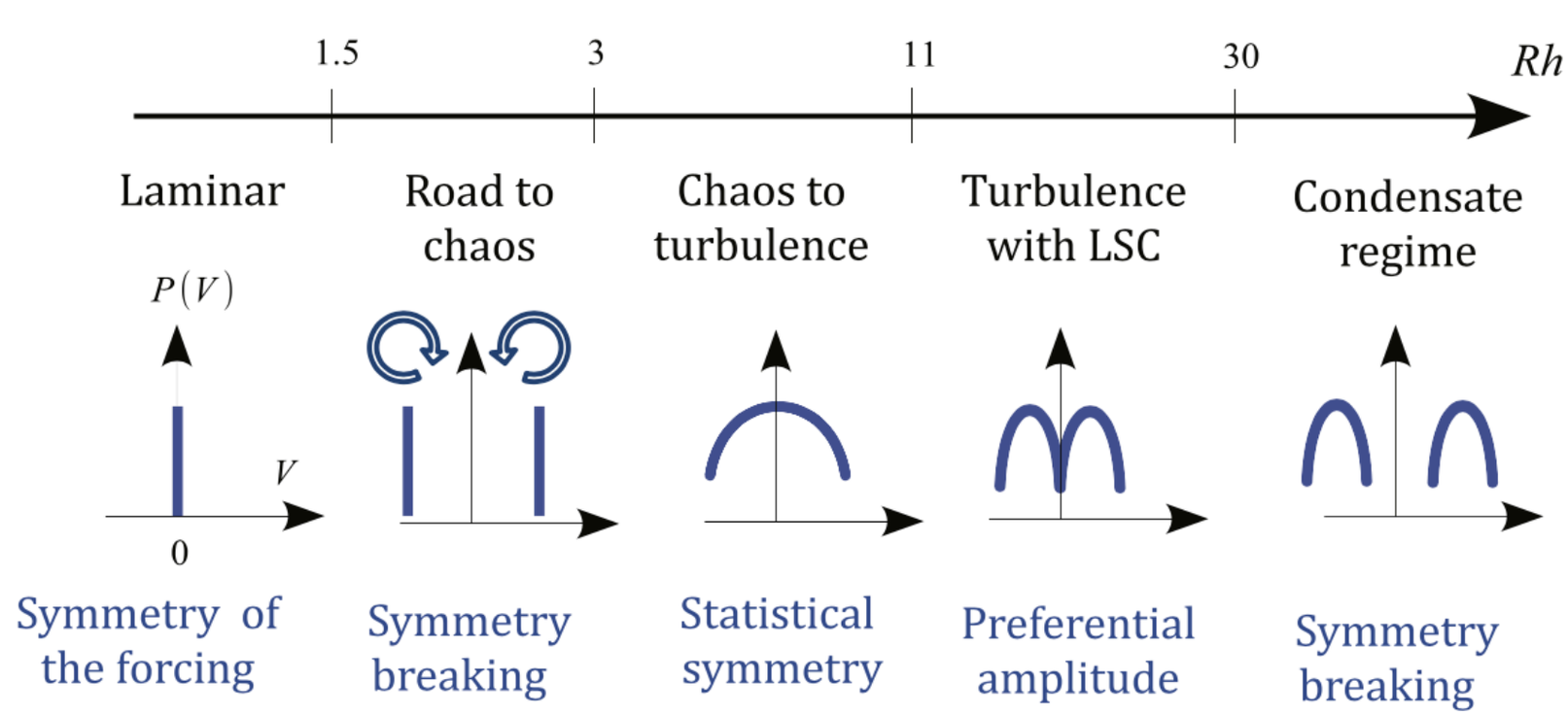

Fig. 1: (Color online) Top: pictures of the flow as a function of Rh. From left to rigth: laminar flow, first bifurcation, chaotic flow, turbulent flow with moderate large-scale flow, turbulent flow with strong large-scale flow (condensate). Bottom: sketch of the PDF of large-scale circulation. Symmetry breaking indicates that depending on the initial conditions one of the two states (*i.e.* one of the two peaks of the PDF) will be observed.

Simulation

Pankaj Kumar Mishra, Johann Herault, Stephan Fauve, and Mahendra K. Verma,
Dynamics of reversals and condensates in two-dimensional Kolmogorov flows,
PHYSICAL REVIEW E 91, 053005 (2015)

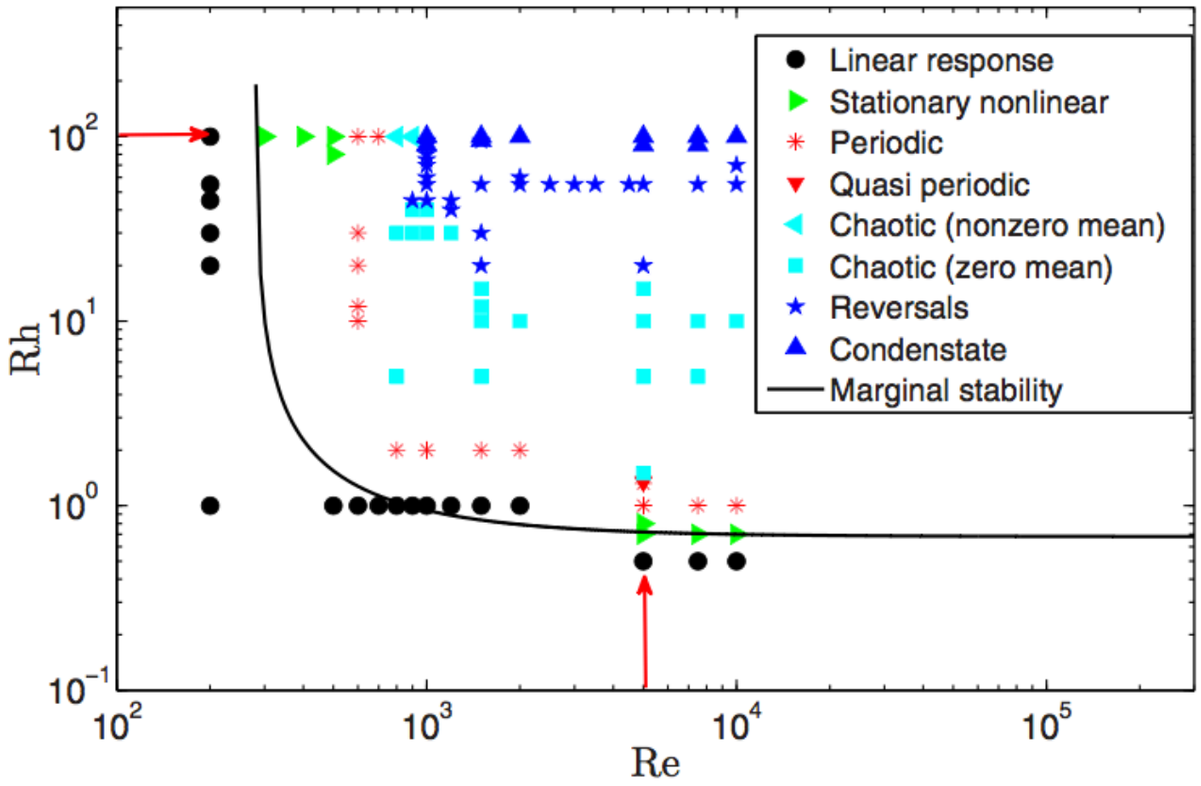

FIG. 1. (Color online) The different flow regimes in the parameter space (Re-Rh): linear response to the forcing (●), stationary nonlinear regime (►), time-periodic regime (∗), quasiperiodic regime (▼), chaotic regime with nonzero mean flow (◄), chaotic regime with zero mean flow (■), random reversals of the large-scale flow (★), and condensate state (▲). The full line is the marginal stability curve of the linear response to the forcing calculated by Thess [10].

$$\frac{\partial \mathbf{u}}{\partial t} + (\mathbf{u}\cdot\boldsymbol{\nabla})\mathbf{u} = -\boldsymbol{\nabla}\sigma - \frac{1}{\mathrm{Rh}}\mathbf{u} + \frac{1}{\mathrm{Re}}\nabla^2\mathbf{u} + \mathbf{F},$$

$$\boldsymbol{\nabla}\cdot\mathbf{u} = 0,$$

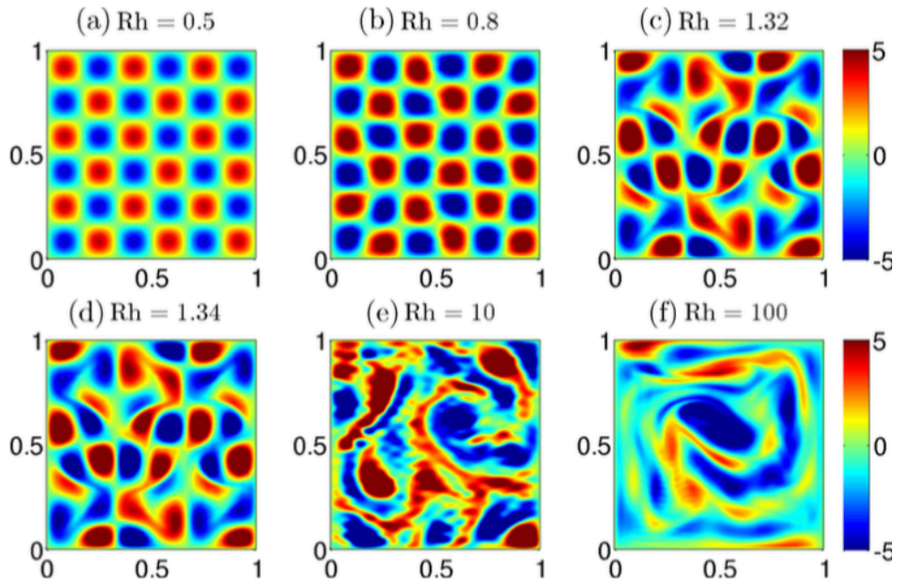

FIG. 2. (Color online) Vorticity patterns for Re = 5000: (a) Linear response to the forcing (Rh = 0.5), (b) stationary nonlinear regime (Rh = 0.8), (c) time-periodic regime (Rh = 1.32), (d) quasiperiodic regime (Rh = 1.34), (e) chaotic flow with zero-mean velocity (Rh = 10), and (f) condensate state (Rh = 100).

2D Navier-Stokes

Vishwanath Shukla, Stephan Fauve, and Marc Brachet,
Statistical theory of reversals in two-dimensional confined turbulent flows,
PHYSICAL REVIEW E 94, 061101(R) (2016)

$$\frac{\partial \psi}{\partial t} - \frac{1}{\nabla^2}\{\psi, \nabla^2 \psi\} = -\frac{1}{\mathrm{Rh}}\psi + \frac{1}{\mathrm{Re}}\nabla^2 \psi + f_\psi$$

$$\psi(x,y) = \sum_{m,n} \hat{\psi}_{m,n} \sin(mx) \sin(ny),$$

$$f_\psi = \tfrac{1}{144} \sin(6\,x) \sin(6\,y).$$

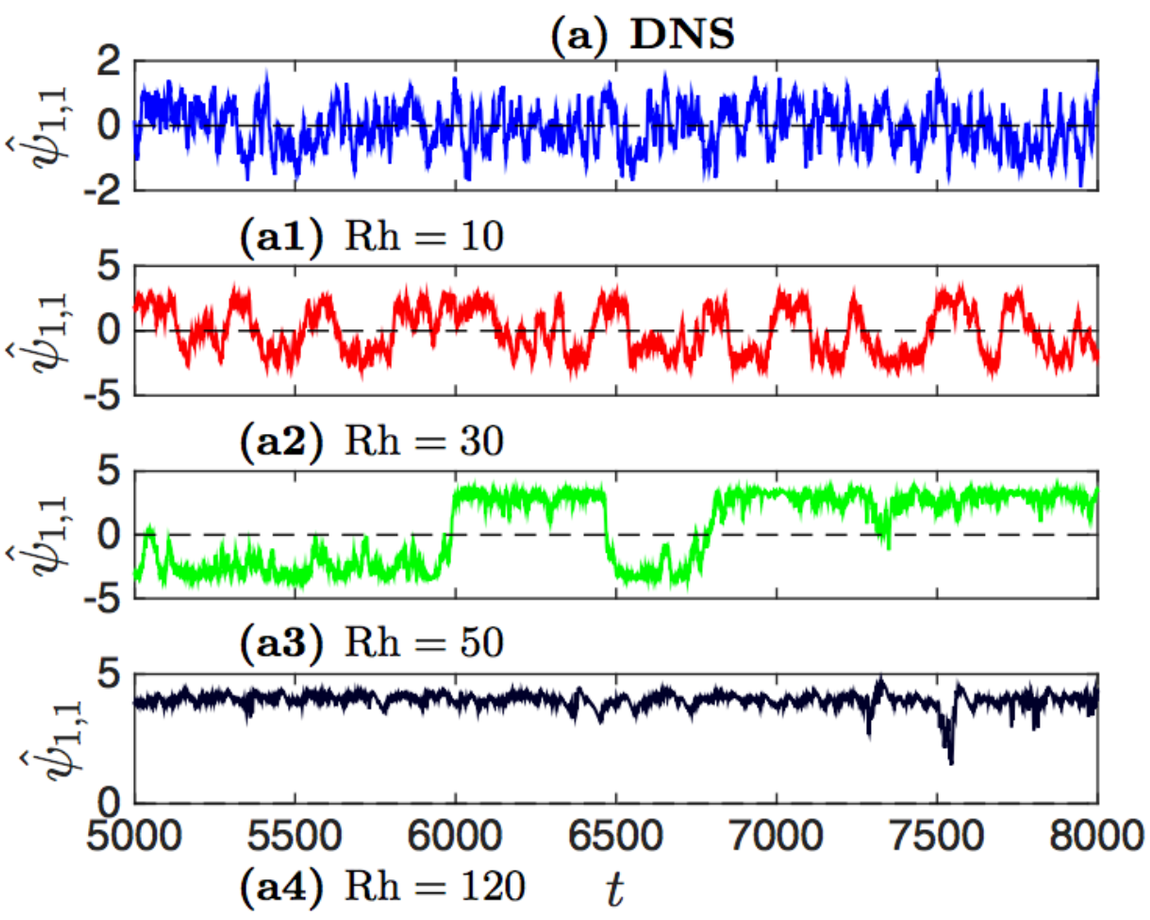

Truncated Euler Equation

The TEE is obtained by performing a circular Galerkin truncation at wave number $k_{\max}$ of the incompressible, Euler equation $\frac{\partial \psi}{\partial t} - \frac{1}{\nabla^2}\{\psi, \nabla^2 \psi\} = 0,$ which is Eq. (1) without forcing or dissipation. The TEE in spectral space reads

$$\frac{\partial \hat{\psi}_{\mathbf{k}}}{\partial t} = \frac{1}{k^2} \sum_{\mathbf{p},\mathbf{q}} (\mathbf{p} \times \mathbf{q}) q^2 \hat{\psi}_{\mathbf{p}} \hat{\psi}_{\mathbf{q}} \delta_{\mathbf{k},\mathbf{p}+\mathbf{q}} \tag{3}$$

with $\delta_{\mathbf{k},\mathbf{r}}$ the Kronecker delta and with Fourier modes satisfying $\hat{\psi}_{\mathbf{k}} = 0$ if $|\mathbf{k}| \geqslant k_{\max}$. Note that, because of the free-slip boundary conditions, Eq. (2), the Fourier modes $\hat{\psi}_{\mathbf{k}}$ are real numbers. This truncated system exactly conserves the quadratic invariants, energy and enstrophy, given in Fourier space by $E = \frac{1}{2}\sum_{\mathbf{k}} |\mathbf{u}_{\mathbf{k}}|^2$ and $\Omega = \frac{1}{2}\sum_{\mathbf{k}} k^2 |\mathbf{u}_{\mathbf{k}}|^2$ [10].

TEE

We now consider the approach introduced by Lee [9] and developed by Kraichnan [1,8] that relies on the 2D TEE. They showed that the Euler equation, truncated between a minimum and a maximum wave number, gives a set of ODEs for the amplitudes of the modes that follow a Liouville theorem [9]. For 2D flows, the kinetic energy E and the enstrophy Ω (integrated squared vorticity) are conserved; therefore, the Boltzmann-Gibbs canonical equilibrium distribution is of the form $\mathcal{P} = Z^{-1} \exp(-\alpha E - \beta\Omega)$, where Z is the partition function and α and β can be seen as inverse temperatures, determined by the total energy and enstrophy. Using this formalism, Kraichnan [1,8] derived the absolute equilibria of the energy spectrum $E(k)$ and showed the existence of different regimes depending on the values of α and β. On the other hand, microcanonical distributions are defined by $\delta(E - E_0)\delta(\Omega - \Omega_0)$, where E_0 and Ω_0 are respectively the energy and enstrophy of the initial conditions, and should be used to compute the PDFs in the reversal and condensed state (see below).

13 modes explicit model

Energie and enstophy

$$E = (1^2+1^2)\hat{\psi}_{11}^2 + (1^2+2^2)\hat{\psi}_{12}^2 + (2^2+1^2)\hat{\psi}_{21}^2 + (2^2+2^2)\hat{\psi}_{22}^2 + (3^2+1^2)\hat{\psi}_{31}^2 + (1^2+3^2)\hat{\psi}_{13}^2 + (2^2+3^2)\hat{\psi}_{23}^2 + (3^2+2^2)\hat{\psi}_{32}^2 + (1^2+4^2)\hat{\psi}_{14}^2 + (4^2+1^2)\hat{\psi}_{41}^2 + (2^2+4^2)\hat{\psi}_{24}^2 + (4^2+2^2)\hat{\psi}_{42}^2 + (3^2+3^2)\hat{\psi}_{33}^2 \quad \text{(A14)}$$

and

$$\Omega = (1^2+1^2)^2\hat{\psi}_{11}^2 + (1^2+2^2)^2\hat{\psi}_{12}^2 + (2^2+1^2)^2\hat{\psi}_{21}^2 + (2^2+2^2)^2\hat{\psi}_{22}^2 + (3^2+1^2)^2\hat{\psi}_{31}^2 + (1^2+3^2)^2\hat{\psi}_{13}^2 + (2^2+3^2)^2\hat{\psi}_{23}^2 + (3^2+2^2)^2\hat{\psi}_{32}^2 + (1^2+4^2)^2\hat{\psi}_{14}^2 + (4^2+1^2)^2\hat{\psi}_{41}^2 + (2^2+4^2)^2\hat{\psi}_{24}^2 + (4^2+2^2)^2\hat{\psi}_{42}^2 + (3^2+3^2)^2\hat{\psi}_{33}^2. \quad \text{(A15)}$$

$k_c^2 = \Omega / E,$ $\psi(x,y) = \sum_{m,n} \hat{\psi}_{m,n} \sin(mx)\sin(ny),$ $\hat{\psi}_{m,n}$ is a real number

$k_c^2 = \Omega / E < 5$ with $\Omega = (1^2+1^2)^2 y_0^2 + (1^2+2^2)^2 y_1^2 + \cdots$ and $E = (1^2+1^2) y_0^2 + (1^2+2^2) y_1^2 + \cdots$ implies that $y_0 \neq 0$.

Thus the microcanonical PDF of y_0 has to obey $p(0) = 0$ for $k_c^2 < 5$ which forbids reversals of the large-scale circulation.

We give here explicitly the set of 13 ODEs for the amplitudes of the Fourier modes $\hat{\psi}_{m,n}$ that define the TEE in the case $k_{\max} = 2\sqrt{5}$. Note that $\psi_{m,n}$ are real numbers because of the free-slip boundary conditions (see text).

$$\frac{d\hat{\psi}_{11}}{dt} = \frac{1}{2}[(2\hat{\psi}_{12} + 5\hat{\psi}_{14})\hat{\psi}_{23} + \hat{\psi}_{13}(2\hat{\psi}_{22} + 5\hat{\psi}_{24}) - 2\hat{\psi}_{22}\hat{\psi}_{31} - \hat{\psi}_{32}(2\hat{\psi}_{21} + 5\hat{\psi}_{41}) + 3\hat{\psi}_{33}(\hat{\psi}_{24} - \hat{\psi}_{42}) - 5\hat{\psi}_{31}\hat{\psi}_{42}], \quad \text{(A1)}$$

$$\frac{d\hat{\psi}_{12}}{dt} = \frac{1}{20}[25\hat{\psi}_{13}\hat{\psi}_{21} + 54\hat{\psi}_{14}\hat{\psi}_{22} + \hat{\psi}_{11}(9\hat{\psi}_{21} - 11\hat{\psi}_{23}) + 25\hat{\psi}_{21}\hat{\psi}_{31} + 21\hat{\psi}_{23}\hat{\psi}_{31} + 56\hat{\psi}_{24}\hat{\psi}_{32} - 39\hat{\psi}_{21}\hat{\psi}_{33} + 49\hat{\psi}_{31}\hat{\psi}_{41} + 9\hat{\psi}_{33}\hat{\psi}_{41}], \quad \text{(A2)}$$

$$\frac{d\hat{\psi}_{21}}{dt} = \frac{1}{20}[-49\hat{\psi}_{13}\hat{\psi}_{14} - \hat{\psi}_{11}(9\hat{\psi}_{12} - 11\hat{\psi}_{32}) - 21\hat{\psi}_{13}\hat{\psi}_{32} - \hat{\psi}_{12}(25\hat{\psi}_{13} + 25\hat{\psi}_{31} - 39\hat{\psi}_{33}) - 9\hat{\psi}_{14}\hat{\psi}_{33} - 54\hat{\psi}_{22}\hat{\psi}_{41} - 56\hat{\psi}_{23}\hat{\psi}_{42}], \quad \text{(A3)}$$

$$\frac{d\hat{\psi}_{22}}{dt} = \frac{1}{4}[-9\hat{\psi}_{12}\hat{\psi}_{14} - 4\hat{\psi}_{11}(\hat{\psi}_{13} - \hat{\psi}_{31}) + 5\hat{\psi}_{14}\hat{\psi}_{32} + 9\hat{\psi}_{21}\hat{\psi}_{41} - 5\hat{\psi}_{23}\hat{\psi}_{41}], \quad \text{(A4)}$$

$$\frac{d\hat{\psi}_{13}}{dt} = \frac{1}{10}\{\hat{\psi}_{11}(6\hat{\psi}_{22} - 9\hat{\psi}_{24}) + 7\hat{\psi}_{21}(3\hat{\psi}_{14} + 2\hat{\psi}_{32}) + 11\hat{\psi}_{32}\hat{\psi}_{41} + \hat{\psi}_{31}[4\hat{\psi}_{22} + 25(\hat{\psi}_{24} + \hat{\psi}_{42})]\}, \quad \text{(A5)}$$

$$\frac{d\hat{\psi}_{31}}{dt} = \frac{1}{10}\{-14\hat{\psi}_{12}\hat{\psi}_{23} - 11\hat{\psi}_{14}\hat{\psi}_{23} - 21\hat{\psi}_{12}\hat{\psi}_{41} - \hat{\psi}_{11}(6\hat{\psi}_{22} - 9\hat{\psi}_{42}) - \hat{\psi}_{13}[4\hat{\psi}_{22} + 25(\hat{\psi}_{24} + \hat{\psi}_{42}]\}, \quad \text{(A6)}$$

$$\frac{d\hat{\psi}_{23}}{dt} = \frac{1}{52}[35\hat{\psi}_{12}\hat{\psi}_{31} + 77\hat{\psi}_{14}\hat{\psi}_{31} + \hat{\psi}_{11}(3\hat{\psi}_{12} - 75\hat{\psi}_{14} + 55\hat{\psi}_{32}) + 90\hat{\psi}_{22}\hat{\psi}_{41} + 42\hat{\psi}_{24}\hat{\psi}_{41} + 120\hat{\psi}_{21}\hat{\psi}_{42}], \quad \text{(A7)}$$

$$\frac{d\hat{\psi}_{32}}{dt} = \frac{1}{52}\{-\hat{\psi}_{11}(3\hat{\psi}_{21} + 55\hat{\psi}_{23} - 75\hat{\psi}_{41}) - 7\hat{\psi}_{13}(5\hat{\psi}_{21} + 11\hat{\psi}_{41}) - 6[20\hat{\psi}_{12}\hat{\psi}_{24} + \hat{\psi}_{14}(15\hat{\psi}_{22} + 7\hat{\psi}_{42})]\}, \quad \text{(A8)}$$

$$\frac{d\hat{\psi}_{14}}{dt} = \frac{1}{68}[-35\hat{\psi}_{13}\hat{\psi}_{21} + 18\hat{\psi}_{12}\hat{\psi}_{22} + 55\hat{\psi}_{11}\hat{\psi}_{23} - 33\hat{\psi}_{23}\hat{\psi}_{31} + 50\hat{\psi}_{22}\hat{\psi}_{32} + 117\hat{\psi}_{21}\hat{\psi}_{33} - 15\hat{\psi}_{33}\hat{\psi}_{41} + 98\hat{\psi}_{32}\hat{\psi}_{42}], \quad \text{(A9)}$$

$$\frac{d\hat{\psi}_{41}}{dt} = \frac{1}{68}[-18\hat{\psi}_{21}\hat{\psi}_{22} - 50\hat{\psi}_{22}\hat{\psi}_{23} - 98\hat{\psi}_{23}\hat{\psi}_{24} + 35\hat{\psi}_{12}\hat{\psi}_{31} - 55\hat{\psi}_{11}\hat{\psi}_{32} + 33\hat{\psi}_{13}\hat{\psi}_{32} - 117\hat{\psi}_{12}\hat{\psi}_{33} + 15\hat{\psi}_{14}\hat{\psi}_{33}], \quad \text{(A10)}$$

$$\frac{d\hat{\psi}_{24}}{dt} = \tfrac{1}{10}[8\hat{\psi}_{12}\hat{\psi}_{32} + 2\hat{\psi}_{11}(\hat{\psi}_{13} + 6\hat{\psi}_{33}) + 7\hat{\psi}_{23}\hat{\psi}_{41} + 18\hat{\psi}_{22}\hat{\psi}_{42}], \quad \text{(A11)}$$

$$\frac{d\hat{\psi}_{42}}{dt} = \frac{1}{10}[-8\hat{\psi}_{21}\hat{\psi}_{23} - 18\hat{\psi}_{22}\hat{\psi}_{24} - 2\hat{\psi}_{11}\hat{\psi}_{31} - 7\hat{\psi}_{14}\hat{\psi}_{32} - 12\hat{\psi}_{11}\hat{\psi}_{33}], \quad \text{(A12)}$$

$$\frac{d\hat{\psi}_{33}}{dt} = -\frac{3}{2}[\hat{\psi}_{14}\hat{\psi}_{21} - \hat{\psi}_{12}\hat{\psi}_{41} + \hat{\psi}_{11}(\hat{\psi}_{24} - \hat{\psi}_{42})]. \quad \text{(A13)}$$

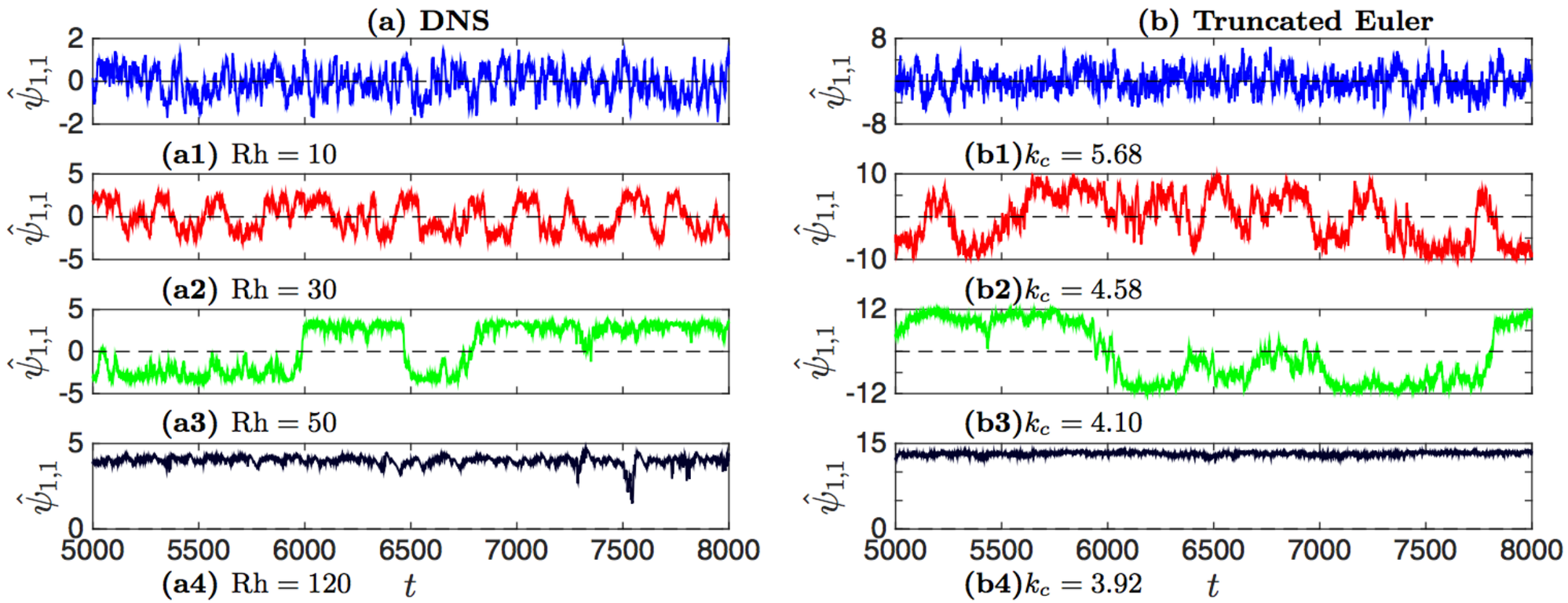

FIG. 1. Flow transitions: Time series of $\hat{\psi}_{1,1}$ obtained from the DNS of the (a) Navier-Stokes equation (NSE) for different values of Rh and Re $= 5000/\pi^2$, and (b) truncated Euler equation (TEE) for different values of k_c. $\hat{\psi}^{\rm NSE}_{1,1}$ and $\hat{\psi}^{\rm TEE}_{1,1}$ have been divided by 10^4 and 10^2, respectively. (c) Plot of $k_c = \sqrt{\Omega/E}$ versus Rh from the DNS of the NSE for two different Reynold's numbers Re $= 3000/\pi^2$ (blue circles) and Re $= 5000/\pi^2$ (red crosses). Inset: Log-linear plots of the PDFs of $\hat{\psi}^{TEE}_{1,1}$ for different values of k_c. (d) Log-linear plots of the PDFs of $\hat{\psi}_{1,1}$ for different values of k_c obtained from the finite-mode minimal model based on the TEE; the lines on top of these PDFs indicate the estimation from our analytical method.

Outlook: TEE and transitions

Transitions between different mean flows are widely observed in turbulent regimes, the most famous example being the drag crisis for which the wake of a sphere becomes narrower. Using the Navier-Stokes equation with noisy forcing [19] is a way to describe this type of transition. The TEE as presented here, can provide an alternative method to describe the dynamics of large scales in turbulence and to model a bifurcation of the mean flow on a strongly turbulent background.

See also an MHD case:

P. Dmitruk, P. D. Mininni, A. Pouquet, S. Servidio, and W. H. Matthaeus Phys. Rev. E 83, 066318 (2011)

Can truncated Euler describe the large scales of 3D turbulence forced at small scales?

- The relation between forced 3D Navier Stokes and truncated 3D Euler was studied in 2 related recent papers

- Alexandros Alexakis and Marc-Etienne Brachet, On the thermal equilibrium state of large-scale flows, J. Fluid Mech., vol. 872, pp. 594–625 (2019)

- Alexandros Alexakis and Marc-Etienne Brachet, Energy fluxes in quasi-equilibrium flows, J. Fluid Mech., vol. 884, A33 (2020)

- Here I only shortly indicate some of the main conclusions of these works

Thermal equilibrium state of large-scale flows

We examined 12 different simulated flows forced at small scales with a scope to understand better the behaviour of large scale flows and their relation to the absolute equilibrium solutions predicted by Kraichnan (1973).

There is a variety of behaviours for the large-scale components of turbulent flows. In particular, the absolute equilibrium solutions are well reproduced by the large scales of turbulent flows when a few modes are forced (spectrally sparse forcing), and when the forcing of these modes is sufficiently short time correlated.

Small deviations from the absolute equilibrium solutions were observed when the forcing correlation time was increased.
Strong deviations from the absolute equilibrium solutions were observed when the forcing was applied to all modes inside a spherical shell (spectrally dense forcing).

Thermal equilibrium state of large-scale flows

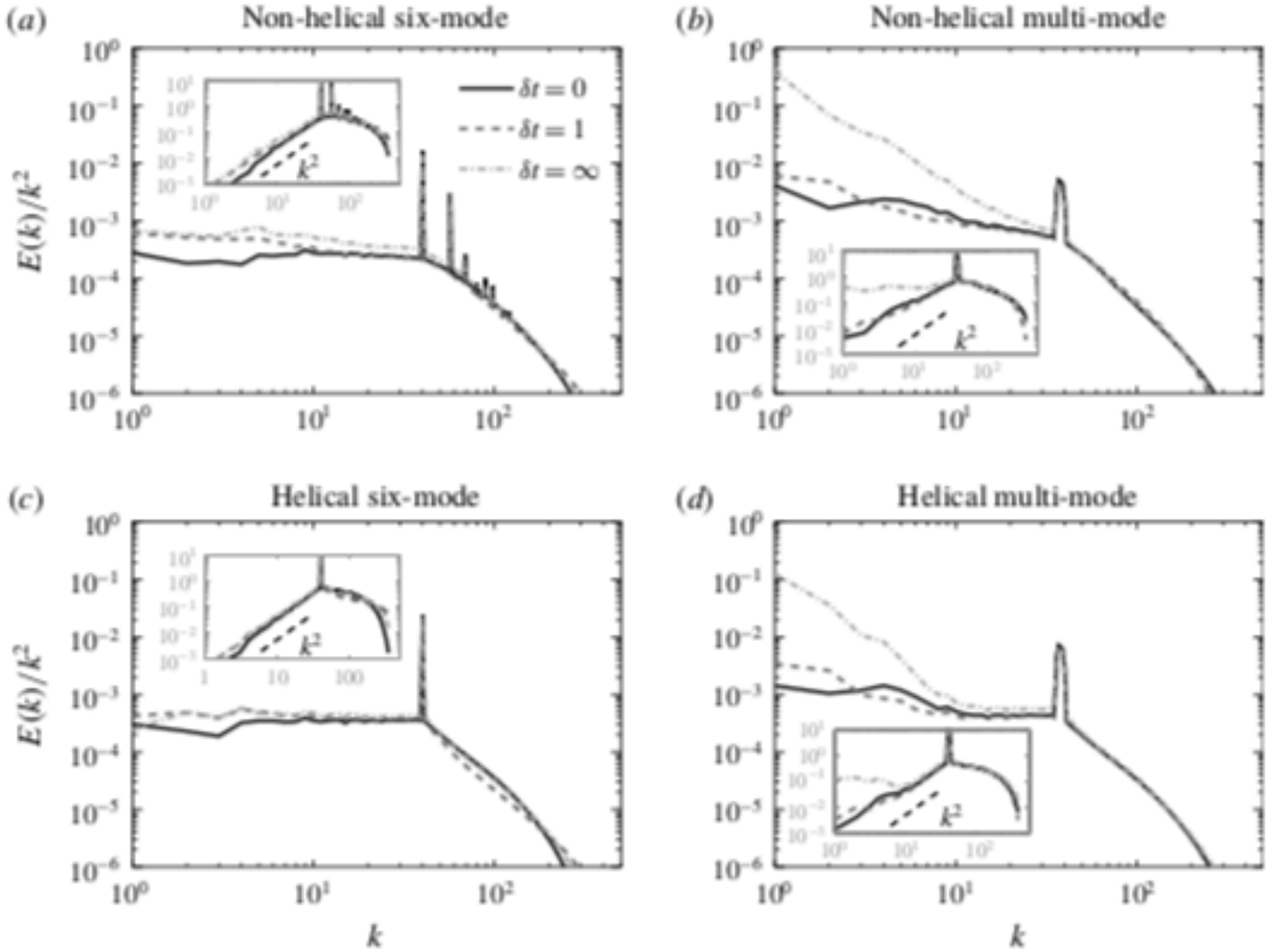

FIGURE 2. Energy spectra $E(k)$ compensated by k^{-2} for the 12 different runs given in table 1. (*a–d*) Show the spectra for the non-helical/helical flows and (*a*,*c*), (*b*,*d*) show the spectra for the six-mode/multi-mode forced flows. The insets show the same spectra uncompensated.

Energy fluxes in quasi-equilibrium flows

We examine the relation between the absolute equilibrium state of the spectrally truncated Euler equations to the forced and dissipated flows of the spectrally truncated Navier–Stokes (TNS) equations where energy is injected by a body-force and dissipated by the viscosity.

We show, using an asymptotic expansion of the Fokker-Planck equation, that the TNS flow approaches the absolute equilibrium

A transition from the quasi-equilibrium ‘thermal’ state to Kolmogorov turbulence is observed.

Energy fluxes in quasi-equilibrium flows

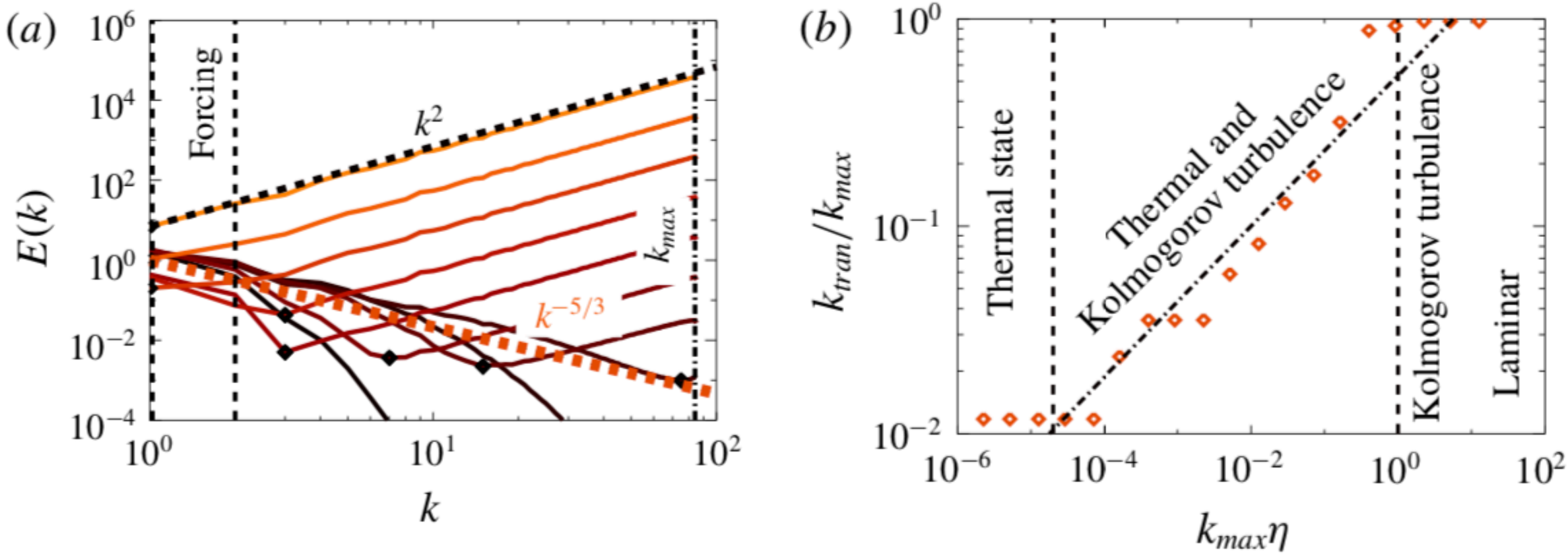

FIGURE 2. (*a*) Energy spectra for six different runs of the TNS equations with $k_{max} = 85$, $\mathcal{I}_\mathcal{E} = 1$ and, from dark to bright, $\nu = 10^{-1}$, $\nu = 10^{-2}$, $\nu = 10^{-3}$, $\nu = 10^{-4}$, $\nu = 10^{-5}$, $\nu = 10^{-6}$, $\nu = 10^{-7}$, $\nu = 10^{-8}$, $\nu = 10^{-9}$, $\nu = 10^{-10}$. The forcing was restricted in the small wavenumbers and the dissipation in the large wavenumbers as indicated. (*b*) The wavenumber k_{tran} where the Kolmogorov spectrum $k^{-5/3}$ transitions to the thermal spectrum k^2 as a function of the Kolmogorov length scale $\eta = (\nu^3/\mathcal{I}_\mathcal{E})^{1/4}$. Here k_{tran} for the simulations (diamonds) is estimated as the wavenumber that $E(k)$ obtains its minimum. The dashed line gives the prediction in (3.1).

Conclusion

- Perhaps turbulence is simpler to resolve starting from GPE rather than Navier-Stokes? The existence of GPE solutions is well established mathematically, see e.g. The Cauchy problem for the Gross–Pitaevskii equation, P. Gérard Ann. I. H. Poincaré – AN 23 (2006) 765–779.
- Statistical mechanics of interacting and reconnecting vortex lines?
- Truncated GPE computations can be used to study finite Temperature effects
- However, the effective viscosity is large: the mean free path needs to be reduced…

Conclusion

- Turbulence is still an open problem [physically and mathematically]
- It is, perhaps, the most important unsolved problem of nonlinear science
- Spectral truncation allows for (pseudo)dissipative effects
- Self truncation: a new direct statistical approach to some conservative PDE's?

Conclusion

- Truncated 2D Euler dynamics appears to describe reversals in two-dimensional confined turbulent flows
- Truncated 3D Euler also appears to describe some of the regimes of forced Navier Stokes turbulence

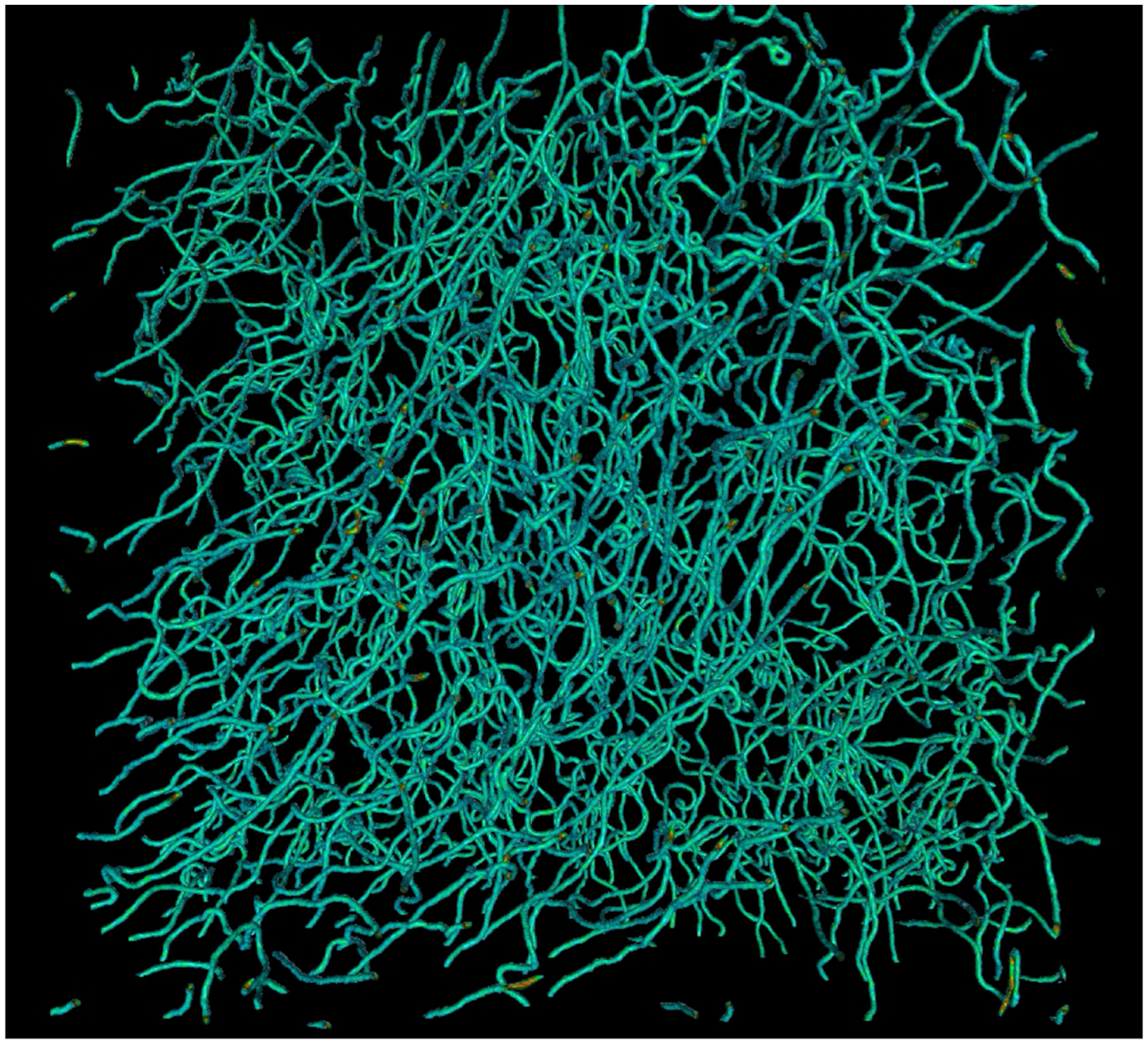

Thank you!

Extra stuff in case I have enough time…

The formation of finite temperatures compact objects in classical-field-self-gravitating dark-matter candidate

Akhilesh Kumar Verma
Rahul Pandit
Marc E. Brachet

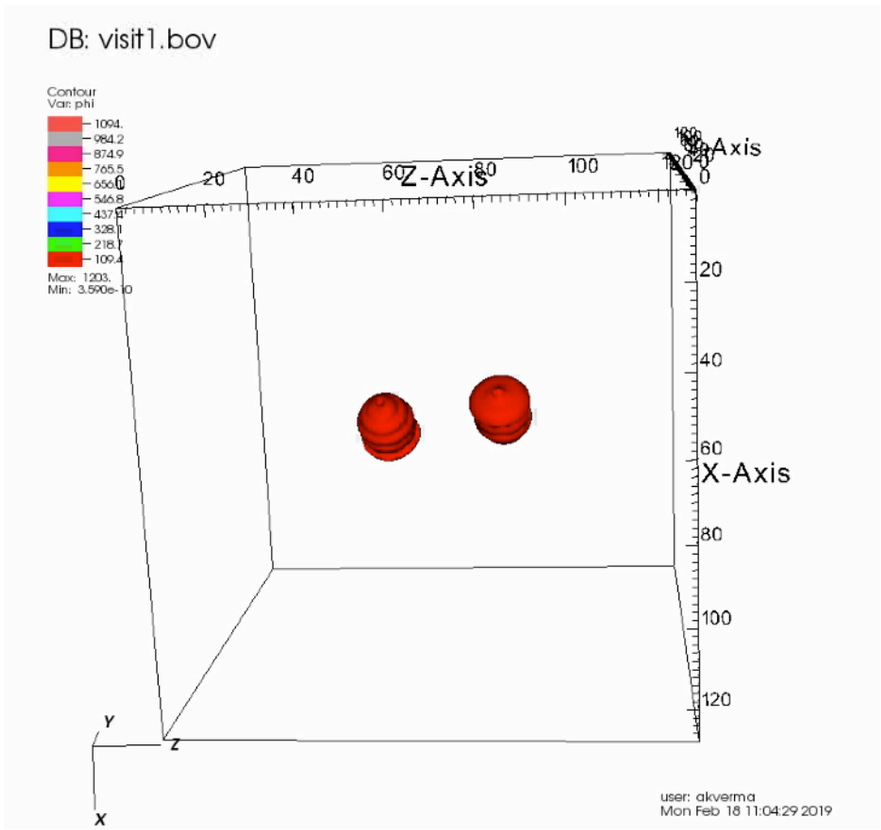

Outline

- Gross-Pitaevskii Poisson Equation (GPPE)
- System definitions and spectral truncation
- TGPPE & conservation laws
- Stochastic Ginzburg-Landau Poisson Equation (SGLP) & equilibrium
- Ground state & finite temperature effects
- GPPE gravitational collapse
- Discussion

System definition

Self-gravitating BEC are described by a complex wave function $\psi(\mathbf{x}, t)$; for weakly interacting bosons, the spatiotemporal evolution of $\psi(\mathbf{x}, t)$ is governed by the GPPE:

$$\begin{aligned} i\hbar\partial_t\psi &= -\frac{\hbar^2}{2m}\nabla^2\psi + \left[G\Phi + g|\psi|^2\right]\psi, \\ \nabla^2\Phi &= |\psi|^2 - <|\psi|^2> \end{aligned} \quad , \tag{1}$$

where m is the mass of the bosons, $n = |\psi|^2$ their number density, $G = 4\pi G_N m^2$ (G_N is Newton's constant), and $g = 4\pi a\hbar^2/m$, with a the s-wave scattering length.

System definition

The subtraction of the mean density $\langle|\psi|^2\rangle$ can be justified either by taking into account the cosmological expansion or by defining a Newtonian cosmological constant. Linearizing around a constant $|\psi|^2 = n_0$ yields the dispersion relation

$$\omega(k) = \sqrt{-Gn_0/m + k^2 g n_0/m + k^4(\hbar/2m)^2},$$

which displays a low-k Jeans instability, for wave numbers

$$k < k_J = \sqrt{\frac{G}{g}}\left[\left(1 + \sqrt{1 + \frac{G\hbar^2}{mg^2 n_0}}\right)/2\right]^{-1/2}.$$

In the absence of gravity ($G = 0$):

speed of sound $c = \sqrt{\frac{gn_0}{m}}$ and coherence length $\xi = \sqrt{\frac{\hbar^2}{2gn_0 m}}$.

Spectral truncation

$3D$ Fourier pseudospectral (2/3-dealiasing): the 2π periodic wave function reads $\psi(x) = \sum_{\mathbf{k}\in\mathbb{Z}^3} \hat{\psi}_{\mathbf{k}} \exp(i\mathbf{k}\cdot\mathbf{x})$. Truncate it spectrally: $\hat{\psi}_{\mathbf{k}} \equiv 0$ for $|\mathbf{k}| > k_{\max}$, with $k_{\max} = [\mathcal{N}/3]$, where $\mathcal{N}$ is the resolution and $[\cdot]$ denotes the integer part.

The Fourier-truncated GPPE reads

$$i\hbar\frac{\partial\psi}{\partial t} = \mathcal{P}_{\mathrm{G}}[-\frac{\hbar^2}{2m}\nabla^2\psi + \mathcal{P}_{\mathrm{G}}[(G\nabla^{-2} + g)|\psi|^2]\psi]. \tag{1}$$

where $\mathcal{P}_{\mathrm{G}}$ is the Galerkin projector [in Fourier space $\mathcal{P}_{\mathrm{G}}[\hat{\psi}_{\mathbf{k}}] = \theta(k_{\max} - |\mathbf{k}|)\hat{\psi}_{\mathbf{k}}$], with $\theta(\cdot)$ the Heaviside function.

Conservation laws

The TGPPE *conserves exactly*:
i) The number of particles

$$N = \int d^3x |\psi|^2.$$

ii) The energy

$$E = E_{kq} + E_{int} + E_G,$$

where $E_{kq} = \frac{\hbar^2}{2m}\int d^3x|\nabla\psi|^2$, $E_{int} = \frac{g}{2}\int d^3x[\mathcal{P}_{\rm G}|\psi|^2]^2$, $E_G = E_{\rm grav} = \frac{G}{2}\int d^3x[\mathcal{P}_{\rm G}|\psi|^2]\nabla^{-2}[\mathcal{P}_{\rm G}|\psi|^2]$.

iii) The momentum

$$\mathbf{P} = \frac{i\hbar}{2m}\int d^3x\left(\psi\nabla\overline{\psi} - \overline{\psi}\nabla\psi\right),$$

where over-bar denotes complex conjugation.

The Stochastic Ginzburg Landau equation (G=0)

The studies of Davis *et al.* [22] and of Connaughton *et al.* [23] showed that if the Fourier truncated version of the GPE is integrated for long enough, the system reaches a thermodynamic equilibrium. The statistical properties of this state are given by the microcanonical ensamble defined with fixed energy E, momentum $\mathbf{P}$, and number of particles $\mathcal{N}$. Moreover, if E is varied, a phase transition akin to that of BECs can be observed, where the zero-wavenumber $A_0 = \langle \Psi \rangle$ mode becomes equal to zero for finite E. But there are two problems with generating thermal states in this way. One is that the truncated GPE takes a very long time to converge to the equilibrium state, making it computationally expensive. The other is that the temperature is not easily accessed nor controlled

The Stochastic Ginzburg Landau equation (G=0)

order to overcome these problems, Krstulovic and Brachet [26, 27] suggested using a Langevin process to generate grand-canonical states with distribution probability $\mathbb{P}_{\rm st}$ given by a Boltzmann weight $\mathbb{P}_{\rm st} = e^{-\beta F}/\mathcal{Z}$, where $\mathcal{Z}$ denotes the grand partition function and

$$F = E - \mu\mathcal{N} - \mathbf{W}\cdot\mathbf{P}, \tag{10}$$

The Langevin process that generates these states has a Ginzburg-Landau equation of the type

$$\hbar\frac{\partial A_{\mathbf{k}}}{\partial t} = -\frac{\partial F}{\partial A^*_{\mathbf{k}}} + \sqrt{\frac{2\hbar}{\beta}}\hat{\xi}(\mathbf{k},t), \tag{11}$$

$$\langle \xi(\mathbf{r},t)\bar{\xi}(\mathbf{r}',t')\rangle = \delta(t-t')\delta(\mathbf{r}-\mathbf{r}'), \tag{12}$$

where $A_{\mathbf{k}}$ are the Fourier modes of the wavefunction, and $\hat{\xi}(\mathbf{k},t)$ is the Fourier transform of the Gaussian delta-correlated noise $\xi(\mathbf{r},t)$. In [27] it is shown that the sta-

SGLPE (finite G)

The spectral truncation generates a classical-field model that allows to study finite-T effects in the GPPE. The spectrally truncated GPPE can describe dynamical effects and, *at the same time*, yield thermalized states, which we can obtain both by thermalization of the long-time GPPE dynamics or directly, by using SGLPE:

$$\begin{aligned} \hbar\frac{\partial\psi}{\partial t} &= \mathcal{P}_{\mathrm{G}}[\frac{\hbar^2}{2m}\nabla^2\psi + \mu\psi - \mathcal{P}_{\mathrm{G}}[(G\nabla^{-2}+g)|\psi|^2]\psi] \\ &\quad + \sqrt{\frac{2\hbar}{\beta}}\mathcal{P}_{\mathrm{G}}\left[\zeta(\mathbf{x},t)\right], \end{aligned}$$

where the zero-mean, Gaussian white noise $\zeta(\mathbf{x},t)$ has the variance

$$\langle\zeta(\mathbf{x},t)\zeta^*(\mathbf{x}',t')\rangle = \delta(t-t')\delta(\mathbf{x}-\mathbf{x}'),$$

with $\beta = \frac{1}{k_B T}$ the inverse temperature; the chemical potential μ is tuned at each time step to conserve the total number of particles N.

SGLPE vs TGPPE

The finite-T SGLPE dynamics does not describe any physical evolution; but it converges more rapidly, than does the GPPE dynamics, toward a thermalized state.

Clearly, the SGLPE leads to a state with a given temperature; but the GPPE yields a state with a given energy.

Ground states

The energy of spherically symmetric ground state with radius R and N bosons can be estimated as

$$E(R) = \frac{\hbar^2 N}{2mR^2} + \frac{gN^2}{2R^3} - \frac{GN^2}{2R}$$

the equilibrium radius follows from

$$dE/dR|_{R=R_0} = 0,$$

yielding

$$R_0 = \frac{R_Q}{4\pi}(1 + \sqrt{1 + 48\pi^2(\frac{R_a}{R_Q})^2},$$

with $R_Q = \frac{\hbar^2}{G_N m^3 N}$ and $R_a = \sqrt{\frac{a\hbar^2}{G_N m^3}}$.

SGLPE convergence to ground state at T=0

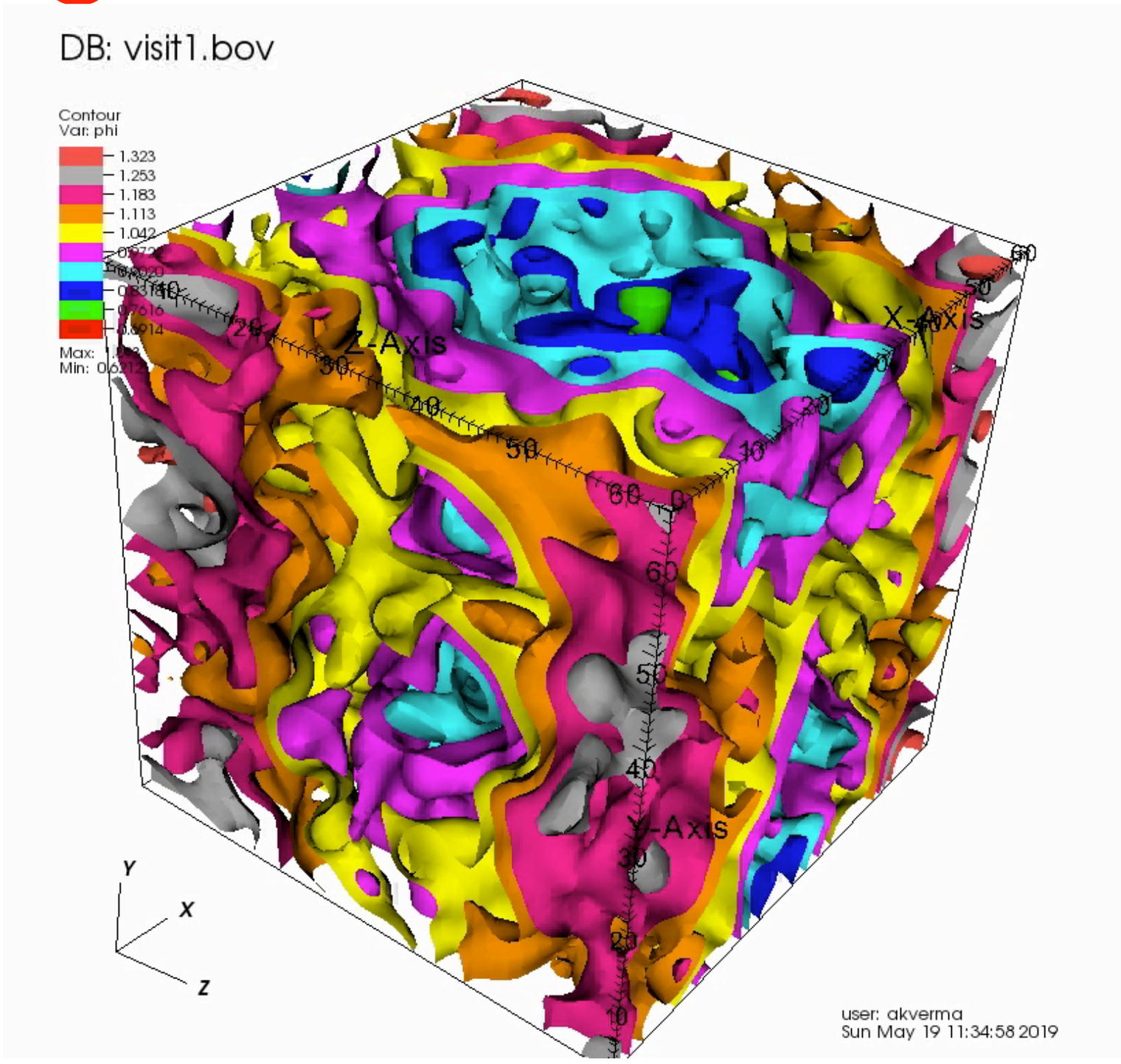

SGLPE convergence to ground state at finite T

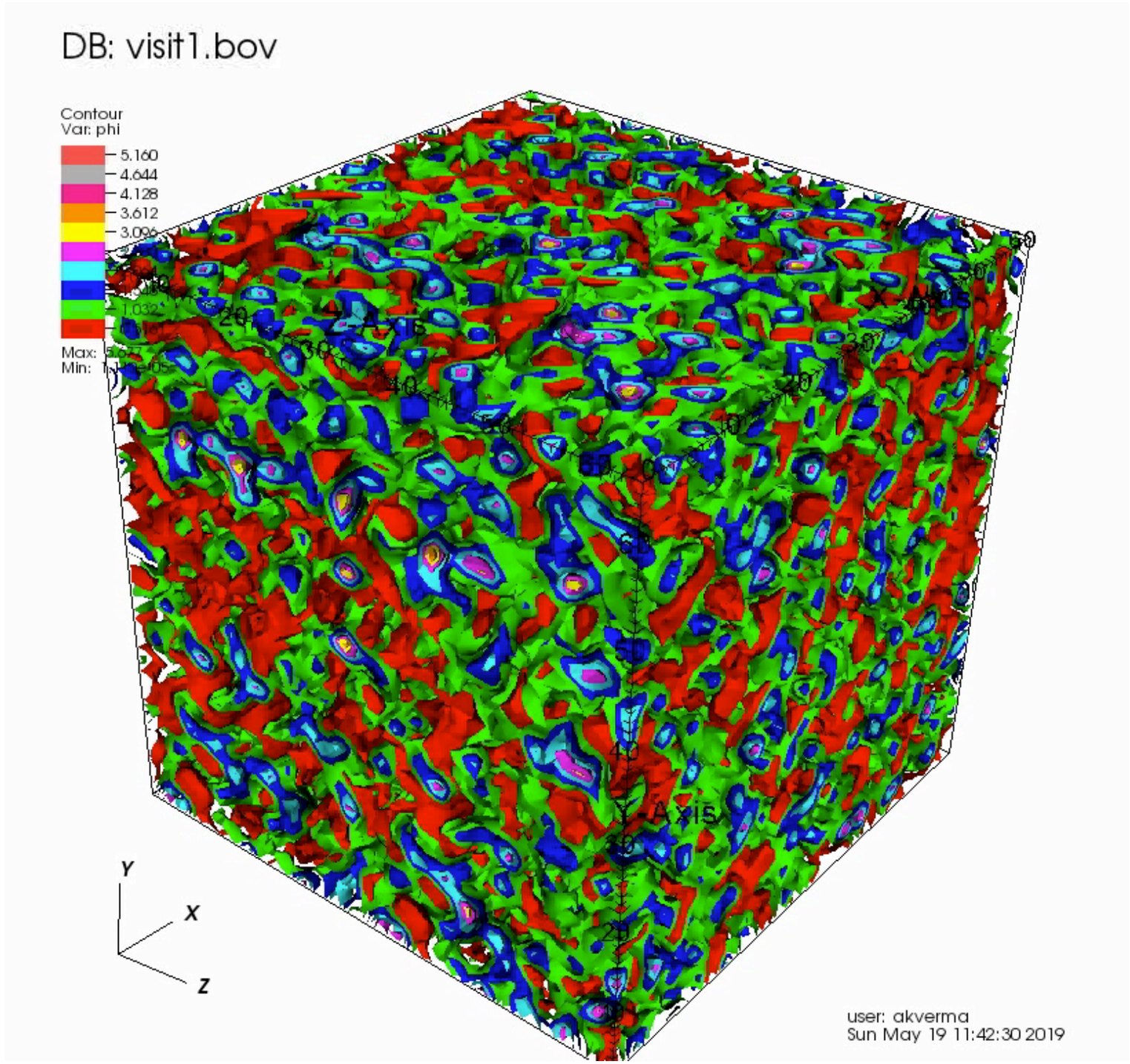

GPPE collapse

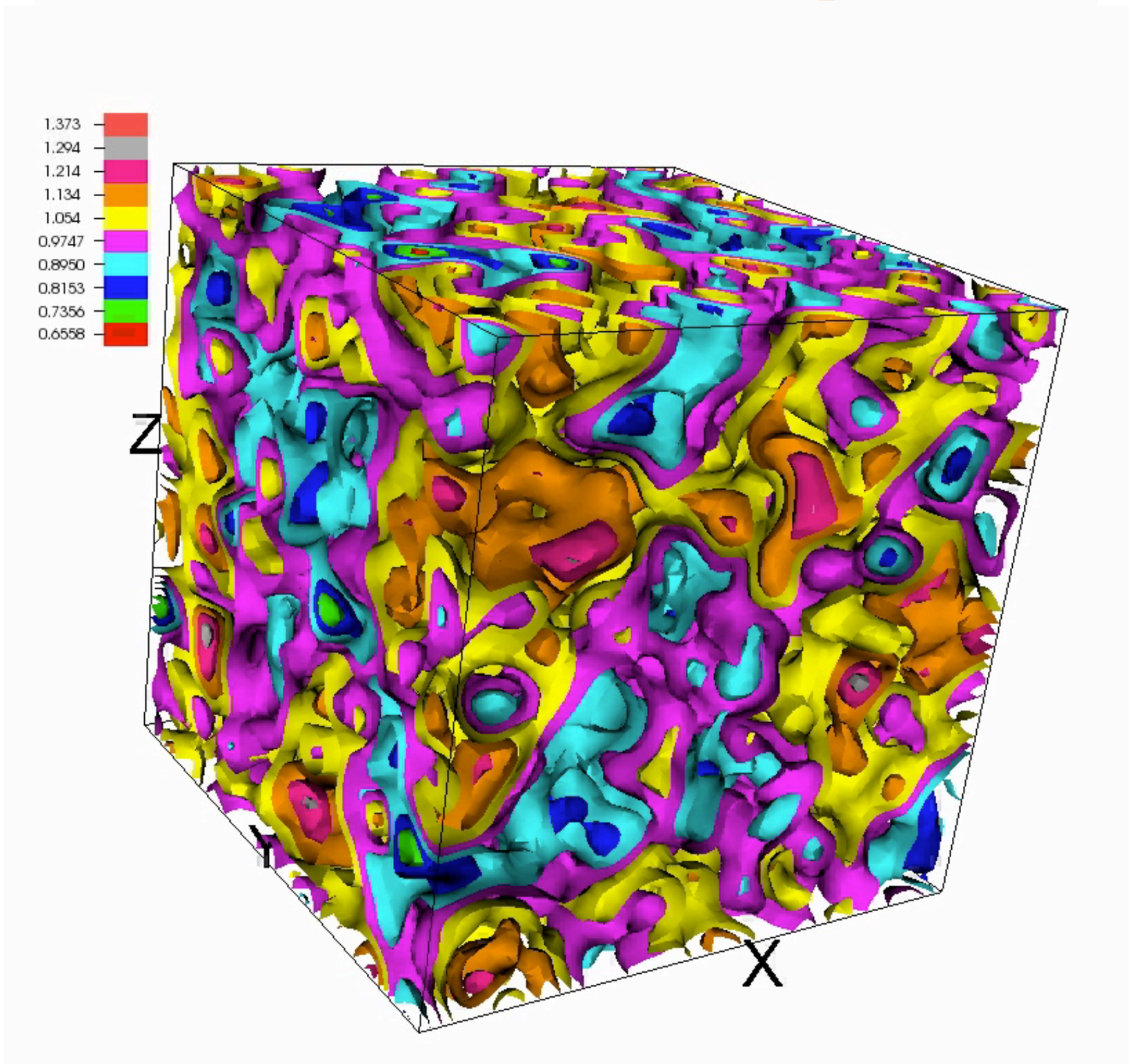

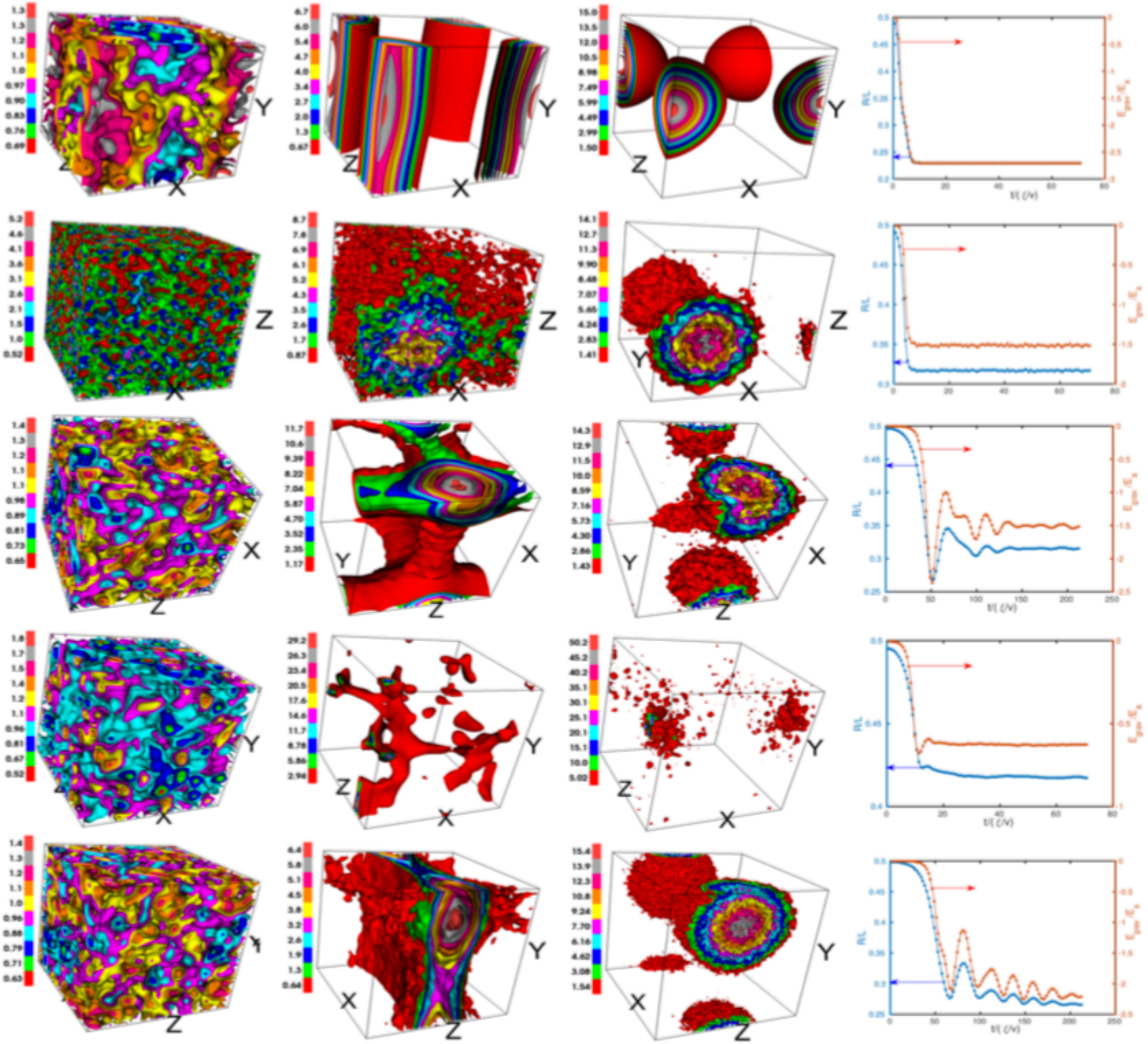

FIG. 1: Columns $(1)-(3)$: Ten-level contour plots of $|\psi(\mathbf{x},t)|^2$, at representative times: $(T=0)$ (top row, run $R1$), SGLPE (second row, run $R2$), GPPE (third row, run $R3$), GPPE (fourth row, run $R4$), and 256^3 GPPE (fifth row, run $R5$) DNSs [the videos V1-V5 (Supplemental Material [13]) show, respectively, the complete spatiotemporal evolution for these cases]. Column(4): Plots of the scaled radius of gyration $R=\sqrt{\frac{\int_V \rho(r) r^2\, d\mathbf{r}}{\int_V \rho(r)\, d\mathbf{r}}}$, R/L, (blue) and the scaled gravitational energy, E_{grav}/E_a (red) versus scaled time $t/(\xi/v)$ for the different runs.

Hysteresis

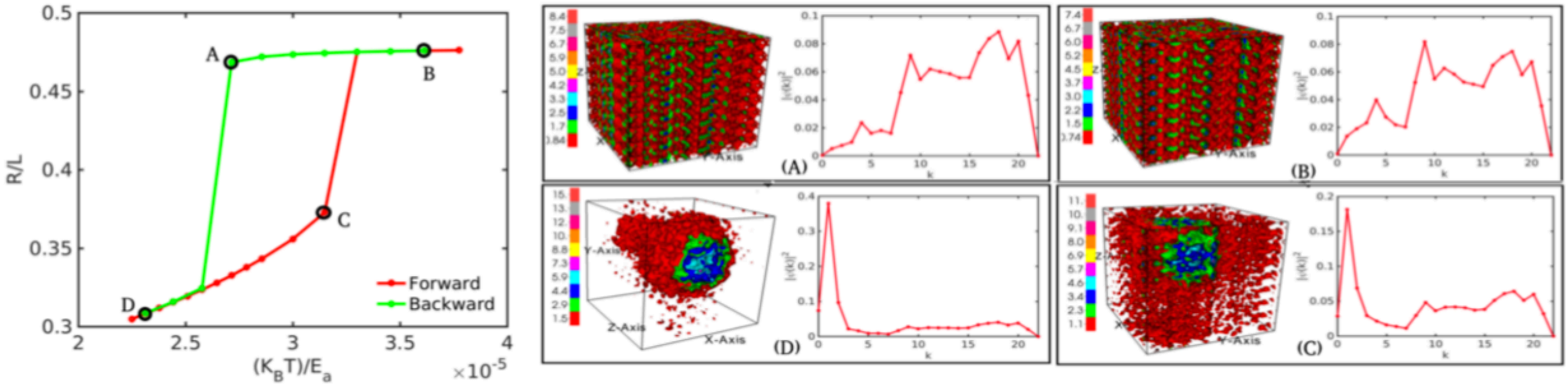

FIG. 3: Plots (in the middle) of dimensionless radius (R/L) versus dimensionless temperature (K_BT/E_a), the red curves is corresponding to increasing the temperature (in forward direction) and green curve is corresponding to decreasing the temperature (in backward direction). The left and right top plots show the density distribution and density spectra of non-collapse state corresponding to green line and the left and right bottom plots of the density distribution and density spectra of collapse state corresponding to red lines.

Binary Star

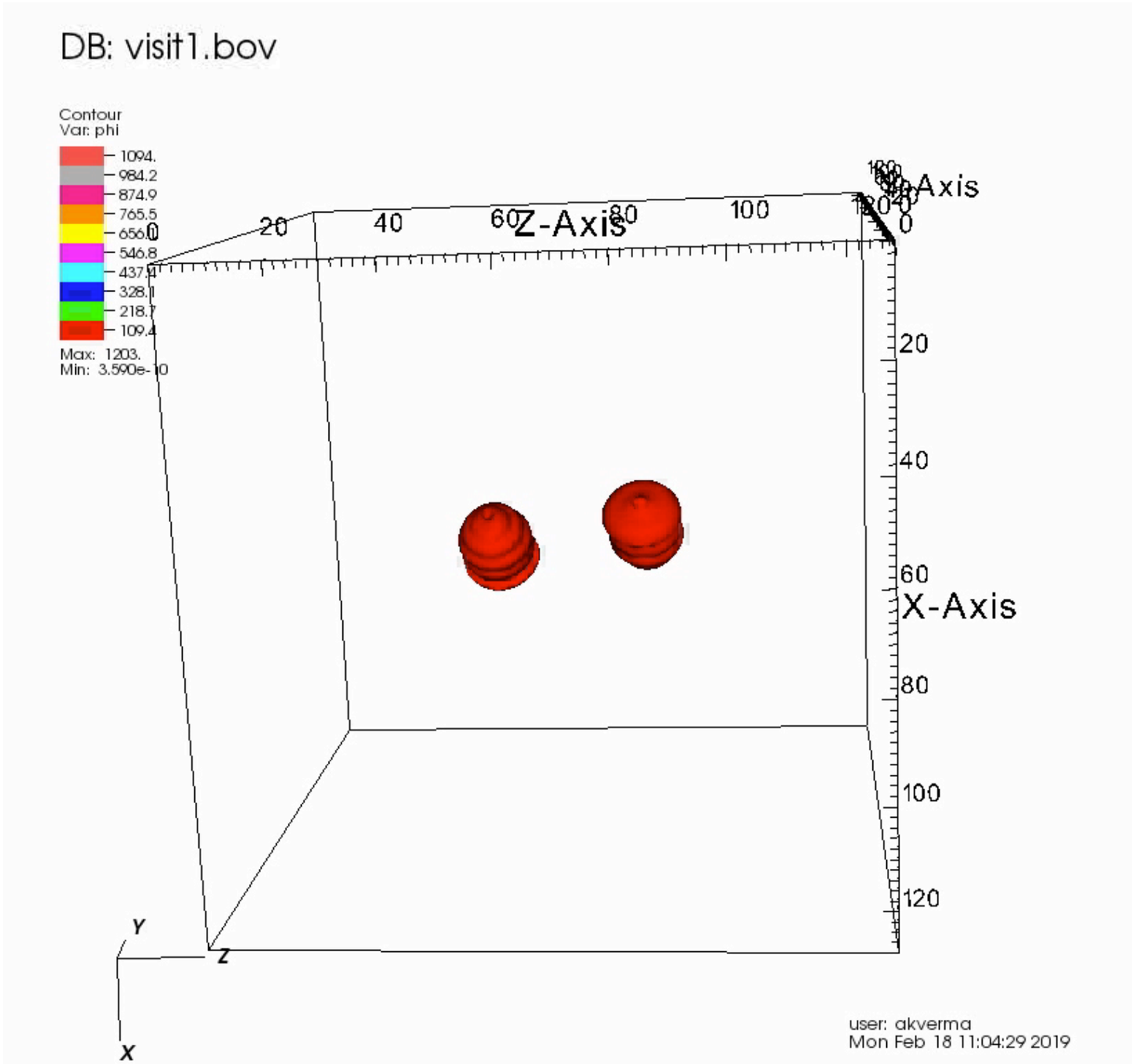
DB: visit1.bov
Contour
Var: phi
1094.
984.2
874.9
765.5
656.0
546.8
437.4
328.1
218.7
109.4
Max: 1203.
Min: 3.590e-10
0
20
40
60
80
100
Z-Axis
0
20
40
60
X-Axis
80
100
120
Y
Z
X
user: akverma
Mon Feb 18 11:04:29 2019

Discussion

- Dark matter candidates: axions
- Long-range interactions and thermodynamic limit
- Structure formation
- Relativistic generalisation